
This manuscript is a preprint and is currently under review in Earth Science Reviews. Subsequent versions of this manuscript may have slightly different content. If accepted, the final version of this manuscript will be available via the 'Peer-reviewed Publication DOI' link on the right-hand side of this webpage. Please feel free to contact any of the authors; we welcome feedback

Surging glaciers in Svalbard: Observing their distribution, characteristics and evolution

William D. Harcourt^{*1,2}, Danni M. Pearce^{1,3}, Wojciech Gajek⁴, Harold Lovell⁵, Erik S. Mannerfelt^{6,7}, Andreas Kääb⁶, Douglas I. Benn⁸, Adrian Luckman⁹, Richard Hann¹⁰, Jack Kohler¹¹, Tazio Strozzi¹², Rebecca McCerery¹³, Bethan J. Davies¹⁴

¹*School of Geosciences, University of Aberdeen, Aberdeen, United Kingdom*

²*Interdisciplinary Institute, University of Aberdeen, Aberdeen, United Kingdom*

³*Faculty of Environmental Sciences and Natural Resource Management, Norwegian University of Life Sciences, Ås, Norway*

⁴*Institute of Geophysics, Polish Academy of Sciences, Warsaw, Poland*

⁵*School of the Environment and Life Sciences, University of Portsmouth, Portsmouth, United Kingdom*

⁶*Department of Geosciences, University of Oslo, Oslo, Norway*

⁷*Arctic Geology, The University Centre in Svalbard, Longyearbyen, Norway*

⁸*School of Geography & Sustainable Development, University of St Andrews, St Andrews, United Kingdom*

⁹*Department of Geography, College of Science and Engineering, Swansea University, Swansea, United Kingdom*

¹⁰*Department of Engineering Cybernetics, UAV Icing Lab, Norwegian University of Science and Technology, Trondheim, Norway*

¹¹*Norwegian Polar Institute, Fram Centre, Tromsø, Norway*

¹²*GAMMA Remote Sensing AG, Gümligen, Switzerland*

¹³*Department of Geography and Environmental Science, Northumbria University, Newcastle Upon Tyne, UK*

¹⁴*School of Geography, Politics and Sociology, Newcastle University, Newcastle Upon Tyne, UK*

*Corresponding author: William D. Harcourt (william.harcourt@abdn.ac.uk)

38 **Abstract**

39 Glacier surges are episodes of significantly increased ice flow due to ice-dynamical feedbacks, and
40 are often repeated in a quasi-periodical manner. Ice mass is redistributed during a surge, which leads
41 to surface lowering at high elevation as ice is transferred down-glacier and thickening nearer the
42 terminus. In this paper, we review different approaches for monitoring and detecting glacier surges in
43 Svalbard, one of the most prominent global clusters of surge-type glaciers. Current surge detection is
44 mainly based upon tracking the speed of glaciers over time, measuring elevation and frontal changes,
45 and more recently automatically detecting surface changes such as increased crevassing. Thermal
46 and hydrological changes near the glacier bed drive surge dynamics and can be measured using
47 geophysical sensors such as ground-penetrating radar (GPR) and seismometers. When glaciers
48 surge, they often produce diagnostic landforms in subglacial and proglacial environments, allowing
49 historical surging to be identified even if surges have not been directly observed. Through this review,
50 we have compiled an updated database of surge-type glaciers in Svalbard and find that 36% of
51 glaciers display surge-type behaviour, rising to 52% when removing glaciers smaller than 1 km². Only
52 9% of all glaciers have been directly observed to surge. Svalbard surge-type glaciers have gentler
53 slopes, are generally longer, and extend across a larger elevation range. We find that the behaviour of
54 surge-type glaciers is variable and more closely resembles a continuum from glaciers that do not
55 surge to those which redistribute mass in a single event of strongly enhanced ice flux. We can
56 describe the variability in surge behaviour using the concept of enthalpy and a six-stage surge model
57 that characterises the build-up of energy at the glacier bed driven initially by thermal change and then
58 ice acceleration which is prompted by changes in subglacial hydrology. Observations of glacier surges
59 have improved significantly with routine mapping from satellites such as Sentinel-1, Sentinel-2 and the
60 Landsat satellite series. Furthermore, an increasing number of geophysical measurements is enabling
61 an improved understanding of subglacial processes before, during and after a surge, which is crucial
62 for improving models of surge behaviour. As our observations of surges continue to improve, we
63 expect to uncover new elements and details of surge behaviour which suggests we need to rethink the
64 binary classification of glaciers as either 'surge-type' or 'not surge-type' in Svalbard and across the
65 world.

66

67 **Keywords:** Glacier surging; satellite remote sensing; geophysics; palaeo-glaciology; continuum of
68 behaviour

69

70 **Highlights**

- 71 • Approximately 36% of glaciers in Svalbard have been observed to surge or show clear
72 evidence of having surged in the past, rising to 52% when removing glaciers smaller than 1
73 km².
- 74 • Surges can be readily identified from satellite data, landforms representative of fast flow (e.g.
75 crevasse squeeze ridges), and geophysical sensors.
- 76 • Svalbard surges may be described by a six-stage model from gradual speed-up, ice
77 acceleration and then peak velocity, before a slow dissipation of energy and glacier slow-down.
- 78 • There is a continuum of glacier surge behaviour: full catchment surges, pulses of tributary
79 glaciers, partial acceleration, and no surge behaviour.
- 80 • Key knowledge gaps include understanding the surge potential of small valley glaciers, the
81 relationship between surges and mass balance, and the evolution of surge-type glaciers and
82 surging from the Little Ice Age through to the present day and into the future.

83

84

85

86

87

88

89

90

91

92

93 1. Introduction

94 1.1. Glacier surges

95 Surge-type glaciers undergo quasi-periodical changes in their flow regime from accelerated velocities
96 during an ‘active’ surge to low velocities during quiescence (Benn et al., 2019a). This behaviour
97 contrasts to the flow dynamics of non-surging glaciers, which are governed by the ongoing adjustment
98 to the difference between mass accumulation at higher elevation and ablation at lower elevation i.e.
99 the balance velocities, with short-term velocity variations (e.g. diurnal, seasonal) superimposed on this
100 long-term pattern. The surge cycle between fast and slow flow results from internal dynamical
101 instabilities, whereby fast flow initiates due to frictional feedbacks (Thøgersen et al., 2019; 2024) and
102 may be expedited by external factors such as dynamic thinning from enhanced surface melt (Sevestre
103 et al., 2018). The subsequent enhanced down-glacier discharge of ice can increase the mass loss
104 over short time periods during a multi-year active surge (McMillan et al., 2014; Dunse et al., 2015;
105 Morris et al., 2020) and subsequently expose more ice to higher air temperatures leading to enhanced
106 surface melting (Oerlemans, 2018). In addition, the influx of freshwater into the ocean/fjord caused by
107 a glacier surge may impact circulation and stratification, whilst also affecting downstream marine and
108 terrestrial ecosystems through local changes in biogeochemistry (Hopwood et al., 2020). More
109 recently, there is clear evidence linking Arctic glacier retreat to the release of subsurface methane
110 (Klebar et al., 2023). Conversely, the link between surge-type glaciers advancing into proglacial
111 permafrost terrain and disrupting methane stores is less clear, but high subglacial water pressure may
112 increase this flux (Kleber et al., 2025) and is therefore relevant to consider in the context of surging. All
113 these impacts vary spatio-temporally in response to the quasi-periodic behaviour of glacier surges
114 (Raymond, 1987). Glacier surges can also cause a number of hazards through the direct impact of
115 their advance on land and infrastructure, river damming and flooding, and ice avalanching (Truffer et
116 al., 2021; Kääb et al., 2021). On Svalbard, a key impact of glacier surging is through enhanced
117 crevassing that makes travel routes dangerous or at least more complicated.

118 Glacier surges involve changes in subglacial conditions (Meier and Post, 1969; Kamb et al. 1985;
119 Benn et al., 2019a). Traditionally, surges were thought to be governed by one of two potential
120 mechanisms - the ‘thermal switch’ and the ‘hydrologic switch’. In the ‘thermal switch’ model (Clarke,
121 1976; Fowler et al., 2001), surges begin and end due to a change in basal temperature that leads to
122 an increase or loss of meltwater availability for basal sliding. In contrast, in the ‘hydrologic switch’
123 mechanism (Kamb, 1987; Fowler et al., 1987), surges initiate due to a change in the configuration of
124 the subglacial hydrological system from a channelised system to a distributed one.

Recent studies have suggested that surge cycles can be explained by oscillations in the coupled mass and basal enthalpy (thermal energy and water) budgets, which occur when glaciers are unable to settle on a stable steady state (Benn et al., 2019a). The enthalpy balance model can explain both the broad evolution of glacier surge dynamics and the occurrence of surge-type glaciers in climatically controlled clusters. In its current form, it takes a simplified approach to representing basal friction and hydrology and adopts a lumped (non-spatial) framework and thus cannot represent the details of individual surges. Thøgersen et al. (2019; 2024) aimed to explain oscillatory dynamics such as surges through a rate and state friction framework, whereby basal shear stress evolves as subglacial cavities expand due to an increase in subglacial water pressure. As a glacier gains mass, basal shear stress increases and ice velocity ‘strengthens’ to a point at which subglacial cavities form and the glacier surges. During a surge, mass is redistributed leading to a reduction in basal shear stress, the velocity ‘weakening’ regime. In this phase, there is a negative feedback between basal friction and subglacial hydrology beneath hard-bedded glaciers (Gilbert et al., 2022). For a glacier to move back into a velocity ‘strengthening’ regime, glacier sliding must then incorporate subglacial sediments, or the glacier margins become cold-based so that subglacial cavities can persist. After surge termination, mass will build up and the basal stress increases again, hence the cycle between velocity ‘strengthening’ and ‘weakening’ continues quasi-periodically. This model was developed for hard beds but has since been extended to include sliding over deformable sediments (Minchew and Meyer, 2020; Thøgersen et al., 2024). However, coupling enthalpy changes to sliding remains difficult. Terleth et al. (2021) suggested combining both the enthalpy and basal sliding theories by considering the transient nature of friction and deformation at the bed as the fundamental component, with enthalpy as the forcing component. Resolving the causes, drivers, and triggers of glacier surges may yield insights into the fundamental physics that govern ice flow, and in particular processes at the glacier base, where direct observations are scarce due to its inaccessibility.

The presence of unstable ice flow raises a pertinent question: why do some glaciers surge and others do not? Sevestre and Benn (2015) found that surge-type glaciers are located in geographical clusters with specific temperature and precipitation regimes optimal for surge-type ice flow cycles to exist. In the Arctic, a ring of surging glacier clusters can be found extending from Alaska Yukon to Novaya Zemlya. The ‘Arctic ring’ encapsulates Svalbard, an archipelago with a long history of glaciological observations and consequently measurements of glacier surges. Around 56% of the Svalbard archipelago area is covered by 1,583 glaciers and ice caps (RGI 7.0, 2023; Figure 1). Furthermore, there are three primary regions with bases in Svalbard: central (Longyearbyen and Barentsberg), northwest (Ny Ålesund), and southwest (Hornsund) Spitsbergen. All three locations can be accessed all year round either by air, boat or snowmobile, making field measurements much more cost-effective and logistically possible. As a result, many of Svalbard’s glaciers located around these central

research hubs have long-term records of glacier changes, with more sites being added as more of the archipelago becomes accessible via improved logistics. Using these observations alongside remote sensing data is enabling a better understanding of the physical processes driving glacier surges. Svalbard is therefore an ideal natural laboratory for studying glacier surges, their drivers, and their changes in the past and into the future. Here, we review the current knowledge of Svalbard surges, including the main techniques used for detecting and monitoring surges, and provide an update on the spatial and temporal distribution of surge-type glaciers and glacier surges.

FIGURE 1

1.2. Surging glaciers in Svalbard

Svalbard is an Arctic archipelago located between 76°N and 81°N. It is approximately 700 km east of Greenland and 300 km west of the Russian Arctic. There is a large climatic gradient across the archipelago (Hanssen-Bauer et al., 2019) as Svalbard is located at the boundary between warm Atlantic waters to the west, which travel northwards along the Fram Strait, and the cold Polar waters in the Barents Sea to the east. Warm Atlantic water is transported along the west coast of Svalbard via the West Spitsbergen Current, releasing heat and moisture that leads to higher temperatures than average found at this latitude. In comparison, the East Spitsbergen Current transports colder water from the Arctic Ocean into the Barents Sea, which leads to the formation of seasonal sea ice (Rieke et al., 2023). The formation of sea ice in western Svalbard is generally limited to the fjords (e.g. Swirad et al., 2024). The presence of sea ice to the north and east of Svalbard (Onarheim et al., 2018) limits available moisture sources and hence average precipitation rates are low, averaging less than 700 mm per year (Hanssen-Bauer et al., 2019). Spitsbergen is the largest island in Svalbard with an area of 40,000 km² and is covered by ice fields in the northwest, northeast and south, with many smaller glaciers and ice masses found in valleys in between. The second largest island is Nordaustlandet to the northeast where the two largest ice caps in Svalbard, Austfonna (8,100 km²) and Vestfonna (2,500 km²), are located. Kvitøya, covered almost completely by the Kvitøygjøkulen ice cap, is located a further 90 km east. The islands of Barentsøya and Edgeøya are located to the southeast of Spitsbergen where several large ice caps and valley glaciers can be found. During the last glacial maximum, the Barents Sea Ice Sheet extended from mainland Russia to Franz Josef Land and then to the continental shelf break to the west of Svalbard (Ingólfsson and Landvik, 2013). At the start of the Holocene, ice in Svalbard was restricted to the archipelago (Farnsworth et al., 2020), after which there was a rapid deglaciation (12.0-10.5 ka) before several episodes of re-advances culminating in the Little Ice Age. Since 1936, Svalbard glaciers have been losing mass at a rate of ~8 Gt per year

192 (Geyman et al., 2022) and this trend is expected to continue as Svalbard is currently warming 4-6
193 times faster than the rest of the planet (Rantanen et al., 2022).

194 The number of surge-type glaciers in Svalbard has been estimated to range between 10% and 90%
195 depending on the classification technique used (Lefauconnier and Hagen, 1991; Jiskoot et al., 1998;
196 Sevestre and Benn, 2015; Kääb et al., 2023; Koch et al., 2023). Therefore, although Svalbard is
197 considered to have a large share of surge-type glaciers compared to other regions, not all glaciers
198 have displayed this behaviour, suggesting local factors may control the ability of a glacier to surge.
199 Jiskoot et al. (1998; 2000) found that glacier geometry (width, thickness, surface and bed slope) has a
200 significant influence on the likelihood of a glacier to be of surge type. This is in agreement with
201 Sevestre and Benn (2015), who found that surge-type glaciers globally tend to be longer, have lower
202 slopes and have larger catchment sizes. In Svalbard, most surge-type glaciers are most likely to
203 overlay deformable sedimentary bedrock (Hamilton and Dowdeswell 1996; Jiskoot et al., 2000).
204 Complex glacier configurations (i.e. the presence of multiple tributaries feeding into a larger glacier, or
205 multiple flow-units within a glacier system) may also partly control Svalbard surges (Jiskoot et al.,
206 2000; Sevestre and Benn, 2015).

207 To better understand the causes, triggers and impacts of glacier surges in Svalbard, improved
208 monitoring is required and new techniques developed to extend the observational record of active
209 surge dynamics. Observations of sediment-landform assemblages formed by past surging have
210 partially bridged this gap (Farnsworth et al., 2016; Flink et al., 2018; McCerery et al., 2024; 2025),
211 particularly when combined with absolute dating methods (Kempf et al., 2013; Flink and Noormets,
212 2018; Lovell et al., 2018b), but such records can be compromised by erosion and sedimentation.
213 Historical aerial photographs / archival maps have revealed past surges as far back as 1850
214 (Lefauconnier and Hagen, 1991; Hagen et al., 1993; Geyman et al., 2022) but these are intermittent
215 observations and do not document surge velocities, terminus advance rates, mass transfer, triggers or
216 subglacial conditions. Even in the satellite era, with dense observations that can be used to detect
217 active surges (Kääb et al., 2023; Koch et al., 2023), only in situ geophysical observations are capable
218 of directly studying subglacial drivers of a surge (Sevestre et al., 2015; Bouchayer et al., 2024). The
219 influence of environmental factors such as calving and surface melt has been less studied with only a
220 few studies (e.g. Dowdeswell et al., 1995; Sevestre et al., 2018; Benn et al., 2022) commenting on the
221 potential causes of surge initiation. Consequently, the lack of detailed long-term surge observations
222 has also inhibited our understanding of their impact on regional glacier mass balance, which may be
223 significant (e.g., McMillan et al., 2014; Dunse et al., 2015).

224 1.3. Aims of review

225 The primary aim of this paper is to review the techniques used to observe surges and the distribution
226 of surge behaviour in Svalbard. Through this review, we will highlight research gaps and opportunities
227 for future research. Our specific objectives are to:

- 228 1) Review the techniques used to detect glacier surges, monitor their characteristics, and
229 measure their causal processes.
- 230 2) Compile existing databases of surge-type glaciers in Svalbard to generate an updated estimate
231 of their distribution across the archipelago.
- 232 3) Evaluate the role of the different monitoring techniques to advance our knowledge of surge
233 behaviour in Svalbard and their causal mechanisms.
- 234 4) Identify key gaps in process knowledge and monitoring capabilities to inform future research
235 priorities.

236 2. Previous compilations of surge-type glaciers in Svalbard

237 One of the first reliable sources of a glacier surge in Svalbard is linked to the 1838 French La
238 Recherche Expedition, which painted Recherchebreen as extensively crevassed, and mapped the
239 terminus position to an extent that far exceeded both previous and subsequent maps (Figure 2). Since
240 then, and with ever more observations of glacier surges, there have been several attempts to
241 compose a database of surge-type glaciers in Svalbard based on different methodologies.
242 Lefauconnier and Hagen (1991) compiled a detailed list of surge-type glaciers in eastern Svalbard that
243 were marine-terminating and discharged icebergs into the Barents Sea, concluding that 90% of
244 glaciers in Svalbard were likely to be surge-type. Hagen et al. (1993) developed the first Svalbard-
245 wide inventory of surge-type glaciers, documenting recorded surges from historical observations,
246 satellite imagery and archival aerial photographs. In comparison, statistical analysis of variables that
247 control surging (e.g. bed lithology, glacier geometry) have suggested that only 13% of Svalbard's
248 glaciers are surge-type (Jiskoot et al., 1998; 2000). Sevestre and Benn (2015) compiled a global
249 database of surge-type glaciers from ice flow velocities, detected terminus advances and
250 geomorphological evidence (see section 4). They also compiled a list of glaciers that are possibly
251 surge-type after showing signatures of past surge behaviour, and glaciers very likely to be surge-type
252 that display several well-preserved surge features but have not been directly observed to surge. An
253 updated version of this database is currently available in the Randolph Glacier Inventory (RGI) version

254 7 (RGI 7.0 Consortium, 2023). In this database, Sevestre and Benn (2015) estimated that 17% (n =
255 263) of glaciers in Svalbard have shown past surge activity, of which only 8% (n = 125) have been
256 directly observed to surge.

257 **FIGURE 2**

258 Other studies have suggested that the presence of diagnostic landforms associated with surging, such
259 as crevasse-squeeze ridges (CSRs; Sharp, 1985; Evans and Rea, 1999), represent evidence of past
260 surge activity. Farnsworth et al. (2016) interrogated centimetre resolution aerial imagery and found
261 that 431 forefields in Svalbard contained CSRs, which equates to 43% of glaciers in Svalbard
262 (although only 27% of the Randolph Glacier Inventory (RGI) 7.0 glaciers, see section 5). The absence
263 of CSRs does not necessarily mean that a glacier has not previously surged as these landforms may
264 not be well preserved due to erosion, weathering, sedimentation, or deposition in water. Other
265 landforms diagnostic of surging have been recognised, such as glaciotectionic moraines and mud-
266 aprons (Croot, 1988; Kristensen et al., 2009; Lovell and Boston, 2017; Lovell et al., 2018b), and these
267 can also be used to assess Svalbard-wide prevalence of surges.

268 Because of the difficulty in directly observing glacier surges before the satellite era, statistical models
269 have been developed to classify the probability of a glacier being surge-type based on the correlation
270 of local geometric and climatic factors with known surge-type glaciers. Hamilton and Dowdeswell
271 (1996) found that Svalbard glaciers had a higher probability of being surge-type as their centrelines
272 were generally longer than other glaciated regions. This finding is in agreement with other studies
273 using logistic regression (Jiskoot et al., 1998; 2000), which found length and surface slope to be key
274 determinants of surge prevalence in Svalbard and suggested 13% of glaciers were surge-type. More
275 recently, advanced machine learning techniques have been employed to map the probability of
276 glaciers across the archipelago being surge-type. Bouchayer et al. (2022) trained several models with
277 data on mass balance, glacier geometric features and climatic data and found that 17% of all glaciers
278 larger than 1km² could be of surge-type, although when considering glaciers of all size classes, this
279 equates to 10%. Whilst these statistical models give new insights into the potential local environmental
280 drivers of surging and the possibility of currently unidentified surge-type glaciers, they do not represent
281 direct observations.

282 To complement these existing inventories, we now review the techniques used to monitor past and
283 present glacier surges and their processes in Svalbard. This review focuses on five key
284 characteristics: 1) ice velocities; 2) mass redistribution; 3) ice front changes; 4) surge drivers; and 5)
285 subglacial conditions. These techniques inform the creation of a new Svalbard surge database, which
286 is described in section 5, and contributes to the discussion of surge behaviour in section 6.

287 **3. Monitoring glacier surges**

288 **3.1. Observational pyramid**

289 Comprehensive monitoring of surges in Svalbard and their associated processes relies upon remote
290 sensing at multiple scales. The observational pyramid provides a conceptual framework for integrating
291 the various technologies used to monitor glacier surges in Svalbard (Figure 3). It spans satellite
292 remote sensing, airborne platforms, and ground-based and uncrewed maritime systems, each
293 contributing observations at different spatial and temporal scales. Satellites offer long-term, large
294 spatial coverage through sensors such as optical imagers and synthetic aperture radar (SAR).
295 Medium-resolution satellite sensors (e.g. Landsat, Sentinel satellites, ASTER) typically have coarse
296 (5-50 m) spatial resolution. In comparison, commercial satellite systems (e.g. SkySat, Planet, ICEYE,
297 Capella) can offer spatial resolution imagery down to 30 cm and acquire data when tasked by an end-
298 user. Uncrewed aerial vehicles (UAVs), by contrast, capture high-resolution (down to a few cm) data
299 at lower altitudes, using a range of sensors to focus on specific areas such as glacier fronts, or to map
300 entire glaciers with more complex missions. Geophysical sensors, such as seismometers and ground-
301 penetrating radar (GPR), enable detailed observations of subsurface and dynamic processes that are
302 otherwise inaccessible and are crucial for observing subglacial conditions driving surges. Marine
303 uncrewed systems—including autonomous and remotely operated underwater vehicles (AUVs and
304 ROVs)—extend observational capabilities below the terminus for marine-terminating glaciers, enabling
305 the study of calving fronts, meltwater discharge, subglacial outflows and the former glacier bed that
306 are otherwise difficult to access (Howe et al., 2019; Inall et al., 2024).

307 Rather than viewing these techniques in isolation, the observational pyramid highlights their
308 complementarity. It allows for coordinated observations where coarse-scale satellite data can guide
309 the targeted deployment of close-range or subsurface sensors, and in situ measurements can validate
310 and refine interpretations of remotely sensed signals. Improving the spatio-temporal resolution and
311 coordination of these methods is paramount in order to fully understand glacier surge dynamics and
312 their driving processes. The observational pyramid thus represents not just the current state of
313 monitoring, but a future-oriented framework that can accommodate new technologies and support
314 adaptive strategies for detecting and investigating glacier surges across Svalbard.

315 **FIGURE 3**

316 **3.2. Satellite Earth Observation (EO)**

317 The most detailed record of glacier surge behaviour in Svalbard has been captured over the satellite
318 era extending back to the 1960s. These observations were infrequent up to the 1990s, around which
319 time the launch of several satellites with optical imaging and SAR payloads (e.g. ERS-1, ERS-2,
320 RADARSAT-1, Landsat 7, ASTER) enabled routine mapping of glaciers in Svalbard. The launch of
321 CryoSat-2 in 2010 improved spaceborne monitoring of glacier volume changes, while the density of
322 satellite measurements has increased dramatically since 2014 with the launch of several new NASA
323 satellites (Landsat 8 and 9), and the initiation of the Copernicus satellite programme launching
324 Sentinel-1 (SAR) and Sentinel-2 (optical). Sentinel-1 imagery offers revisit periods of 1-2 days in extra-
325 wide swath mode (EW) and 6-12 days in interferometric-wide swath mode (IW), whilst Sentinel-2 has
326 almost daily coverage in Svalbard between March and October. Meanwhile, the long time series of
327 Landsat imagery is key for detecting surges back to the 1980s. The major benefits of satellite EO is
328 their ability to continuously and systematically monitor the dynamics of glacier surges over time and
329 therefore detect anomalous changes associated with unstable ice flow, whilst doing so across the
330 whole archipelago. However, these sensors can only detect surface changes, and do not provide
331 direct data on subglacial conditions.

332 An active glacier surge in Svalbard typically undergoes a multi-year speed-up and then decelerates
333 gradually (Figure 4). Although the magnitude of this pattern differs between glaciers, the premise is
334 that velocity data can be used to detect an active surge from continuous satellite monitoring.
335 Techniques such as feature-tracking and radar interferometry (InSAR) are employed to measure the
336 surface displacement between image pairs, enabling the detection of surge events (Murray et al.,
337 2003b; Koch et al., 2023). Before 2000, velocity maps were restricted to image pairs covering limited
338 spatial regions in Svalbard due to the longer revisit periods (Dowdeswell and Collin, 1990; Rolstad et
339 al., 1997). In the 2000s, velocity data were primarily acquired from satellites such as ERS-1/2,
340 ENVISAT, RADARSAT-1/2 and ASTER (Murray et al., 2003a,b; Mansell et al., 2012), often with
341 variable revisit periods which detected only large surges of glaciers with extensive catchments. In the
342 case of ERS-1/2, the revisit times over Svalbard were either too short (1-3 days) to capture the
343 displacement of surface features or too long (35 days) causing surface decorrelation, despite the
344 images being of high quality. Older Landsat 1-5 imagery had lower quality (e.g. radiometric resolution)
345 compared to more recent Landsat 7-9 imagery, resulting in larger geolocation errors and lower
346 contrast between surface features, which hinder the image matching during feature-tracking. Despite
347 the relative paucity of appropriate SAR images over Svalbard, InSAR has successfully been used to
348 detect unstable ice flow, such as during the surges of Fridtjovbreen (Murray et al., 2003b) and
349 Monacobreen (Luckman et al., 2002). A recent addition to surge detection has been the use of InSAR

coherence loss as the primary signal to identify surge-related instabilities, instead of only using it to explain why regular processing fails (Mannerfelt et al., 2025). Also, with the open release of historical satellite imagery, it is now possible to generate long-term velocity time series (e.g. Strozzi et al., 2017), enabling the detection of previously unidentified surges (Figure 5). In addition, extracting velocity data from satellites such as ALOS PALSAR has enabled a more complete understanding of complex surge dynamics, such as those at Nathorstbreen in southern Spitsbergen Svalbard (Nuth et al., 2019). Finally, high-resolution TerraSAR-X images have been used to capture the evolution of two major surges at Aavatsmarkbreen and Wahlenbergbreen (Sevestre et al., 2018), demonstrating the benefits of high-resolution velocity time series for understanding surge dynamics.

FIGURE 4

FIGURE 5

Since 2014, the density of ice velocity observations has significantly increased primarily due to the simultaneous orbits of Sentinel-1, Sentinel-2, Landsat 8 and Landsat 9, leading to several global open access databases (Friedl et al., 2021; Lei et al., 2022; Gardner et al., 2025). The velocity time series in Figure 4 is taken from ITS_LIVE and demonstrates the simplicity of tracking large surges in near real-time. The dense time series of ice velocity measurements in Svalbard has led to the development of automated anomaly detection methods for surge identification (Koch et al., 2023). The higher temporal resolution also enables tracking of surge dynamics in more detail, such as the impact of seasonal ice flow variations which may be imprinted on the surge velocity pattern (Benn et al., 2022). These observations have been used to test glacier surge theories (Benn et al., 2019b) and assess drivers of surges (e.g., Sevestre et al., 2018), aiding advancement towards a general theory of surge behaviour. However, these methods encounter difficulties when detecting anomalous flow patterns on smaller valley glaciers where flow rates are typically much slower. The surge of Scheelebreen (Figure 4b) is somewhat of an anomaly, as it is a glacier flowing into a small, narrow valley yet experienced a rapid acceleration from 0.5 m/d to ~9.5 m/d in a short time period when measured by ITS_LIVE, although velocity mapping from higher resolution SAR imagery suggests its velocity reached 30 m/d at its peak.

Surges typically lead to pervasive surface crevassing due to the high strain rates induced by the sudden discharge of ice down-glacier. This leads to a change in surface texture which is visible between satellite images taken before and during a surge and is particularly pronounced in SAR imagery as the heavy crevassing increases surface roughness and consequently radar backscatter (Figure 6). Leclercq et al. (2021) found that by differencing SAR imagery between 2018 and 2019, locations of increases in radar backscatter can be related to surge activity. They identified 11 ongoing surges in Svalbard using this approach. Käab et al. (2023) extended this analysis to between 2017

383 and 2022, enabling detection of 26 surges in Svalbard during this time period, thus more than doubling
384 the initial estimate by Leclercq et al. (2021). The extension of this technique to other satellite time
385 series (e.g. ERS-1/2, JERS-1, ENVISAT, ALOS-1, RADARSAT-2) is expected to yield even further
386 information on historical glacier surges. While texture changes in optical imagery have not yet been
387 explored in Svalbard, they hold potential as a tool for monitoring and detecting glacier surges (Trantow
388 and Herzfeld, 2018).

389 **FIGURE 6**

390 Whilst the velocities can be used to track ice discharge and frontal ablation (Dunse et al., 2015;
391 Luckman et al., 2015), glacier mass balance requires mapping of volume changes associated with a
392 surge (Figure 7). Ice accumulates in the reservoir zone during quiescence but is redistributed down-
393 glacier during a surge, leading to increased thinning at high elevation and thickening at low elevation,
394 often with an advance of the terminus. Long-term changes in Svalbard's ice volume can be readily
395 quantified by differencing a modern-day digital elevation model (DEM) with a 1930s DEM generated
396 from historical aerial photographs (Geyman et al., 2022; Mannerfelt et al., 2024; see section 3.3). DEM
397 differencing has been used to measure ice build-up before a surge and the subsequent transfer of
398 mass down-glacier towards the margin (Sund et al., 2009; Murray et al., 2012; Sevestre et al., 2018).
399 Longer time series of surge activity has been developed from historical maps created by explorers in
400 the 1900s (Melvold and Hagen, 1998; Ottesen et al., 2008), but these are of lower quality compared to
401 modern-day sensing systems.

402 **FIGURE 7**

403 Similar to the velocity data, surface elevation mapping of surging glaciers in Svalbard increased
404 significantly after 2000 with the availability of repeat stereoscopic satellite imagery (ASTER,
405 ArcticDEM), laser altimeters (ICESat, ICESat-2) and radar altimeters (CryoSat-2, ENVISAT). ASTER
406 has a revisit period of 16 days and can be used for detailed analysis of geometric changes during a
407 surge. Nuth et al. (2019) used ASTER stereoscopic pairs with 2-4 year intervals to map the geometric
408 evolution of the Nathorstbreen system during its multiple phases of surge activity and compared it to
409 earlier DEMs from 1936 and 1990. This long-term elevation mapping has been used by other studies
410 (Sund et al., 2009; Rolstad et al., 1997; Sund et al., 2014; Sevestre et al., 2018) and has revealed the
411 mass redistribution resulting from a surge. Coarser resolution CryoSat-2 data has been instrumental in
412 acquiring Svalbard-wide elevation changes and has been used to quantify the mass loss of the large
413 Basin-3 surge in Austfonna (McMillan et al., 2014; Morris et al., 2020). However, the 500 m resolution
414 of CryoSat-2 products inhibits quantification of volume changes on smaller glaciers. More recently, the
415 release of 2 m resolution ArcticDEM data has been used to assess elevation changes alongside other

416 DEMs from ASTER and Tandem-X (Figure 7; Haga et al., 2020; Kavan et al., 2022). Since 2003,
417 regional surface elevation maps have been available covering the entire archipelago and derived from
418 ICESat (Nuth et al., 2010), CryoSat-2 (Morris et al., 2020) and more recently ICESat-2 (Sochor et al.,
419 2021). Although these do not specifically target the detection of surges and are generally coarser
420 compared to ASTER, aerial photos and ArcticDEMs, the measurements have high temporal resolution
421 and enable detailed mapping of elevation changes suitable for monitoring geometric changes of
422 glaciers during a surge. Combined with similar repositories of terminus changes (Li et al., 2024; 2025),
423 mass balance can be quantified and the impact of surges assessed, but this remains to be analysed
424 fully. The multi-modal elevation data sets can be used to generate a coarse time series of geometric
425 changes during surge activity after 2000, but large gaps further back in time hinder more detailed
426 understanding of past surge activity.

427 EO monitoring of surges in Svalbard has transformed our understanding of their distribution, scales
428 and dynamics, relationship to mass balance, and detection capabilities, but these methods struggle to
429 observe surge dynamics of smaller glaciers with lower ice fluxes. Small satellite constellations (e.g.
430 ICEYE, Planet, Capella) might fill this gap in the observational pyramid but this requires financial
431 investment (the data is not free to use) and the development of new computational tools.

432 **3.3. Airborne remote sensing**

433 Aerial images using crewed aircraft are a crucial tool for surge identification, which has previously
434 been adopted to show an apparent variable surge frequency on the archipelago (Dowdeswell et al.,
435 1995). Aerial image campaigns by the Norwegian Polar Institute started in 1936 (Geyman et al., 2022)
436 and have since been performed in recurring intervals of at most 30 years, with the most notable
437 campaigns near the years 1960, 1990 and 2009/2011, accompanied by sporadic campaigns of
438 smaller extent in between. Using photogrammetric techniques, these aerial images can be used to
439 generate DEMs, enabling the quantification of almost 100 years of ice volume changes across
440 Svalbard. In particular, the 1930s aerial images and DEM (Geyman et al., 2022; Mannerfelt et al.,
441 2024) act as a baseline data set from which to compare glacier geometry changes. They have also
442 been utilised in more detailed studies to derive terminus positions and volume changes for discussing
443 surge incidence (e.g., Ottesen et al., 2008, Lovell et al., 2018b, Mannerfelt et al., 2024). However, the
444 infrequent repetition interval of about 30 years means that many smaller events are missed altogether,
445 and even large surges could occur in between without the possibility to detect them with certainty. This
446 leads to a temporal bias, especially in inland regions, in detecting surges around these acquisition
447 dates. In addition, a DEM generated from 1990s aerial imagery also offers a baseline year to study
448 surge activity (Rolstad et al., 1997; King et al., 2016) but is likely to miss surges with small ice fluxes.

449 Instead, some glaciers have been mapped during dedicated airborne field campaigns, such as
450 Fridtjovbreen before and after its surge in the 1990s (Murray et al., 2012) and Finsterwalderbreen
451 during quiescence (Nuttall et al., 1997), enabling a better understanding of geometric changes as a
452 surge cycle evolves. More recently, there have numerous airborne flights covering smaller regions in
453 Svalbard, including: hyperspectral surveys using the Dornier aircraft in 2020 ([https://sios-](https://sios-svalbard.org/AirborneRS)
454 [svalbard.org/AirborneRS](https://sios-svalbard.org/AirborneRS)) and 2021 (https://sios-svalbard.org/AirborneRS_Call2021), sea ice surveys
455 by the Alfred Wegener Institute (AWI) that also covered glaciers in Svalbard (Haas et al., 2023; Kolar
456 et al., 2025), and opportunistic flights using a helicopter (e.g. Girod et al., 2017). Compiling available
457 airborne data covering Svalbard surge-type glaciers would generate a useful data set to fill gaps in
458 satellite time series.

459 **3.4. Close-range sensing**

460 Satellite sensors can detect large-scale patterns in glacier surge activity in Svalbard, but close-range
461 sensors are required to capture detailed surface processes associated with a surge such as iceberg
462 calving, surface melt, and flow patterns. Terrestrial laser scanners (TLS), surface-mapping radars,
463 such as the GAMMA Portable Radar Interferometer (GPRI) (Werner et al., 2008; Strozzi et al., 2017)
464 and millimetre-wave radar (Harcourt et al., 2022), provide high-resolution data but are relatively costly
465 to build. However, UAVs with visible imager payloads and time-lapse cameras are relatively
466 inexpensive, although to date their application to understanding surge behaviour is limited.

467 UAVs have been used to monitor critical aspects of glacier surges with very high spatial resolution
468 (Hann et al., 2021, Hann et al., 2022). Typically relying on Red-Green-Blue (RGB) cameras, UAVs use
469 photogrammetric methods (Smith et al., 2016) to extract DEMs and orthomosaics (Figure 8). These
470 data sets have been used to detect surface elevation changes, flow velocities, calving rates, and the
471 spatial extent and structure of crevasses (e.g. Dachauer et al., 2021 and Karušs et al., 2022).
472 Commercial off-the-shelf multirotor systems (e.g. DJI), are relatively inexpensive and logistically
473 straightforward to deploy. These systems offer valuable data, particularly for short-range surveys over
474 smaller glaciers or discrete areas of interest. More sophisticated UAV platforms, such as fixed-wing
475 and vertical take-off and landing (VTOL) systems, allow for larger-area coverage and more complex
476 mission profiles, often with increased endurance, payload capacity, and autonomy (Solbø & Storvold,
477 2013). However, they come with significant operational challenges, including more complex logistics,
478 specialised training requirements, certification, and permits from the aviation authorities. In general,
479 most UAV operations in Svalbard are also constrained by regulatory restrictions, particularly within
480 national parks or protected areas, which limit deployment without special permits (Hann et al., 2023).

482 The use of TLS for monitoring surges is limited despite showing significant potential for 3D monitoring
483 of tidewater calving fronts (Pettlicki et al., 2015; Köhler et al., 2019). The limited application of this
484 technique may be due to the potential for signal absorption of visible and infrared wavelengths into
485 pure ice, but the rougher surface of a highly crevassed surging glacier may suggest TLS instruments
486 are better suited to monitoring surface conditions during unstable ice flow. Time-lapse photography
487 appears to be the most commonly used close-range sensor for monitoring glacier surges in Svalbard
488 and has been used to generate dense observations of terminus conditions during an active surge
489 (Sund and Eiken, 2010), such as the dynamics between adjacent flow-units during a surge of the
490 Paulabreen system in 2005 (Kristensen and Benn, 2012). For surging glaciers, time-lapse
491 photography is especially useful as it can capture fast and transient changes that are often missed by
492 other monitoring techniques. These advantages also mean surges can be tracked from quiescence to
493 an active surge (Vallot et al., 2018) whilst they may also be employed in a network to track surface
494 melt, iceberg calving and surface flow patterns (How et al., 2017).

495 Close-range sensors are not currently widely used for monitoring the dynamics of glacier surges. A
496 reason for this is the unpredictability of surges and an inability to plan and fund the deployment of
497 close-range sensors during the short time window of a surge. Permanent installations at glacier
498 systems that are known to surge relatively frequently (e.g. Nathorstbreen glacier system, Paulabreen,
499 Tunabreen) or are predicted to surge soon (e.g. Kongsvegen, Edvardbreen) might enhance monitoring
500 efforts. An improved strategy for deploying close-range sensors at surging glaciers is required, e.g. a
501 portable observing system for detailed monitoring of glacier surges.

502 **3.5. Geophysical measurements: surface**

503 Global navigation satellite systems (GNSS) are used to measure 3D surface changes on glaciers over
504 time at specific geographic points. Offering high temporal resolution (seconds) and greater accuracy
505 than satellite measurements, GNSS is particularly effective at detecting subtle movements, such as
506 anomalous flow at the onset of a surge when velocities remain near quiescent levels. This capability
507 proved crucial in identifying the activation of a surge at Basin-3, Austfonna (Figure 9; Dunse et al.,
508 2012; 2015) and is currently being used to study the slow surge initiation at Kongsvegen (Bouchayer
509 et al., 2024). Similarly, Nuttall et al. (1997) measured annual and seasonal velocity variations using
510 stakes on Finsterwalderbreen and detected a reduction in ice flux consistent with mass accumulation
511 in the reservoir zone. GNSS data can also be used to validate satellite measurements of ice velocity
512 and confirm the existence of ice flow acceleration during a surge (Pohjola et al., 2011). GNSS can

513 also track elevation changes associated with surge activity, including the down-glacier progression of
514 a surge bulge. For example, Hodgkins et al. (2007) measured ice accumulation on Finsterwalderbreen
515 during quiescence and subsequent downwasting in the ablation zone, revealing the mass gradient
516 imbalance associated with the quiescent-stage phase of the surge cycle. Similar processes have been
517 observed at Kongsvegen (Eiken et al., 1997; Hagen et al., 2005), highlighting the ability of GPS to
518 bridge the temporal resolution gap left by satellite data.

519 However, the deployment and maintenance of GNSS instruments on surging glaciers is challenging
520 due to their highly deformable and fractured surfaces, often rendering suitable deployment sites
521 inaccessible. Even when successfully installed, GNSS units face significant risks of damage or loss.
522 Similar to other close-range sensing methods, deploying GNSS sensors in advance of a surge
523 requires accurate predictions of surge timing. This may be feasible for glaciers with multiple surge-
524 type tributaries, such as Nathorstbreen or Paulabreen/Bakaninbreen, but logistical and financial
525 constraints make it impractical to cover the entire archipelago. A strategic sampling approach is
526 therefore necessary. Alternatively, internal GNSS data produced from seismic stations or other GNSS-
527 equipped field instruments can provide information about sliding velocity while avoiding the need to
528 install multiple instruments on a surging glacier surface (Gajek et al., 2025), although the positional
529 information has low accuracy.

530 **FIGURE 9**

531 **3.6. Geophysical measurements: subsurface**

532 **3.6.1. Ground-penetrating radar (GPR)**

533 Ground-penetrating radar (GPR) is a non-invasive method that uses low frequency electromagnetic
534 waves to penetrate and image the subsurface. These capabilities make GPR a useful technique for
535 studying surge-type glaciers as changes at the bed are key to understanding glacier evolution
536 throughout a surge cycle (Kamb et al., 1985; Benn et al., 2019a). Land-based GPR systems are
537 usually manually operated, requiring the radar system to be dragged or towed over surfaces (Figure
538 10b). As a result, land-based GPR surveys are relatively slow and can be challenging or dangerous to
539 apply in steep or heavily crevassed areas, particularly during ongoing glacier surges. However, it may
540 be possible if glacier surfaces can be navigated safely, which was the case for the GPR survey of the
541 actively surging Vallåkrabreen in 2022 (Figure 11a). In comparison, airborne GPR systems,
542 traditionally mounted on helicopters, are now increasingly deployed on UAVs (Figure 10a, López et
543 al., 2022), enabling rapid surveys over extensive areas, especially in remote or inaccessible regions.

544 Recently, multi-rotor UAVs have gained popularity for GPR surveys (Jenssen et al., 2024), offering
545 improved flight path precision, denser spatial sampling, and lower operational costs compared to
546 helicopters, albeit with reduced range. However, while effective for large-scale surveys, airborne GPR
547 typically offers lower spatial resolution than land-based methods due to limited spatial sampling and is
548 more reliant on favorable weather conditions. An alternative approach is to deploy an Autonomous
549 phase-sensitive Radio Echo Sounder (ApRES) at a fixed location to measure subtle changes in the
550 distance between the radar and reflective targets (such as ice layers, bedrock, or subglacial water)
551 over time. ApRES has been successfully applied in Antarctica (Kingslake et al., 2014; Lok et al., 2014)
552 and Greenland (Gillet-Chaulet et al., 2011) but has only recently been applied to study glacier surges
553 in Svalbard (Harcourt et al., 2024).

554 **FIGURE 10**

555 Englacial and subglacial scattering of electromagnetic waves is strongly influenced by the glacier
556 thermal regime (Björnsson et al., 1996), with warm ice typically scattering more than cold ice. This is
557 typically driven by ice thickness and pressure melting (Murray et al., 2000), with thick ice over 100 m
558 usually leading to warm basal ice, and thinner ice being cold-based due to conductive heat losses.
559 GPR data has revealed the presence of a basal layer of temperate ice overlain by cold ice in
560 polythermal surge-type glaciers (Ødegård et al., 1992; Björnsson et al., 1996; Sevestre et al., 2015)
561 (Figure 11). At the snout of surge-type glaciers, a cold ice dam extending the full ice thickness can
562 block outflow of subglacial water, although it may be removed through iceberg calving (Sevestre et al.,
563 2015) leading to the presence of warm ice across the whole glacier bed. The thermal regime of
564 Bakaninbreen during and after its 1985-1995 surge was extensively studied with GPR (Murray et al.,
565 1998; 2000; Smith et al., 2002). Murray et al. (2000) interpreted an internal reflecting horizon (IRH)
566 with 60 MHz GPR data acquired at Bakaninbreen to show the position of the surge front where the
567 thermal regime transitioned from warm to cold, which was subsequently confirmed by borehole and
568 seismic data (Murray and Porter, 2001; Smith et al., 2002). The presence of ice lenses below the bed
569 indicated the presence of permafrost-trapped meltwater in a thin ice-bed interface (Murray et al.,
570 2000), from which it was inferred that the slow leakage of water through pores in the permafrost and
571 through fractures in the basal ice was responsible for gradual surge termination. Similar thermal
572 characteristics have been observed at land-terminating surge-type glaciers such as Hørbyebreen
573 (Malecki et al., 2013) and Von Postbreen (Sevestre et al., 2015; Delf et al., 2022). GPR has also been
574 used to uncover changes in thermal conditions associated with surge-like behaviour. Several small
575 valley glaciers that were previously warm-based have been shown to now be predominantly cold-
576 based and frozen to their beds (Hodgkins et al., 1999; Bælum & Benn, 2011; Lovell et al., 2015a;

577 Sevestre et al., 2015), suggesting mass loss has reduced the ability of these smaller glaciers to
578 undergo dynamic ice flow (Mannerfelt et al., 2024).

579 **FIGURE 11**

580 The presence of englacial or subglacial liquid water is similarly important when considering the role of
581 subglacial drainage configurations on surge cycles (Kamb 1987; Fowler et al., 1987). Because
582 meltwater has a different dielectric permittivity compared to ice it can be observed in GPR data as a
583 strong contrast in radar backscatter and be used to infer water accumulations at depth. Barrett et al.
584 (2008) detected distributed scatterers in GPR data at the bed of Bakaninbreen representing the
585 presence of large water bodies. Furthermore, bright reflectors within Von Postbreen were interpreted
586 as small water bodies that stored meltwater all year round (Delf et al., 2022) and often held more
587 water than the bed. Crevasses that form during an active surge will close up during surge termination
588 and quiescence as the glacier decelerates. Meltwater located within the crevasses will refreeze and
589 lead to the formation of superimposed ice layers that can be detected within GPR surveys (Brandt et
590 al., 2008). The detection of such features may indicate the presence of past surge activity.

591 Both land-based and airborne GPR systems can reveal detailed internal structures to reveal past
592 dynamics related to surging (Murray et al., 1998; Woodward et al., 2003) and internal stratigraphy
593 (Dunse et al., 2009; Barzycka et al., 2019; Barzycka et al., 2020). Saturated sediment is squeezed
594 and deformed into basal fractures that open during surges, which can be detected in GPR data
595 (Murray et al., 1998; Woodward et al., 2003; Murray and Booth, 2010; Temminghoff et al., 2019).
596 Linear bands of 'dark' internal layering that were dipping 45° relative to the bed were found in both
597 Bakaninbreen (Murray et al., 1998) and Kongsvegen (Woodward et al., 2003) and interpreted to be
598 sediment thrust faults formed during surging. The presence of debris-rich englacial structures, which
599 are also often exposed at the margins of surge-type glaciers and melt-out to form diagnostic
600 geometrical ridge networks and crevasse-squeeze ridges (Glasser et al., 1998; Lovell et al., 2015b;
601 Lovell and Fleming, 2023), provides strong evidence for past unstable ice flow. These features are
602 particularly useful in determining whether smaller valley glaciers have previously surged (Lovell et al.,
603 2015a; Sevestre et al., 2015) and determining the changing distribution of surging behaviour across
604 the archipelago. The formation of surface crevasses below snow and firn may also be identified using
605 GPR surveys and indicate the initiation of glacier acceleration (Dunse et al., 2015). In addition, the
606 scattering properties of different zones on the glacier (e.g. superimposed ice) can also be used to infer
607 melt and refreezing properties (Langley et al., 2007; 2009), aiding the interpretation of mass build-up
608 and enthalpy production.

609 Importantly, GPR surveys are essential for mapping ice thickness and bedrock topography, both of
610 which are critical for modelling surge-type behaviour (Benn et al., 2019a; Thøgersen et al., 2019).
611 Several studies have mapped subglacial topography in Svalbard (Smith et al., 2002; Saintenoy et al.,
612 2013) and quantified ice volumes (Navarro et al., 2014; Sevestre et al., 2018; Karušs et al., 2022),
613 whilst recent compilations of existing data using ice flow models have improved coverage in recent
614 years (Fürst et al., 2018; van Pelt and Frank, 2025). Furthermore, GPR measurements of the glacier
615 bed may also reveal the lithology of the subglacial environment, which may help to determine the
616 likelihood that a glacier will surge (Jiskoot et al., 1998; Murray and Porter, 2001). Additional GPR
617 surveys of a wider range of glaciers are required to further test the link between surging and bedrock
618 types.

619 Although GPR is a powerful tool for glacier monitoring, challenges remain. Glacier ice is a favorable
620 medium for electromagnetic wave propagation due to its limited number of internal scatterers
621 (Woodward and Burke, 2007). However, surveying actively surging glaciers remains difficult due to the
622 presence of surface crevasses (e.g., Dunse et al., 2015) which significantly hinders land-based
623 access, and attenuates the radar signal and may reduce signal penetration through the surface layers.
624 Furthermore, data resolution remains a key limitation. Due to the physical principles governing wave
625 propagation, a trade-off exists between resolution and depth penetration. For instance, while GPR
626 systems can image the first meters of the subsurface with centimeter-scale resolution, obtaining
627 information from the glacier base requires increasing the signal wavelength and, in turn, reducing the
628 resolution to the meter scale. In temperate ice, scattering bodies necessitate even longer
629 wavelengths, further lowering resolution to meters.

630 Land-based GPR provides high-resolution data with denser and more controlled spatial sampling but
631 is restricted in spatial range and accessibility. Its use is often limited to spring months, when snow
632 cover facilitates faster data acquisition with antennas towed behind snow machines (Figure 10b). In
633 contrast, airborne GPR enables surveys across larger areas regardless of snow cover, but often at
634 lower vertical resolution, as longer wavelengths are commonly used, and spatial sampling is less
635 controlled, particularly with helicopter-mounted systems.

636 Future research should aim to combine these methods to enhance overall data quality and coverage.
637 One promising advancement is spectral GPR, which acquires a wide range of frequencies within a
638 single cycle, effectively integrating the advantages of different frequency antennas into a single device
639 (Dyrda et al., 2023). Additionally, combining GPR data with remote sensing and other geophysical
640 techniques, such as seismic surveys and GNSS measurements, can provide a more comprehensive
641 understanding of glacier surges and their controlling factors.

642 **3.6.2. Seismology**

643 Seismological methods have been used to study glaciers for decades (Crary, 1955; Röthlisberg, 1955;
644 Hatherton & Evison 1962; Weaver & Malone, 1979), including in Svalbard (Lewandowska & Teisseyre,
645 1964; Cichowicz, 1983; Górski & Teisseyre, 1991) and is now recognized as the field of
646 cryoseismology. Seismic instruments like geophones or seismometers are used to record ground
647 shaking. Installing them in the vicinity of, or directly on, glaciers (drilled in the ice, Figure 10d) may
648 provide information about the dynamics of glacier surge processes, particularly processes at the bed.
649 Cryoseismology may complement traditional glaciological observations from fieldwork or remote
650 sensing by operating independently of visibility conditions, including the polar night, providing wide
651 spatial imaging beyond single observation points and achieving high temporal resolution on the sub-
652 second scale (e.g., Bartholomaus et al., 2012). Furthermore, it enables systematic analysis of
653 continuous seismic records from permanent stations, facilitating the study of long-term trends and
654 seasonal patterns of cryo-seismicity over years or even decades (e.g., Köhler et al., 2016; Gajek et al.,
655 2017). Seismological findings can also complement GPR surveys (e.g. Smith et al., 2002) to cross-
656 validate interpretations of subglacial conditions, including surge-related changes at the glacier bed
657 (Zhan, 2019).

658 Short-term and multi-season deployments of seismometers in close proximity to, or directly on,
659 surging glaciers provide detailed insights into various englacial phenomena. For example, analysis of
660 recorded seismic events enable the study of ongoing crevassing by mapping thousands of surface
661 icequakes per day (Mikesell et al., 2012; Walter et al., 2015). Studying basal icequakes has enabled
662 the inference of frictional processes at the glacier bed (Gräff & Walter, 2021), while analysis of shear-
663 wave splitting from the same events has revealed daily expansion and contraction of englacial
664 channels (Gajek et al., 2021). Analysis of long-lasting monochromatic tremors can be used to infer
665 moulin formation (Röösli et al., 2014; Walter et al., 2015) and quantify subglacial discharge
666 (Bartholomaus et al., 2015). In addition, ambient noise can be used, for instance, to observe the
667 development of subglacial channels (Zhan, 2019; Nanni et al., 2020) and provide estimates of
668 subglacial channel geometries and efficiency (Gimbert et al., 2016; Bouchayer et al., 2024).
669 Comprehensive reviews, such as those by Podolskiy & Walter (2016) and Aster & Winberry (2017), as
670 well as the 2019 SESS Report ‘CRYOSEIS’ focusing on cryoseismology in Svalbard (Köhler et al.,
671 2020), illustrate its value as a powerful method for advancing our understanding of glacier surge
672 dynamic processes and measuring englacial and subglacial conditions.

673 Despite its potential, seismological studies of glacier surges are scarce due to the difficulties in
674 deploying instruments on heavily crevassed surging glacier surfaces (Raymond and Malone, 1986),

675 but a few case studies from Svalbard exist. A study of Bakaninbreen (Stuart et al., 2005) identified
676 near-field seismic signals associated with an ongoing surge, while Köhler et al. (2015) observed
677 exceptional far-field surge-related variations in long-term seismic emissions from Tunabreen and
678 Nathorstbreen (Figure 12). At Kongsvegen, the subglacial hydraulic gradient and the radius of the
679 channelized subglacial drainage system were inferred from the power of recorded seismic signals
680 (Bouchayer et al., 2024). Most recently, seismology has been employed to monitor the ongoing surge
681 of Borebreen (Harcourt et al., 2024, Gajek et al., 2025). These examples highlight the importance of
682 seismology in monitoring surge-type glaciers and their driving processes.

683 **FIGURE 12**

684 New technologies, such as Distributed Acoustic Sensing (DAS), which consist of kilometres long fibre-
685 optic cables used as seismic receivers (Figure 10c) offer great potential for surge monitoring. DAS has
686 already proven to be effective in studying icequakes in alpine glaciers (Walter et al., 2020) and
687 Antarctic ice streams (Hudson et al, 2021), providing unprecedented insight into dynamic processes
688 due to the sensor density and spatial sampling down to the metre scale. The first on-ice installation of
689 DAS in Svalbard took place in 2023 on Hansbreen (Gajek et al., 2024), but the potential of DAS for
690 surging glaciers has not been explored yet. Notably, DAS may be installed underwater in the proximity
691 of the terminus enabling insights into calving front dynamics. Another way to install underwater
692 seismic stations is to use Ocean Bottom Seismometers (OBS) which, after being dropped and sunk in
693 the glacial fjord, record seismic waves at a single location at the seabed. Such stations installed close
694 to the terminus are less hazardous to maintain and offer less noisy recordings. Podolskiy et al. (2021)
695 have demonstrated that OBS data may be used to monitor calving rates and to use seismic noise as a
696 proxy for glacial sliding velocity, even when using a single station. The ability of these new techniques
697 to provide high-resolution cryoseismological data, and the potential to use pre-existing fibres (e.g.,
698 ocean bottom telecom cables) suggests they should be seriously considered for future monitoring of
699 surges.

700 **4. Identifying historical and palaeo glacier surges**

701 Reconstructing long-term histories of surging is necessary to help contextualise contemporary surge
702 data. Extending surge records back beyond the remote sensing era relies on two main approaches:
703 investigations of sediment-landform assemblages formed by surges and interrogations of historical
704 observations and archival evidence of surging.

705 The dynamic glacier flow during surges shapes the subglacial and proglacial environment producing
706 sediments and landforms that can be linked to surge processes (Evans and Rea, 1999). Where these
707 sediment-landform assemblages are revealed and preserved during quiescent phase ice stagnation
708 and retreat, they provide diagnostic geomorphological evidence for past surging - often extending far
709 back beyond the observational record (e.g., Flink et al., 2018; Lovell et al., 2018b). This is particularly
710 valuable in Svalbard, where glaciers have often experienced multiple surges that are decades to
711 centuries apart (Dowdeswell et al., 1991), and other glaciers that may have surged in the past but are
712 no longer able to (e.g., Lovell et al., 2015a; Mannerfelt et al., 2024). As a result, geomorphological
713 investigations have helped to identify past surging of many glaciers that have not been directly
714 observed to surge (e.g., Farnsworth et al., 2016; Ottesen et al., 2017; Aradóttir et al., 2019; Ben-
715 Yehoshua et al., 2023; Mannerfelt et al., 2024; Osika and Jania, 2024). These approaches require an
716 understanding of the sediments and landforms associated with surging and typically combines field
717 mapping, visual observations, sediment logs and sample measurements with remote sensing
718 approaches (i.e., mapping using aerial and UAV photography and satellite imagery in a GIS)
719 (Chandler et al., 2018).

720 Geomorphological investigations commonly focus on the best-preserved sediment-landform
721 assemblages. For surge-type glaciers, the clearest evidence is typically associated with a glacier's
722 most-recent surge, particularly in terrestrial settings and where subsequent surges may have erased
723 any landform records of previous surges. For most glaciers that last surged prior to the observational
724 period, it is likely their most-recent surge occurred during or close to the Little Ice Age (LIA) Neoglacial
725 maximum approximately at the end of the 19th/start of the 20th centuries (Mannerfelt et al., 2024).
726 However, where repeated surges have reached successively less-extensive positions, particularly in
727 marine settings, it can be possible to explore preserved sediment-landform assemblages associated
728 with multiple surges (e.g. Ottesen et al., 2008; Flink et al., 2015). Combined with a well-constrained
729 geochronology, this can allow surge timings to be reconstructed beyond the immediate observation
730 period (i.e., during the LIA), further back into the Holocene (e.g., Hald et al., 2001; Kempf et al., 2013;
731 Flink et al., 2017; 2018; Flink and Noormets, 2018; Larsen et al., 2018; Lovell et al., 2018b; Lyså et al.,
732 2018; Streuff et al., 2018), and can even allow surge-like behaviour of ice streams within the Barents
733 Sea Ice Sheet during the glaciation to be identified (e.g., Andreassen et al., 2014; Bjarnadóttir et al.,
734 2014; Kurjanski et al., 2019). Sedimentary archives recorded in proglacial lakes have significant
735 potential to provide insights on past surging of land-terminating glaciers (e.g., Striberger et al., 2011;
736 Larsen et al., 2015). In Svalbard, such records have allowed glacier dynamics to be reconstructed
737 (e.g., Røthe et al., 2015) but are yet to be directly linked to surging. This represents an exciting
738 avenue for future research.

739 **4.1. The surging glacier landsystem**

740 The sediments and landforms associated with surging have been documented in both terrestrial and
741 marine settings in Svalbard (Ottesen and Dowdeswell, 2006; Ottesen et al., 2008, 2017; Flink et al.,
742 2015; Streuff et al., 2015; Farnsworth et al., 2016; Lovell et al., 2018a,b; Osika and Jania, 2024;
743 McCerery et al., 2025). To interpret these landscapes, Svalbard scientists, as elsewhere, typically
744 employ a 'landsystems' approach (Figures 13 and 14). This concept seeks to identify, describe, and
745 interpret the diverse range of sediments and landforms observed in glacial environments to
746 reconstruct processes and thus the dynamics of the ice that previously covered the terrain (cf. Evans,
747 2005; Evans and Rea, 1999). Unlike other glacial environments, where changes may occur gradually
748 over time, surging glaciers produce rapid, extensive modifications to the landscape that leave behind a
749 specific suite of landforms. Surging glacier landsystems are most accessible in terrestrial settings
750 (Figure 15), which can be investigated in the field and from remote imagery, but preservation of
751 features can be heavily impacted by fluvial and gravitational reworking processes during ice
752 stagnation. In contrast, landforms associated with marine-terminating glacier surges are often
753 excellently preserved on the seafloor (Figure 16), but analysis of these is reliant on the availability of
754 high-resolution bathymetry data (Ottesen and Dowdeswell, 2006; Ottesen et al., 2017). However, in
755 most cases, marine-terminating glacier surges also leave behind landform evidence on the adjacent
756 terrestrial fjord margins that can be utilised instead (Bennett et al., 1996; Lovell et al., 2018b).

757 **Figure 13 Terrestrial Landsystem**

758 **Figure 14 Marine Landsystem**

759 **FIGURE 15 Terrestrial landforms**

760 **FIGURE 16 Marine landforms**

761 **4.2. Key components of the surging glacier landsystem**

762 Glaciotectonic moraines: In Svalbard, the maximum extent of a surge is sometimes delineated by a
763 large moraine system (Croot, 1988; Boulton et al., 1999; Lovell and Boston, 2017; Ottesen et al.,
764 2017). These are most common in a marine setting, where they typically have a low-gradient debris
765 flow lobe extending from the distal flank (e.g. Ottesen and Dowdeswell, 2006; Flink et al., 2015;
766 Ottesen et al., 2017; Aradóttir et al., 2019) (Figure 13C). In terrestrial settings, the moraine systems
767 often have multiple ridge crests, forming complexes known as composite ridge systems (Croot, 1988;
768 Hart and Watts, 1997; Boulton et al., 1999; Lovell and Boston, 2017; Lovell et al., 2018a) (Figure

769 15a;b). These features have also been referred to as 'push moraines/complexes', although these
770 terms can be ambiguous since they are employed for a broad range of landforms at various scales. In
771 both terrestrial and marine settings, these moraine systems are formed by glaciotectonic deformation
772 as the glacier advances rapidly into unconsolidated sediment in the proglacial zone.

773 Crevasse-squeeze ridges (CSRs): CSRs form when highly-saturated, deformable subglacial sediment
774 is squeezed into a highly fractured glacier base (Evans and Rea, 1999; Rea and Evans, 2011). During
775 recession, CSRs melt out in situ to form a system of cross-cutting ridges composed of diamicton that
776 are typically aligned transverse or subparallel (i.e., 40-60°) to ice-flow, mimicking surface crevasse
777 patterns (Figure 15c;d). During the early parts of the quiescent phase following a surge, CSRs can
778 often be observed emerging from crevasses in terrestrial settings. The required conditions for their
779 formation are (1) a saturated subglacial environment, (2) a glacier base fractured by extensive ice
780 flow, and (3) ice mass stagnation following the surge in order to promote their preservation, making
781 CSRs arguably the most diagnostic landform evidence for surging (Farnsworth et al., 2016). CSRs are
782 found in both terrestrial and submarine settings (Figures 15c;d and 16b) and have been studied
783 extensively in Svalbard (e.g., Bennett et al., 1996; Boulton et al., 1996; Woodward et al., 2002; 2003;
784 Rea and Evans, 2011; Flink et al., 2015; Lovell et al., 2015b; Farnsworth et al., 2016; Ben-Yehoshua
785 et al., 2023, Osika and Jania, 2024). They form a key line of evidence for identifying past surges when
786 there is no direct observational data (e.g., Farnsworth et al., 2016; Ben-Yehoshua et al., 2023).
787 Because CSRs form beneath surging glaciers, in situ geotechnical measurements could provide a
788 valuable data set on stresses and strains in the subglacial environment right before the stagnation of
789 surges.

790 Flutes: Flutes are streamlined ridges of sediment formed subglacially and are often found in front of
791 surging glaciers in Svalbard, both in terrestrial and marine settings (Figures 15e and 16a). Their
792 formation during surges is associated with rapid advance causing flow-parallel deformation of the
793 underlying basal sediments. In marine settings they can be over 1 km in length (e.g., Borebukta,
794 Ottesen and Dowdeswell, 2006). Flutes often form in a close geomorphological association with
795 CSRs, with both forming in the subglacial environment (e.g., Christoffersen et al., 2005).

796 Eskers: Eskers are sinuous ridges of sand and gravel that form in channelised subglacial or englacial
797 meltwater systems, which can be preserved in the foreland during glacier retreat. Their formation is
798 not uniquely linked to surging, but eskers are often found as part of the Svalbard surging landsystem
799 (e.g., McCerery et al., 2024; 2025). In some cases, geometrical ridge networks similar to CSRs but
800 composed of sand and gravels have been reported (Evans et al., 2022) (Figure 15f). These likely
801 reflect pressurised meltwater exploiting the heavily fractured glacier towards the end of a surge and

are probably similar to 'zig-zag' or 'concertina' eskers reported from some surging glacier forelands in Iceland (Evans and Rea, 1999). Morphologically, such eskers are hard to distinguish from CSR networks without detailed sedimentological investigations. Large sinuous seafloor eskers are often revealed during quiescent-phase retreat of marine-terminating eskers (e.g., Ottesen et al., 2008, 2017).

Quiescent phase stagnation and retreat: Most landforms associated with surging form during the active phase due to the combination of fast ice flow, frontal advance and a highly saturated glacier bed. The geomorphological signature of the quiescent phase is typically less diagnostic of surging but can still be identified. In terrestrial settings, the cessation of surging leads to widespread stagnation and subaerial downwasting of the over-extended glacier front. Surging glaciers often transport large volumes of debris, creating extensive areas of ice-stagnation topography in the form of ice-cored hummocky moraine (e.g., Schomacker and Kjaer, 2008). Debris flows and kettle holes are common as buried ice degrades over time, which, together with extensive glaciofluvial erosion, can impact the preservation of landforms such as CSRs and flutes. At tidewater surging glaciers, annual retreat moraines can form on the seafloor during quiescent phase retreat (e.g., Ottesen and Dowdeswell, 2006; Flink et al., 2015) (Figure 16d), whilst subaerial stagnation terrain will likely be common along their terrestrial fjord margins (e.g. Lovell et al., 2018b).

4.3. Historical observations and archival evidence for surging

Nineteenth and early 20th century expeditions to Svalbard produced a wealth of maps, photographs and written observations (e.g., Hamberg, 1894; Conway, 1897; Gregory et al., 1897; Garwood and Gregory, 1898; Hoel, 1914; Gripp, 1929), which both directly and indirectly provide an important insight into the state of glaciers at that time. The end of the 18th century featured substantial improvements in topographic mapping techniques (Holmlund and Martinsson, 2016), meaning the geographical accuracy of maps became reliable enough for intercomparisons. In some cases, maps, qualitative observations, and subsequently photographs, strongly suggest that glaciers were actively surging. For example, one of the first reliable sources of a surge was by the 1838 French La Recherche Expedition, who painted the glacier Recherchebreen as extensively crevassed and mapped its terminus to an extent that far exceeded both previous and subsequent maps and is corroborated by modern observations of a submerged moraine (Zagórski et al., 2023). Other events such as the ~1908 surge of Wahlenbergbreen was captured through repeated mapping campaigns showing a ~6.6 km advance between 1896 and 1908 (Figure 17), with accompanying photographs detailing its highly crevassed surface (de Geer, 1910). While these unique data points are useful for historical accounts of surging, they are strongly biased towards large events along the coast. The

835 quality of these historical maps and observations prohibits the detection of small (<1km) scale events,
836 and most studies were carried out from a ship, with very few exceptions to this rule.

837 **FIGURE 17**

838 One of the only historical sources of non-coastal observations is from the Conway Expedition of 1896
839 crossing of Spitsbergen (Conway 1897, Gregory et al., 1897, Garwood and Gregory, 1898). They
840 walked eastward from Adventalen (where Longyearbyen has since been established) and
841 photographed “Booming Glacier” (today Drønbreen), noting its “aggressive front” (Figure 18; Gregory
842 et al., 1897). They also passed other glaciers such as Rieperbreen, Foxbreen, Ayerbreen and Scott
843 Turnerbreen and provided observational and photographic leads to infer the ongoing or imminent
844 surges (Mannerfelt et al., 2024). Additional Norwegian photography and mapping campaigns between
845 1906 and 1928 yield further potential for detecting inland surges (Figure 18d), but not all of these
846 thousands of archived photographs have been analysed and published. Photographic and
847 observational evidence is invaluable for further understanding the past dynamics of terrestrial glaciers
848 in Svalbard, but information is sparsely distributed along the path of the associated expeditions,
849 leading to the need for extrapolation to establish a wider picture.

850 **FIGURE 18**

851 **5. Svalbard surge-type glacier database**

852 **5.1. Database structure**

853 We have developed a new database of surge-type glaciers in Svalbard (Harcourt et al., 2025b) by
854 combining existing compilations and reviewing studies examining surge dynamics, many of which
855 have been discussed in the previous sections. Through this literature review we have documented
856 where they exist, years of surge onset and termination, active and quiescent velocities, and terminus
857 changes. We record these characteristics using the RGI 7.0 digital glacier database (RGI 7.0
858 Consortium, 2023). Observations of surges are generally limited to the period ~1850-2025 (time of
859 writing), which broadly corresponds to the end of the LIA through to the present, but some palaeo-
860 glaciological evidence for surging may relate to activity occurring prior to this.

861 Our compilation of existing Svalbard-wide glacier surge databases is sourced from several studies:
862 Lefauconnier and Hagen (1991) [LH1991]; Hagen et al. (1993) [H1993]; Sevestre and Benn (2015)
863 [SB2015]; Farnsworth et al. (2016) [F2016]; Kääb et al. (2023) [KA2023]; and Koch et al. (2023)
864 [KO2023]. The compilation of LH1991 only covers eastern Svalbard and mostly focuses on marine-

terminating glaciers but is included as it contains details on surge characteristics. H1993 is the original database of glaciers across Svalbard and similarly contains details of historical surges. The current RGI 7.0 database defines the 'surge status' of each glacier according to Sevestre and Benn (2015): (0) no evidence of surging; (1) possible surge, (2) probable surge, and (3) observed surge. Most of the evidence for surge behaviour in this database has been verified through independent studies. The F2016 compilation was manually translated into the RGI 7.0 database. The glacier names described in F2016 often referred to tributaries which are now combined into single glacier catchments (e.g. Nuddbreen / Strongbreen), hence we manually combined these entries. The recent compilations from KA2023 and KO2023 were manually transcribed from tables in PDF files.

The KA2023 data are based on manual surge identification from annual Sentinel-1 interferometric wide-swath (IW) satellite radar backscatter differences between 2017 and 2022 (Kääb et al. 2023). For the present review we updated the data by mapping more recent surges from winter-to-winter differences 2022-2023, 2023-2024, and 2024-2025 using new IW data. Before 2017, we use 2015-2016 and 2016-2017 extended wide-swath (EW) data instead, acknowledging that these coarser data (compared to IW) might lead to less detailed surge identification, or overlooking of surges of small glaciers or surges accompanied by only limited backscatter changes. Based on these additional data, we are also able to update some surge information contained in the original KA2023, for instance concerning surge start and end years, and by adding the last year of strongly enhanced backscatter (before backscatter reduction). The new 2015-2025 backscatter-derived surge inventory over Svalbard now contains 39 surging glaciers (the 2017-2022 KA2023 contained 26 surging glaciers).

We complement these compilations with our own literature review to generate the most comprehensive database of surge-type glaciers in Svalbard. In the following sections, we provide details of the new database and compare it to existing compilations.

5.2. Directly observed surges

Direct observations of glacier surges are defined here as those where studies have presented evidence of glacier velocity changes an order of magnitude above quiescence, surface changes (e.g. heavy crevassing), large iceberg production in imagery, ice mass redistribution as detected through surface elevation changes, or inferred clear evidence of terminus advance from modern imagery or historical maps. Glaciers which have both accelerated (e.g. Sveabreen, Esmarkbreen) and have demonstrable evidence of surging in the past (e.g. presence of CSRs in their foreland) are considered to have been directly observed to surge. Of the compilations used here, only the F2016 database is not used as it infers surges from the landform record. A total of 138 surges have been directly

897 observed in Svalbard (Lefauconnier and Hagen, 1991; Hagen et al., 1993; Sund et al., 2009; Kääb et
898 al., 2023; Koch et al., 2023), which accounts for 9% of all glaciers (Table 1). Of these directly
899 observed surges, 61% are marine-terminating (Table 1). Figure 19 shows the spatial distribution of the
900 directly observed surges. Most of the direct observations cover glaciers with large catchments,
901 particularly where they terminate into the ocean. Dynamical changes on large glaciers can be more
902 easily detected using satellite data and historical imagery, whilst a large advance of a marine-
903 terminating glacier can increase iceberg production which can be detected in historical imagery (e.g.
904 Lefauconnier and Hagen, 1991). Surges on smaller glaciers (e.g. <1 km²) have generally not been
905 detected, especially across Andrée Land (Figure 19b) and Nordenskiöld land (Figure 19c). This may
906 be due to the inability of a smaller glacier to discharge large volumes of ice over a short period of time
907 but could also be due to an inability of current sensing systems to detect lower magnitude changes in
908 velocity or surface elevation. Many direct observations come from historical records (Lefauconnier and
909 Hagen, 1991; Hagen et al., 1993) and were biased towards the eastern margins of the archipelago
910 due to interests in calving glaciers and their impact on offshore structures and shipping routes. Direct
911 observations of historical surges are mostly based on archival aerial imagery and identifying known
912 features of surges (e.g. crevassing, steep surface slopes), whilst after the 1990s satellite
913 measurements have mostly been used due to improvements in mapping glacier velocity changes and
914 terminus advances during a surge. The reliance on these methods likely means smaller surges are
915 missed from this compilation.

916 **FIGURE 19**

917 **TABLE 1**

918 **5.3. Indirectly observed surges**

919 Glacier surges interpreted from the landform record or historical maps (see section 4.3) are classified
920 as ‘indirectly observed surges’. Here, we do not differentiate between ‘possible’ and ‘probable’ surge-
921 type glaciers as used by Sevestre and Benn (2015) and the current RGI7.0 database to avoid
922 potential subjectivity in our database. Here, most evidence is taken from the F2016 database
923 (Farnsworth et al., 2016) although there are several additional studies which have detected surges at
924 outlets not mentioned in Farnsworth et al. (2016) (Sund et al., 2009; Robinson and Dowdeswell, 2011;
925 Flink et al., 2018). We have identified a total of 535 glaciers with evidence of past surging behaviour,
926 representing 34% of all glaciers in Svalbard. This is undoubtedly an underestimate, as Farnsworth et
927 al. (2016) focused on the terrestrial landform record and therefore did not explore marine-terminating
928 glacier forefields, such as several of the outlets in Austfonna, Vestfonna and Kvitøkjökulen. Strikingly,

929 many glaciers never previously considered to be surge-type contain CSRs in their foreland,
930 suggesting these glaciers may have very long quiescent periods towards the upper end of the
931 spectrum in Svalbard (e.g. over 150 years) or have lost the ability to surge. This includes glaciers with
932 long-term observational records (e.g. Kronebreen, Nordenskiöldbreen) which have explicitly been
933 categorised as not surge-type (e.g. Błaszczyk et al., 2021; Kavan et al., 2024). Until recently,
934 Hansbreen in southern Spitsbergen was also not considered to be surge-type, but archival
935 photographs and geomorphological mapping now suggests it underwent a surge in the late 1800s
936 (Osika and Jania, 2024). Furthermore, 20% (n = 108) of the glaciers with past evidence for surging
937 (indirect) have been directly observed to surge. This finding suggests that we will uncover more
938 evidence for glacier surges across the archipelago as we continue to study glacier dynamics in
939 Svalbard.

940 The larger number of surge-type glaciers identified through indirect evidence increases the spatial
941 coverage of surge-type glaciers across Svalbard (Figure 20). Many smaller glaciers across Andrée
942 Land and Nordenskiöld Land have evidence of past surge behaviour, particularly through the
943 presence of CSRs in their foreland. The dynamics of these smaller glaciers is difficult to monitor using
944 satellite methods and so geomorphological evidence for past unstable ice flow is usually the only way
945 to detect past surges. Figure 20 demonstrates that many smaller glaciers across the large ice fields of
946 Spitsbergen in the northwest, northeast and south have evidence for past surge behaviour. Direct
947 evidence for surging has mostly been found on the eastern edges of these three subregions. In
948 comparison, past evidence for surging extends from these eastern regions to the warmer Atlantic side
949 along the west coast of Spitsbergen, and also across Ny-Friesland. There is a distinct lack of
950 geomorphological evidence for surging across the northeast of Svalbard which is likely due to the
951 sparse bathymetry data available to analyse submarine glacial landforms and confirm the presence of
952 past fast flow related to a surge, whilst the geology of this region is also different which may alter
953 surge behaviour as well as CSR formation through differences in sediment supply. Although these
954 observational gaps are being filled through the acquisition of new bathymetric data (e.g. Flink et al.,
955 2018), more surveys are needed to increase spatial coverage in this area and also around Kvitøya.
956 We find that 22% (n = 30) of glaciers directly observed to surge do not have evidence for past surge
957 behaviour. This is most likely due to scarce observations rather than the behaviour representing a
958 different type of flow regime other than a surge, although this remains to be tested. For example, there
959 was no evidence to suggest Monacobreen was a surge-type glacier before its surge in the 1990s
960 (Murray et al., 2003a). Given that our time series only extends back to 1800, and robust evidence for
961 surging is only available since the availability of 1930s aerial imagery, we expect many glaciers
962 previously not identified as surge-type due to lack of indirect evidence to initiate fast flow in the coming
963 years. Finally, we strongly encourage further studies to test the Farnsworth et al. (2016) interpretation

964 of CSR landforms and understand past surge behaviour across the archipelago. Recent studies (e.g.
965 Mannerfelt et al., 2024) are beginning to fill this knowledge and observational gap.

966 **FIGURE 20**

967 **5.4. All surges**

968 Compiling both the direct and indirect databases together, we estimate that 36% (n=565) of glaciers in
969 Svalbard are surge-type. We note here that if a glacier has been both ‘directly’ (e.g. velocity changes)
970 and ‘indirectly’ (e.g. through the presence of CSRs) observed to surge, it is only counted once in the
971 ‘All Surges’ category. Of these glaciers, 24% are marine-terminating and the other 76% are land-
972 terminating (Table 1). In comparison to the entire population of Svalbard glaciers, 12% are marine-
973 terminating and 88% are land-terminating. Figure 21 shows the spatial distribution of surge-type
974 glaciers across Svalbard. The ice fields in northwest, northeast and south Spitsbergen contain several
975 large glacier catchments many of which have exhibited surge behaviour, with only a collection of
976 outlets showing no evidence of past surge behaviour. Regions with many small valley glaciers (Figure
977 21b and 21c) generally have fewer surge-type glaciers but as discussed previously, this pattern may
978 be due to slower dynamics related to surge behaviour with lower ice fluxes that are difficult to detect in
979 historical archives, palaeo-glaciological landforms and modern-day sensing systems. Surge
980 observations in Vestfonna and Austfonna are more limited, most likely due to fewer in situ
981 observations of palaeo-glaciological landforms on the seafloor. We expect that several of the outlets
982 from both ice caps may surge in the future given the past history of surging in the region (Robinson
983 and Dowdeswell, 2011). Finally, there appears to be little evidence for glacier surges across the
984 western coast of Albert I Land in northwest Spitsbergen despite there being several large tidewater
985 glaciers in this region (e.g. Raudfjordbreen, Smeerenburgbreen, Svitjodbreen). Larusbreen, a small
986 glacier in this region that terminates partially on land and in the ocean, was heavily crevassed in 2016
987 and partially advanced which might suggest it was surging but further work, e.g. by mapping velocity
988 changes is required to confirm this. Although the absence of published evidence for glacier surges
989 does not mean a glacier cannot exhibit this type of behaviour, future work should target these less
990 studied regions for studies of past and more recent surging behaviour.

991 **FIGURE 21**

992 There is theoretical basis to assume that glaciers with a surface area below 1 km² may be unable to
993 build up the mass required for a surge. Moreover, they are thin (Bahr et al., 2015) which typically
994 means they are cold-based due to conductive heat losses and, therefore, cannot build up enthalpy at
995 the glacier bed to initiate fast flow. There are 987 glaciers larger than 1 km² in Svalbard and 511 of

these have been classified as surge-type in our database. Therefore, 52% (n=511) of all glaciers larger than 1 km² have demonstrable evidence of surging behaviour. Likewise, half of the glaciers in Svalbard that have the potential to surge have done so since 1800. As mentioned previously, we expect this number to increase as our measurements of past surges improves through new studies of past geomorphological evidence and archival material. Furthermore, 54 glaciers with a surface area smaller than 1 km² were found to be surge-type in our compilation. Some of these are former tributaries of larger surge-type glaciers (e.g. Esmarkbreen, Wahlenbergbreen) or once formed part of a larger lobe (e.g. Smaubreen-Berrklettreen-Vallotbreen). However, there are some isolated valley glaciers such as Meyerbreen and Purpurbreen in Andrée Land, Dumskoltbreen in Sørkapp Land, and Saksbreen in Wedel Jarlsberg Land which have CSRs present in their foreland (Farnsworth et al., 2016) and are therefore likely to have surged in the past. This suggests that small valley glaciers in Svalbard have previously been able to surge and may be undergoing very long quiescence periods and their active surge is yet to be observed. Alternatively, these smaller valley glaciers may have surged in the past when they were larger but are now unable to due to excessive thinning leading to a thermal regime switch to predominantly cold-based (Mannerfelt et al., 2024). For example, it has been suggested that Midtre Lovénbreen transitioned to a non surging state due to a prolonged period of negative mass balance which inhibited sliding due to the presence of cold-based ice at its bed (Hansen, 2003). The physical relationship between glacier size, thermal regime and surging potential, alongside the relative importance of thinning and meltwater production (e.g. Nuth et al., 2019) over time has not yet been tested and requires further study.

5.5. Characteristics of Svalbard surges

It has been suggested that surge-type glaciers in Svalbard have different characteristics from their non-surging counterparts (e.g. Jiskoot et al., 1998; 2000; Bouchayer et al. 2022). Here, we compare our new database of surge-type glaciers in Svalbard with glacier characteristics from the RGI7.0 database (Figure 22). We choose to compare six characteristics available in the RGI7.0 database (e.g. area, elevation range, mean elevation, slope, length, aspect) that have previously been suggested to influence a glacier's ability to surge (Jiskoot et al., 1998; 2000; Bouchayer et al. 2022). We note that we are comparing glaciers with evidence of surging behaviour with the entire list of glaciers in Svalbard, many of which may be surge-type but with no demonstrable evidence. Therefore, this analysis may be more accurately described as a comparison between glaciers with a higher probability of surging compared to those in long quiescent phases that may or may not be surge-type. We find that the average elevation range, slope and length (Figures 22b, d, and e) differs between surge and non-surge-type glaciers. This means that surge-type glaciers have gentler slopes, are generally longer, and extend across a larger elevation range, as has been suggested before (e.g.

Jiskoot et al., 1998; 2000; Bouchayer et al. 2022). It would suggest that the lower slopes precondition glaciers to accumulate more ice. The fact that it occurs over a larger elevation range (hypsometry) might suggest that these glaciers can also reach elevations cold enough to maintain that accumulation. We also find, quantitatively, that surge-type glaciers tend to be larger (Figure 22a), which is consistent with the notion that temperate conditions at the glacier bed can only be sustained through thick ice to avoid conductive heat losses. However, there may be an element of bias due to our ability to more easily observe surges of larger glaciers both now and in the past. Finally, we find no clear relationship between surge classification and both aspect and mean elevation (Figures 22f).

FIGURE 22

Variations in the spatial distribution of Svalbard surges over time is shown in Figure 23. We note that several surges in the historical record have not been accurately dated and there may be errors. We split the time series into three time steps: the LIA maximum (1800-1930), post-LIA warming (1930-2000), and the dense contemporary observational period (2000-2025). During these time periods, we have identified 57 (1800-1930), 80 (1930-2000), and 52 (2000-2025) observed surges. This equates to 0.44 (1800-1930), 1.16 (1930-2000), and 2.1 (2000-2025) surges per year. The greater number of surges per year identified since 2000 likely reflects the denser range of observations available from satellite data. The fewer observations before 1930 similarly probably reflects our reliance on historical archives and geomorphological analyses. Some glaciers, such as Bodleybreen, are likely to have experienced more than once surge during the Holocene (Flink et al., 2017) but it is currently not possible to date these historical surges. Therefore, whilst the spatial and temporal variability likely reflects limitations in our current observational capacities, we can draw some early conclusions from their patterns.

FIGURE 23

The spatial distribution of identified surges is remarkably similar over the three time periods with evident clusters in Oscar II Land and Olav V Land where there are glacier surges present in all three epochs. These two regions are dominated by large surges e.g. Negribreen in Olav V Land. There was a cluster of surges in northwest Isfjorden in both 1800-1930 and 2000-2025 and their apparent synchronicity might suggest their behaviour is partly driven by a common mechanism. In southern Spitsbergen, the Paulabreen system has been active in all three time periods and continues to be in the present day (Kääb et al., 2023; Koch et al., 2023; Lovell and Fleming, 2023). The most prominent surge activity in southern Spitsbergen can be found in van Keulenfjorden (1800-1930 and 2000-2025) where Nathorstbreen and its tributaries are located. In the time period 1930-2000, this system did not appear to be active and instead surges were mostly found along the east coast of Sørkapp Land.

1063 Surges on Edgeøya have been mostly dominated by several advances of the large Stonebreen
1064 catchment.

1065 The lack of evidence for many surges from Vestfonna and Austfonna likely reflects a lack of
1066 submarine data available to reveal past signatures of ice flow. We note that many of the surges
1067 identified with dates are marine-terminating despite representing a smaller percentage of the total
1068 number of Svalbard glaciers. This possibly reflects the better preservation of past fast flow in the
1069 submarine geomorphological record. Therefore, our time series of spatial changes in surges is biased
1070 towards those with clear evidence of surge behaviour. If observational techniques had an increased
1071 sensitivity to smaller magnitude changes or we had more lines of evidence from geomorphological
1072 landforms and/or historical archives, many smaller magnitude surges may be uncovered. We therefore
1073 suggest that our current database is biased towards ice flow from larger glaciers. Unstable fast ice
1074 flow may take many different forms depending on glacier characteristics and other local environmental
1075 controls such as geological substrate, ocean boundary conditions, local climate and many more.
1076 Therefore, as our measurements improve, we expect to observe more complex behaviour related to
1077 glacier surging that is not captured in these plots which are binary in nature i.e. surge-type or not. We
1078 explore this concept in the next section.

1079 **6. Surge behaviour**

1080 **6.1. Continuum of surging**

1081 As we acquire more observations of glacier surges in Svalbard using a diverse range of techniques
1082 that are becoming more accurate and increasingly sensitive to lower magnitude changes in ice
1083 dynamics, the more we observe a larger variability in surge behaviour across the archipelago. This
1084 challenges the assumption that we can simply classify a glacier as ‘surge-type’ or ‘not surge-type’. We
1085 therefore propose that Svalbard surges can be represented as a continuum of behaviours (Figure 24)
1086 that include: (1) full catchment scale surges; (2) pulses from valley glaciers with several tributaries; (3)
1087 low magnitude speed-ups and slow-downs of a glacier; and (4) glaciers which do not surge. This
1088 spectrum of surge behaviour reflects differences in glacier characteristics (geometry, size, elevation
1089 range), spatial variability in subglacial enthalpy (Benn et al., 2019a), subglacial lithology, and local
1090 climatic conditions which influence rates of accumulation and ablation. All these features are likely
1091 typical of polythermal glaciers (Kristensen and Benn, 2012) where spatial variability in thermal regime
1092 leads to differences in surge behaviour. These factors ultimately influence the dynamics of a surge
1093 and whether it manifests as a surge bulge travelling down-glacier (Sund et al., 2009) or is initiated
1094 from the terminus (e.g. Sevestre et al., 2018) which leads to longitudinal stretching of the ice. Both

1095 may lead to mass redistribution and glacier terminus advance, but the magnitude of these changes
1096 depends on where the glacier is positioned along this continuum, with a higher likelihood of terminus
1097 advance when positioned nearer the full-catchment scale surge.

1098 **FIGURE 24**

1099 We consider a large, full-catchment scale surge of a glacier to represent an extreme end-member of
1100 this continuum. The surge of Basin-3 in Austfonna (e.g. Dunse et al., 2015) that started in 2012 and
1101 remains ongoing to this day is the best contemporary example of such an event. A surge of this
1102 magnitude can be readily detected through velocity and elevation changes in remote sensing data and
1103 typically leave behind strong indicators of past fast ice flow e.g. CSRs. Negribreen’s surge since 2016
1104 (Figure 4a; Benn et al., 2022; Trantow and Herzfeld, 2025) is also an example of this end-member
1105 type. Ordonnansbreen, which is a tributary of Negribreen, was not active during this surge. It should
1106 be noted that a ‘catchment-scale surge’ is defined by the RGI7.0 glacier outlines and often combines
1107 tributaries into a single catchment, such as Negribreen and Ordonnansbreen, therefore neglecting the
1108 potential for tributaries to surge independently. At the other end of the spectrum, glaciers that may not
1109 be able to surge are typically those that are cold-based and small (Sevestre et al., 2015; Mannerfelt et
1110 al., 2024). For a glacier to become this end-member type, mass accumulation does not lead to
1111 pressure melting and the bed remains cold-based, inhibiting sliding. In Svalbard, small valley glaciers
1112 across Nordenskiöld Land, Dickson Land and Andrée Land may be characterised by this end-member
1113 type although this is conjecture without additional data on thermal regime and ice dynamics.

1114 Between these end-member types, Svalbard surges exhibit a wide variety of behaviours. For a glacier
1115 system consisting of multiple tributaries, such as Nathorstbreen and Paulabreen, the fjord where these
1116 glaciers coalesce into a single unit often undergo ‘pulses’ of advance in response to surges of
1117 individual tributaries (e.g. Nuth et al., 2019). The pulses of several tributaries might reflect the storage
1118 and release of energy locally within a glacier catchment, reflecting local variations such as bedrock
1119 topography and lithology, or even the surface slope of individual catchments. Therefore, spatial
1120 variability in enthalpy at the glacier bed may play a critical role in the behaviour of glacier surges
1121 across Svalbard. How the individual processes at a single glacier are interconnected across a wider
1122 system is less well known, although it has been previously suggested that surges are more prevalent
1123 from catchments with a higher degree of ‘branchiness’ (Jiskoot et al., 2000). Furthermore, surge
1124 propagation may be restricted by the presence of subglacial conduits incised into the bed (i.e. Nye
1125 channels; Benn et al., 2009), enabling the evacuation of meltwater and therefore reducing enthalpy.
1126 Neighbouring glaciers that are seemingly disconnected may also display apparent synchronicity in
1127 their surge timing but with different ice dynamics. For example, whilst Comfortlessbreen surged and

underwent a 700 m advance in 7 years (Sund and Eiken, 2010; King et al., 2016), the speed-up of the adjacent Uvêrsbreen was barely noticeable on satellite data due to a lack of a considerable terminus advance (Figure 7b). Across the northern coast of Isfjorden, several glaciers have either surged (Sevestre et al., 2018; Harcourt et al., 2024) or accelerated in recent years. Although these are two isolated cases, the synchronicity in surge behaviour suggests there may be a shared process driving glacier dynamics within sub-regions of Svalbard, but this requires further testing.

Between the glaciers that surge and the cold-based glaciers which act as an end-member of this continuum, there are several glaciers which have exhibited fast ice flow of a lower magnitude compared to the aforementioned glaciers (Sund et al., 2009). The surge of Monacobreen between 2017 and 2020 is a prime example (Benn et al., 2022) having undergone a multi-stage pattern of speed-up following seasonal ice flow acceleration which led to an increase in terminus velocities four times relative to pre-surge conditions. Some glaciers have sped-up and slowed down in a cyclical manner, consistent with surge behaviour, yet the magnitude of the velocity change was small (e.g. Hansbreen, Esmarkbreen, Hinlopenbreen; Figure 25). Sveabreen, which terminates in northwest Isfjorden, appeared to speed up at the same time as Wahlenbergbreen's surge but did not evolve into a full-scale surge. Finally, some glaciers appear to be completely out of sync with climate, such as Kvalbreen (Figure 25); seasonal signals of ice flow on these glaciers are almost completely absent and instead appear to be undergoing ice flow regimes almost entirely driven by internal ice dynamics. On the other hand, Hinlopenbreen (Figure 25) has been undergoing a long-term seasonal cycle that does not appear to be dampened by long-term climate. A similar trend is found at Stonebreen (Figure 25). The velocity of Nordsysselbreen and Sefströmbreen has generally fluctuated around 1 m/day but accelerated rapidly to above 10 m/day during their recent surges in 2024 (Figure 25). The ice acceleration of these glaciers would be considered a full-catchment surge. Finally, cold-based glaciers with past evidence of surging such as proglacial CSRs (e.g. Mannerfelt et al., 2024) may not be classified as an end-member type. Instead, these glaciers have the potential to surge again and lie somewhere in between 'no surge' and 'slow acceleration'.

FIGURE 25

6.2. Surge cycles and causality

It has typically been thought that Svalbard surges undergo a three-stage cycle of change from quiescence, active surge and then a gradual slowdown back to quiescence (Dowdeswell et al., 1991; Sund et al., 2009). In this model, subglacial enthalpy builds up before frictional feedbacks lead to a surge peak. This enthalpy, which is defined as the internal availability of glacier energy and is a

function of ice temperature and meltwater (Aschwanden et al., 2012; Benn et al., 2019a), then dissipates after the redistribution of mass that results from a surge. However, observations of Svalbard surges indicate that this process is more complex (Strozzi et al., 2017; Benn et al., 2022; Figure 25) and instead surges typically move through several interconnected stages. The quiescent phase begins after enthalpy is fully dissipated and the glacier reaches a minimum in velocity. The slope of the glacier will typically be shallower compared to the surface slope of an actively surging glacier. The quiescent phase is long due to the 'dry' climate of Svalbard that increases the time taken for mass to build up in the reservoir zone. Our database confirms that the quiescent phase length ranges between 40 and 150 years (Lefauconnier and Hagen, 1991; Hagen et al., 1993; Flink et al., 2015). In comparison, the active phase length is far shorter and estimated to be between 3-10 years (Dowdeswell et al., 1991) which can be verified by satellite measurements of modern-day surges, some of which have been presented in this review. For surges of large glacier catchments (e.g. Basin-3, Negribreen) the active phase appears to be longer, which suggests that the length of the quiescent and active phases scale with glacier size.

As mass accumulates, ice near the bed reaches the pressure melting point and the area of temperate ice slowly increases (Benn et al, 2019a), increasing subglacial thermal energy. This initiates frictional feedbacks that lead to measurable ice flow changes (Benn et al., 2022). Velocity increases are restricted due to the loss of enthalpy through basal refreezing, subglacial outflow through channels, leakage of meltwater through the subglacial groundwater system or other means (Murray et al., 1998). Therefore, thermal conditions and subglacial hydrology work in tandem to alter ice flow. For both land- and marine-terminating glaciers, the slow buildup of enthalpy may last just a few months if the subglacial environment reacts quickly to frictional feedbacks, which may be the case for glaciers smaller than 30 km² (e.g. Drønbreen), but at larger glaciers (e.g. Negribreen, Basin-3) it has been observed to last several years reflecting slow enthalpy production and long response times to external enthalpy inputs (e.g. from supraglacial meltwater). The speed-up may be measured using in situ GNSS, such as at Basin-3 in Austfonna (Figure 8), or through loss of radar-interferometric coherence (Mannerfelt et al., 2025).

A full-scale surge is initiated when a glacier speed-up, observed as a velocity increase over several years, transitions into ice acceleration, where glacier velocities increase by an order of magnitude over a short time period e.g. months. This change results from a switch in ice flow regime from one that is driven by glacier thermal regime to one that is dominated by hydrologically driven basal sliding. Basal sliding transitions from a Weertman-style power law to one that incorporates subglacial cavities such as a regularised Coulomb sliding law which depends on basal water pressure (Weertman, 1957; Lliboutry, 1968; Schoof, 2005). Ice flow acceleration is usually restricted to a small spatial region that

1194 progressively expands in size. For example, acceleration may initiate in the reservoir zone and travel
1195 down-glacier as a surge bulge, or it may progressively propagate from the terminus upwards (e.g.
1196 Sevestre et al., 2018). Ice flow acceleration may last several months (e.g. Wahlenbergreen) or
1197 multiple years when the catchment size is larger (e.g. Basin-3, Negribreen), suggesting that glacier
1198 area is a key control on ice flow acceleration. Environmental conditions may accelerate this ice flow
1199 regime change. Dynamic thinning can induce glacier acceleration and promote surface fracturing that
1200 enables surface meltwater to penetrate to the bed and facilitate accelerated basal sliding (Sevestre et
1201 al., 2018). In addition, high melt years may lead to larger meltwater volumes reaching the glacier bed
1202 and increase basal water pressures leading to basal sliding (Flink et al., 2015). Other potential
1203 environmental factors could include glacier retreat past a subglacial pinning point, steepening of the
1204 glacier surface through increased melting in the ablation zone and mass build up in the accumulation
1205 zone, or changes in ocean thermal forcing.

1206 A short-lived peak in velocity will occur at the point at which enthalpy conditions reach their maximum.
1207 This may last from days or weeks on smaller glaciers to months on larger glaciers. Rapid velocity
1208 fluctuations related to seasonal velocity changes that are not related to the internal dynamics of a
1209 surge may be superimposed on this peak (e.g. Benn et al., 2019a; 2022). In some cases, there can be
1210 more than one documented surge peak (e.g., Kvalbreen in Figure 25), which may reflect the alteration
1211 of subglacial enthalpy due to ice mass redistribution or external forcing (e.g. surface melting). For
1212 example, a surge bulge moving down-glacier may slow down due to surface lowering and conductive
1213 heat losses but may then reactivate when subglacial meltwater can accumulate. This may occur when
1214 the margins of a glacier remain cold-based and reduce subglacial outflow. This implies that spatial
1215 variability in subglacial enthalpy controls the nature of the surge peak.

1216 After a peak in surge velocity, enthalpy reduces, and the glacier decelerates. Several mechanisms for
1217 enthalpy dissipation have been inferred from previous studies (e.g. Murray et al., 2000). The
1218 subglacial drainage system may change from an inefficient one with cavities to one that efficiently
1219 removes subglacial meltwater through channels, as was observed at Moršnevbreen (Benn et al.,
1220 2019a). A thermal regime switch may also occur whereby ice mass redistribution alters the spatial
1221 variability in ice thickness leading to conductive heat losses and loss of basal temperate ice needed
1222 for frictional feedbacks to initiate. Subglacial meltwater may also be lost via basal freeze-on and
1223 seepage into the subglacial permafrost and sediments (Murray et al., 2000). Ice flow deceleration of
1224 Svalbard surges is typically a multi-year process (e.g. Benn et al., 2022; Kääb et al., 2023; Koch et al.,
1225 2023) implying both hydrological and thermal changes contribute to enthalpy dissipation, which is
1226 typical of polythermal glaciers (Kristensen and Benn, 2012). After enthalpy is fully dissipated, the
1227 glacier reverts to quiescence.

1228 **6.3. Future projections**

1229 Svalbard is located within the Arctic ring of surge-type glaciers (Figure 26a) which is defined by a
1230 climatic envelope described by a pair of linear equations relating mean winter precipitation (MWP), to
1231 mean summer temperature (MST) i.e. 2m air temperature in summer:

1232 $MST = 0.001MWP + 8.4$ (1)

1233 $MST = 0.0014MWP - 0.97$ (2)

1234 where MST is in °C and MWP is in mm a⁻¹ (Sevestre and Benn, 2015). Glaciers that sit between the
1235 bounds set by equations (1) and (2) are considered to have a high probability of being surge-type. We
1236 map the modern-day limits of this envelope in Figure 26a using monthly averaged ECMWF Reanalysis
1237 5th Generation (ERA5) data from 2000 to 2009. We note that this envelope can also be defined by
1238 mean annual temperature (MAT) and mean annual precipitation (MAP) which may produce different
1239 results. Furthermore, this analysis also neglects differences between different versions of ERA
1240 reanalysis products (e.g. ERA1 and ERA5) as our focus is solely on the large-scale patterns. Figure
1241 26a shows that Svalbard is currently at the edge of the surging climatic envelope which may partially
1242 explain the large variability in surge behaviour. In the future, we expect the climatic envelope to shift
1243 northwards as summer temperatures and the volume of liquid water precipitation both increase
1244 (Bintanja, 2018; McCrystall et al., 2021; Gutiérrez et al., 2021). By 2100, there are projected increases
1245 in MSTs by up to 5°C and MWP by 30% (Gutiérrez et al., 2021). Applying these crude estimates of
1246 change to Equations 1 and 2, we can estimate the future spatial distribution of the surging climatic
1247 envelope (Figure 26b). The changes suggest Svalbard will remain in this climatic envelope up to 2100
1248 and hence surging activity is expected to remain prevalent across the archipelago. However, this
1249 interaction of a changing climate with surging prevalence is unlikely to be linear and the changes are
1250 expected to be more complex than the basic analysis presented here. Nonetheless, the changing
1251 overlap between the envelope and Svalbard might lead to changes in surge behaviour and also lead
1252 to surging of currently inactive ice masses such as Kvitøya. Post-LIA warming may have similarly
1253 altered the distribution of surge-type glaciers across Svalbard through changes in Svalbard's climate.
1254 Therefore, comparing past and present surge dynamics may yield insights into how future climate
1255 change will impact surging behaviour in Svalbard.

1256 **FIGURE 26**

1257 As changes in the prevalence of surge behaviour is driven by MST and MWP (Sevestre and Benn,
1258 2015), it follows that the changing nature of surging is driven by surface melt and ice thickness

1259 changes. Where surface meltwater can reach the bed, enthalpy will increase and drive glacier
1260 acceleration during a surge. However, long-term increases in surface melt can enhance the
1261 channelisation of the subglacial drainage system and reduce ice velocity. This effect has been
1262 observed in Greenland (e.g. Tedstone et al., 2015) and could lead to a negative feedback cycle in
1263 Svalbard and inhibit surging. It is not known whether an increase in surface melting due to climate
1264 change (van Pelt et al., 2019) could accelerate this process in Svalbard. However, because the
1265 surging climatic envelope is expected to remain over Svalbard up to 2100 and likely beyond (Figure
1266 26), higher surface melt rates will likely act to enhance enthalpy rather than reduce it. Furthermore,
1267 although MWP is projected to increase, increased surface melt will counteract this process and lead to
1268 Svalbard-wide glacier thinning (van Pelt et al., 2021), increasing conductive heat losses. For smaller
1269 glaciers, this will shift their thermal regime to predominantly cold-based (Sevestre et al., 2015;
1270 Mannerfelt et al., 2024). For larger glaciers, increased accumulation at higher elevation could increase
1271 the prevalence of subglacial meltwater generation and enhance sliding, whilst enhanced ablation near
1272 the terminus could steepen the glacier surface and promote faster flow, initiating frictional feedbacks
1273 (Thøgersen et al., 2019; 2024). The increasing prevalence of liquid precipitation in Svalbard
1274 (McCrystall et al., 2021) could also promote glacier sliding and surging. The impact of ocean thermal
1275 forcing on surging has not been studied but it is possible that regional warming could lead to
1276 synchronous glacier thinning and acceleration, initiating fast ice flow.

1277 If the Arctic ring of surges is normally distributed, we would expect glaciers at the edges of the
1278 envelope to have a lower probability of surging compared to those near the centre. Svalbard is
1279 currently near the edge of the envelope (Figure 26a) but will progressively move to the centre as the
1280 envelope moves northwards. This might suggest enthalpy availability will increase and surge
1281 behaviour will change. In particular, a glacier will pass through each of the stages outlined in Section
1282 6.1 at different times and at variable timescales, altering the length of the active and quiescent phases
1283 which are particularly sensitive to changes in meltwater inputs (Benn et al., 2019a). For example, the
1284 advances of Tunabreen during its multiple surges between the late 1800s and present day were
1285 progressively smaller as a result of smaller ice fluxes related to glacier mass loss (Flink et al., 2015).
1286 In comparison, Wahlenbergbreen and Borebreen have recently surged for the first time in ~100 years
1287 (e.g. Ottesen and Dowdeswell, 2006; Sevestre et al., 2018), demonstrating that the build-up of internal
1288 energy can still take several decades to accumulate despite ongoing climatic changes post-LIA.
1289 Finally, it is unclear whether movement in the position of the climatic envelope leads to an
1290 instantaneous change in the surge state of a glacier or whether there is a lagged response consistent
1291 with glacier response times. Unravelling the future behaviour of surges in Svalbard will rely upon
1292 understanding the response of surge-type glaciers to external forcing and how this relates to the build-
1293 up and release of energy during a surge.

7. Summary and outlook

Svalbard is a natural laboratory to study glacier surges given its high density of surge-type glaciers, ease of access in an Arctic context and availability of historical observations. When combined, this makes Svalbard surges arguably the best studied anywhere in the world. In this paper, we have reviewed the methodologies used to monitor glacier surges and compiled a new database of surge-type glaciers in Svalbard together with their characteristics. We estimate that 36% ($n=565$) of the 1,583 glaciers in Svalbard have demonstrable evidence for past surge behaviour, which increases to 52% ($n=511$) when considering only glaciers with a surface area larger than 1 km². Of all the glaciers in Svalbard, only 9% ($n=138$) have been directly observed to surge, with the others being classified as surge-type based on glaciological or geomorphological evidence of past surging. We found that surge-type glaciers are generally longer, have shallower slopes, and can be found across a broader elevation range, in agreement with previous studies (e.g. Jiskoot et al., 2000; Bouchayer et al., 2024). Therefore, surge-type glaciers have specific characteristics that make them more likely to surge. Since the 1990s, observations of glacier surges have increased dramatically with the launch of several new satellites, and since 2014 the launch of the Copernicus Sentinel satellites has simplified continuous monitoring of glacier surges. Analysis of glacial landforms such as CSRs and historical archives including photographs and maps enables the detection of past surges which are critical for increasing the temporal coverage of surge records. In situ geophysical surveys using instruments such as GPR and seismometers enable the study of subglacial conditions but are difficult to conduct in challenging terrain such as heavily crevassed surfaces during an active surge. A more harmonised, integrated approach that combines each of these techniques through the 'observational pyramid' would enhance our capabilities to measure surges at different scales in Svalbard.

As observations of glacier surges increase in number and quality, we are beginning to understand that the phenomenon of a 'glacier surge' is more complex than previously thought and the binary classification of whether a glacier is surge-type or not starts to break down. Instead, our database compiles glaciers with evidence for non-steady ice flow, which has been observed to take many forms. We find that the 3-stage model of Svalbard surges from quiescence-active-quiescence (Dowdeswell et al., 1991; Sund et al., 2009) fails when considering recent observations. Instead, up to 6 stages have been observed including: 1) quiescence; 2) a gradual multi-year velocity build-up; 3) a switch in basal sliding regime from thermal to hydrological; 4) rapid acceleration; 5) surge peak; and 6) gradual slowdown. These stages are typical of polythermal glaciers that are widespread in Svalbard (Sevestre et al., 2015). Furthermore, we note that some glaciers, such as Basin-3 in Austfonna, experience a full surge across their entire catchment whilst others have multiple tributaries or flow-units that surge independently as 'pulses', such as the Nathorstbreen glacier system. Additionally, some glaciers

1328 accelerate over multiple years, similar to the slow build-up phase we have identified, but then
1329 gradually slow down again. We suggest that glacier surges represent a continuum of behavioural
1330 characteristics beginning from a glacier with no apparent non-steady ice flow characteristics to a
1331 glacier that undergoes the traditional model of a Svalbard surge with a distinct acceleration, peak and
1332 then deceleration. The temporal evolution of surges can therefore be described by the 6-stage model
1333 whilst the spatial variability can be represented by the continuum approach.

1334 The variability in surge behaviour may reflect changes in the spatial overlap between the Arctic ring
1335 surge climatic envelope and Svalbard. Currently, Svalbard sits on the edge of this envelope and is
1336 expected to progressively move towards the centre, suggesting surges may become more prevalent.
1337 In addition, we expect that many of the smaller glaciers across the archipelago that have surged in the
1338 past can no longer surge due to thinning and a transition to a predominantly cold-based thermal
1339 regime. Overall, many glaciers in Svalbard have surged and many of these will likely do so again.
1340 Hence, continued monitoring from satellites and in situ geophysical sensors is critical to understand
1341 their surge processes. To improve our understanding of the complex behaviour of surging in Svalbard,
1342 we suggest nine areas of research that should be prioritised:

- 1343 1) Long-term measurements: There is an urgent need to generate a long historical time series of
1344 Svalbard glacier surges and their characteristics by bridging the gap between palaeo
1345 observations and the contemporary satellite record. This may be done by developing methods
1346 to detect surges in the historical record (e.g., developing a new 1960/61 DEM from available
1347 aerial imagery) as well as through new satellite observations.
- 1348 2) Documenting surge characteristics: Initiate systematic cataloguing of fundamental surge
1349 behavioural parameters (e.g., surge onset year, surge termination year, terminus change,
1350 maximum velocity, mean velocity in quiescence, surge propagation rates) to better understand
1351 surge drivers. This should combine existing monitoring results from different research groups
1352 and include analysis of satellite imagery, modelling studies, and artificial intelligence methods.
- 1353 3) Interaction between surges and glacier mass balance: Improved quantification of the impact of
1354 surges on mass balance, e.g., combining close-range sensors with satellite observations of
1355 surface elevation change. This should also include studying the evolution of a glacier before
1356 and after a surge. Integrated field campaigns and combining simultaneous monitoring efforts
1357 will be critical in achieving this. Additionally, analysing how mass balance influences surge
1358 behaviour will improve our understanding of how surges are affected by regional climate.
1359 Modelling of these processes, such as ice discharge changes and surface elevation melt
1360 feedbacks (Oerlemans, 2018) should also be prioritised.

- 1361 4) Subglacial observations: Direct observations of the subglacial environment during a surge are
1362 urgently needed to understand thermal and hydrological conditions. As discussed in this
1363 review, this is not simply due to the logistical complexities of deploying instruments over
1364 heavily crevassed surfaces and the issue of GPR signal attenuation. Interdisciplinary
1365 approaches and new measurement technologies are the recommended path.
- 1366 5) Past surges of small glaciers: Studying the prevalence of past surges at smaller glacier
1367 catchments will help us to understand the impact of catchment size on surge distribution and
1368 the potential for smaller glaciers to undergo fast ice flow during a surge. This will also help us
1369 constrain the changing spatial distribution of surge-type glaciers across Svalbard. In particular,
1370 mapping their thermal regime, understanding their velocities and measuring volume changes
1371 could be quantified using in situ and remote sensing observations.
- 1372 6) Surge causality: Improved analysis of the processes that lead to a surge is recommended. In
1373 particular, the distinction between events happening after a long succession of internal
1374 changes and events happening as the result of some distinct environmental ‘push’ such as
1375 intense surface melt, calving episodes, winter warm spells or surges of physically connected
1376 glaciers. Disentangling these processes is critical.
- 1377 7) Improved modelling: To improve surge process understanding, it is critical to unify models with
1378 observations (e.g. Terleth et al., 2021). This will help to understand the drivers and causality of
1379 surges and their quasi-periodal cycles. Furthermore, new developments in artificial intelligence
1380 should be explored to model the characteristics of glaciers and extend existing models.
1381 Moreover, improved modelling may also enable the detection of older surges by filling in gaps
1382 in time and space e.g. by fine-tuning foundational models. The effectiveness of this approach
1383 is still in its infancy but could lead to a paradigm shift in understanding past surge behaviour.
- 1384 8) Submarine measurements: A significant observation gap for understanding glacier surges is
1385 the submarine environment, where subglacial outflow, iceberg calving processes, and fjord
1386 circulation are key components impacting surge activity. Additionally, bathymetry data is
1387 essential for detecting past surge behaviour from submarine landforms. Measurements using
1388 AUVs, passive underwater acoustics, OBS / DAS systems can fill these gaps
- 1389 9) Research infrastructure: We suggest that new and portable research infrastructure should be
1390 developed to enable rapid deployment on surging glaciers which often start surging abruptly
1391 and without warning. This will enable the measurement of these surges from the start to the

1392 end of a surge. The detailed specific recommendations for developing research infrastructure
1393 in Svalbard are outlined in a recent white paper on Svalbard surges (Harcourt et al., 2025a).

1394

1395

1396

1397

1398

1399

1400

1401

1402

1403

1404

1405

1406

1407

1408

1409

1410

1411 **Acknowledgements**

1412 This work was supported by the Research Council of Norway, project number 322387, Svalbard
1413 Integrated Arctic Earth Observing System – Knowledge Centre, operational phase 2022. AK
1414 acknowledges support from the European Space Agency projects Glaciers_cci and EarthExplorer 10
1415 Harmony (4000127593/19/I-NB, 4000146464/24/NL/MG/ar). We would like to thank Berit Jakobsen
1416 from the University Centre in Svalbard (UNIS) for assisting in acquiring the historical paintings from
1417 the Recherche Expedition. We thank Torbsen Dunse for providing the Basin-3 Austfonna GPS data for
1418 Figure 9.

1419 **Data Statement**

1420 The database that has been created in this review is available via a zenodo repository:
1421 <https://doi.org/10.5281/zenodo.15240754> (Harcourt et al., 2025b).

1422

1423

1424

1425

1426

1427

1428

1429

1430

1431

1432

1433 **Tables**

1434 **Table 1** Number of surge-type glaciers in Svalbard, split into marine- and land-terminating. Total
1435 number of glaciers in Svalbard is 1,583 based on RGI7.0. If a glacier has been both ‘directly’ (e.g.
1436 velocity changes) and ‘indirectly’ (e.g. through the presence of CSRs) observed to surge, it is only
1437 counted once in the ‘All Surges’ category.

	Total	Marine-Terminating	Land-Terminating
All Glaciers	1,583	190	1,393
Directly Observed Surges	138	84	54
Indirectly Observed Surges	535	119	416
All Surges	565	138	427

1438



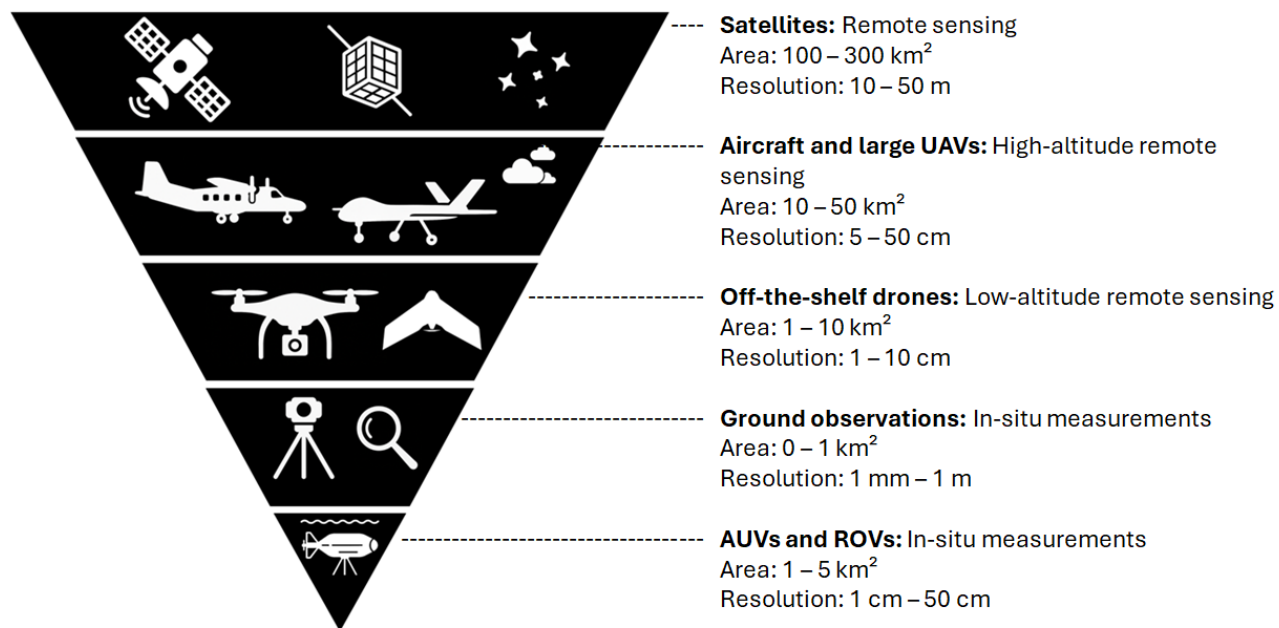
Figure 1 Location map of Svalbard and its position in the Arctic (highlighted in red within the inset panel). Names of different locations mentioned in the paper are highlighted. Land elevation and bathymetry are taken from the International Bathymetric Chart of the Arctic Ocean (IBCAO) (Jakobsson et al., 2024). Bold text indicates the locations of islands, whilst plain text represents different regions.



1450

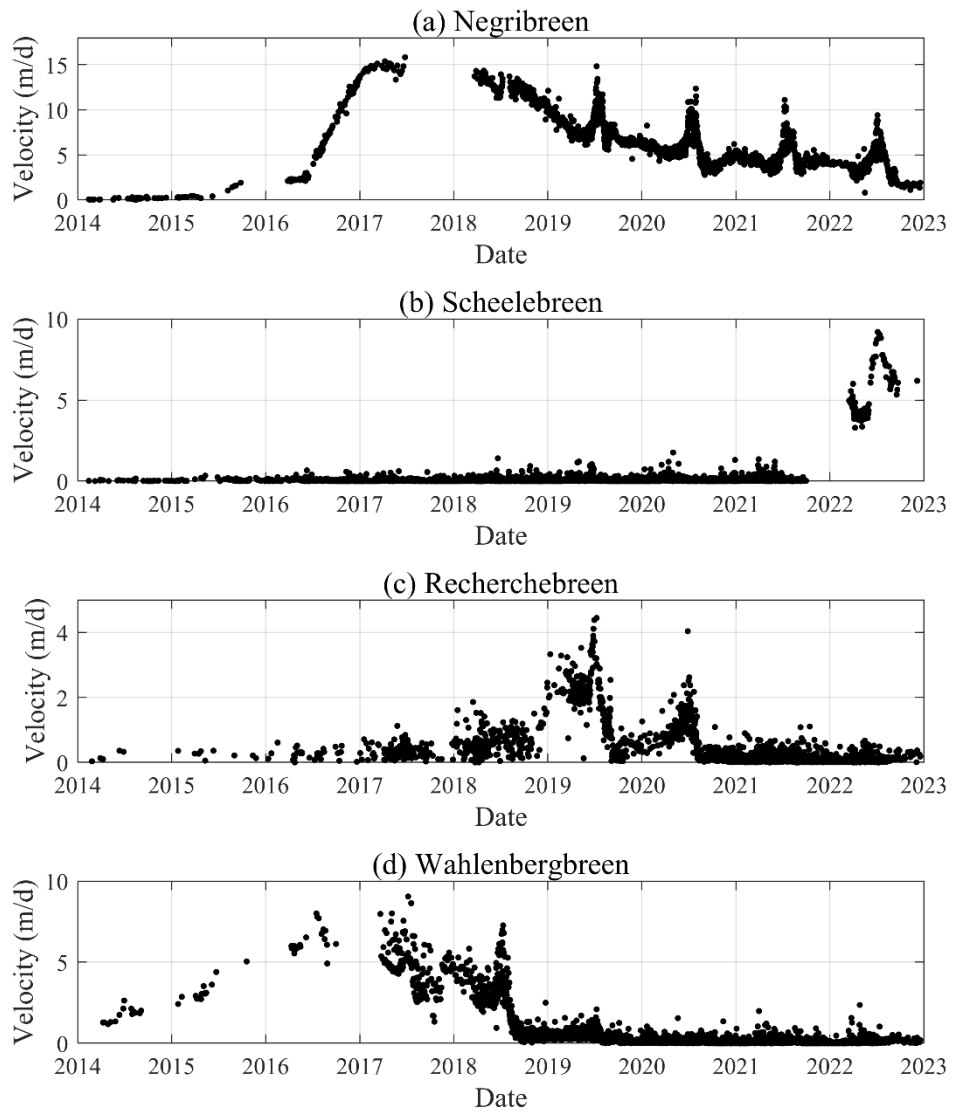
1451 **Figure 2** Painting of the terminus region of Recherchebreen (77.47°N, 14.73°E) from the 'La Recherche'
1452 Expedition between 1838 and 1840 (Commission scientifique du Nord, 1852).

1453



1454

1455 **Figure 3** The 'observational pyramid' that is employed to monitor glacier surges in Svalbard at different
 1456 scales.



1457

1458 **Figure 4** Velocity time series of selected surges that have taken place since 2014 at (a) Negribreen
 1459 (78.57°N, 18.96°E), (b) Scheelebreen (77.75°N, 17.03°E), (c) Recherchebreen (77.47°N, 14.73°E), and
 1460 (d) Wahlenbergbreen (78.47°N, 14.20°E). Data taken from the ITS_LIVE velocity catalogue (Lei et al.,
 1461 2022).

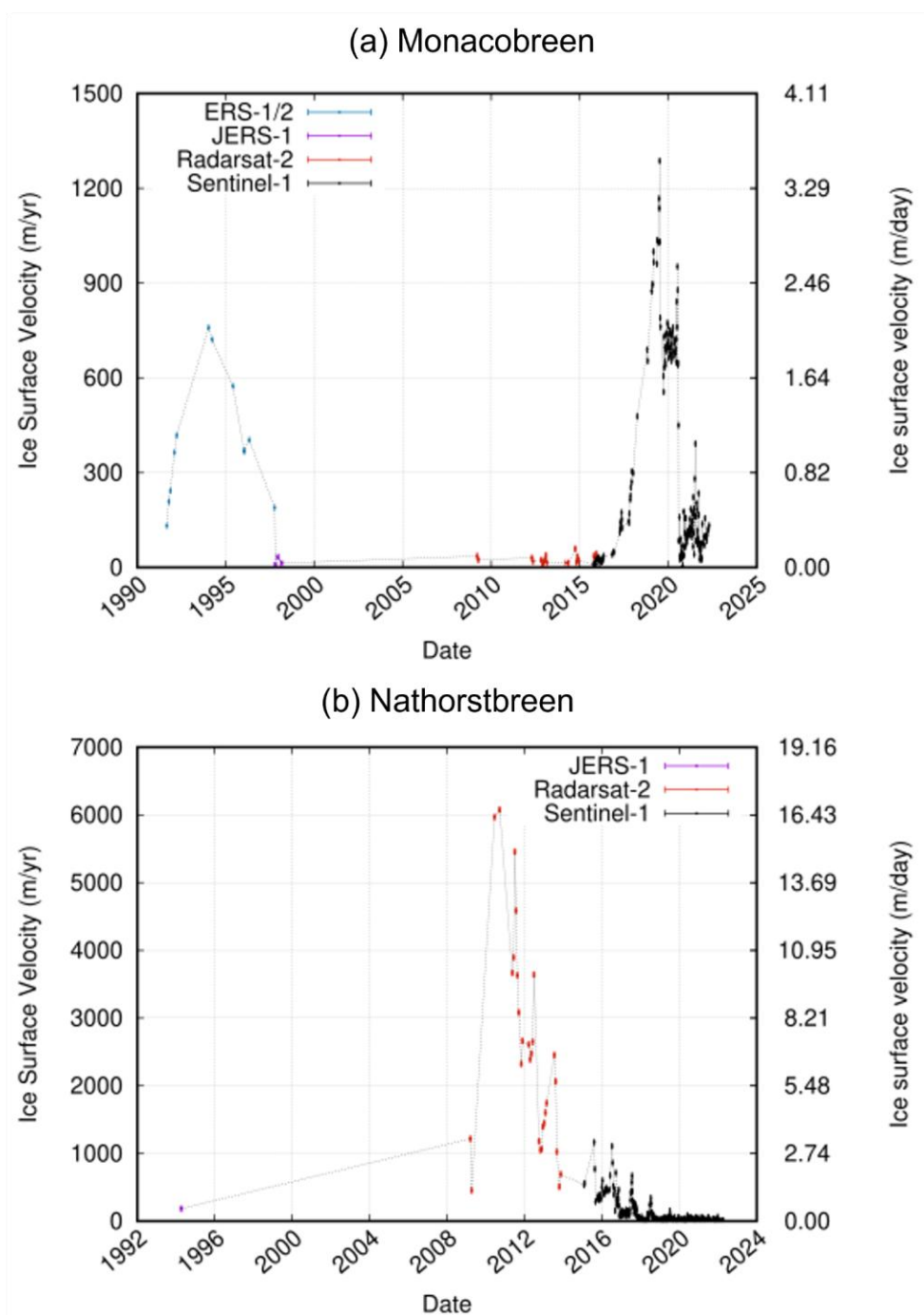
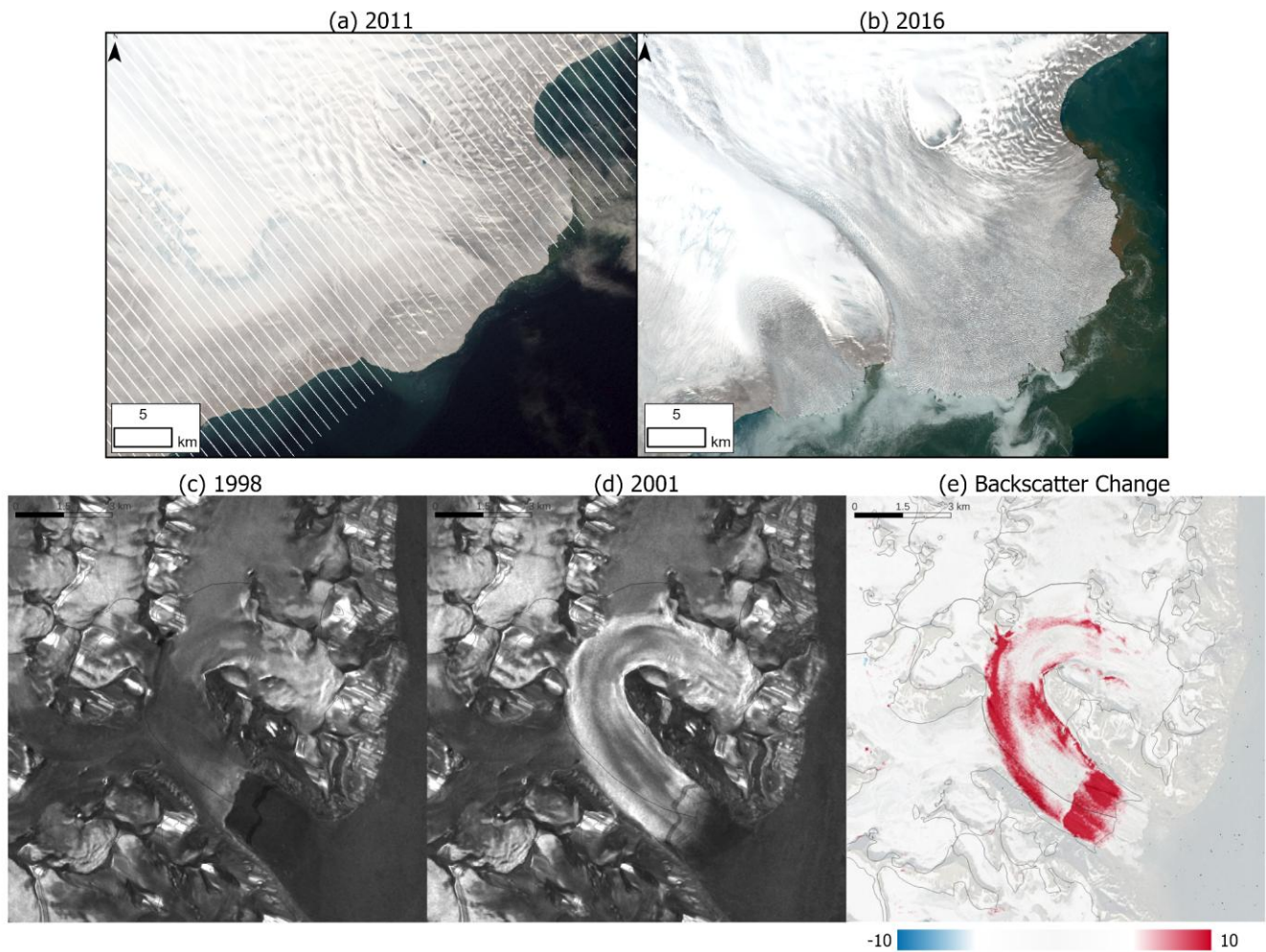


Figure 5: Velocity profiles of (a) Monacobreen (1990-2025; 79.50°N, 12.52°E) and (b) Nathorstbreen (1992-2024; 77.40°N, 16.22°E). These plots illustrate the availability of velocity data before and after the launch of the Copernicus Sentinel satellites.



1466

1467 **Figure 6** Surface conditions before and after a surge viewed from (a-b) optical and SAR (c-e) imagery.
 1468 The optical imagery shows (a) a Landsat 7 scene of Basin-3 in Austfonna (79.42°N, 25.36°E) pre-surge
 1469 and (b) a Landsat 8 image during its surge in 2016. For the SAR imagery, ERS-1/2 from Ingerbreen
 1470 (77.72°N, 18.16°E) in (c) 1998 and (d) 2001 is shown. Note the large increase in radar backscatter in
 1471 panel (d), which is interpreted as increased crevassing (Kääb et al., 2023). (e) Radar backscatter change
 1472 between the ERS-1/2 images.

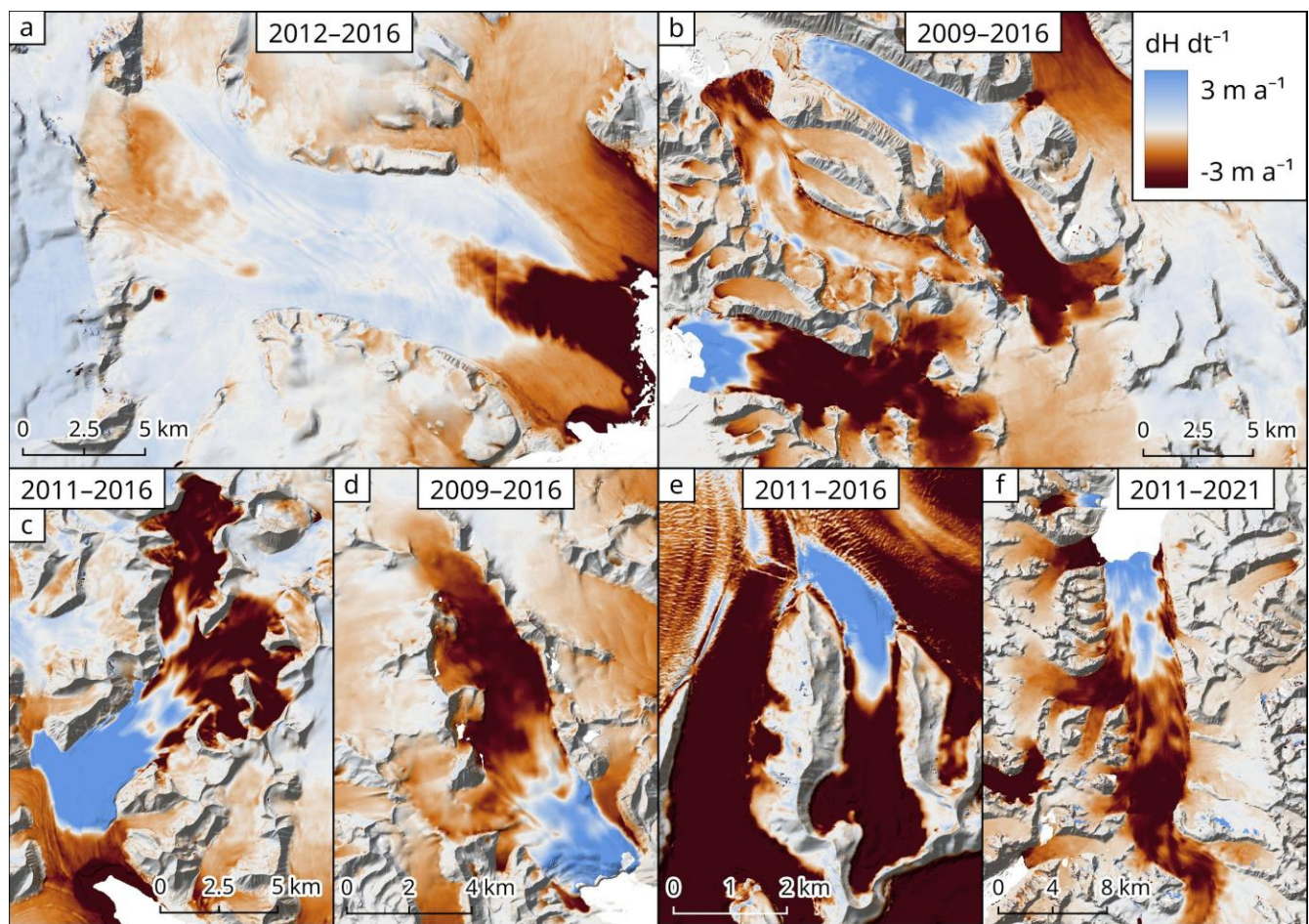


Figure 7: Elevation change rates (dH/dt) of surges in Svalbard: (a) Negribreen (78.57°N , 18.96°E), (b) Aavatsmarkbreen (bottom left; 78.71°N , 12.01°E) and Uvêrsbreen (top; 78.82°N , 12.23°E), (c) Moršnevbreen/Strongbreen (77.58°N , 17.55°E), (d) Esmarkbreen (78.31°N , 13.85°E), (e) Blankfjellbreen (tributary to Nathorstbreen; 77.27°N , 16.48°E), and (f) Monacobreen (center; 79.50°N , 12.52°E) and Emmabreen (top left; 79.55°N , 12.31°E). The maps were made by subtracting ArcticDEMs from the Norwegian Polar Institute 2008–2012 aerial image-derived DEMs. The background hillshade is from each respective ArcticDEM.

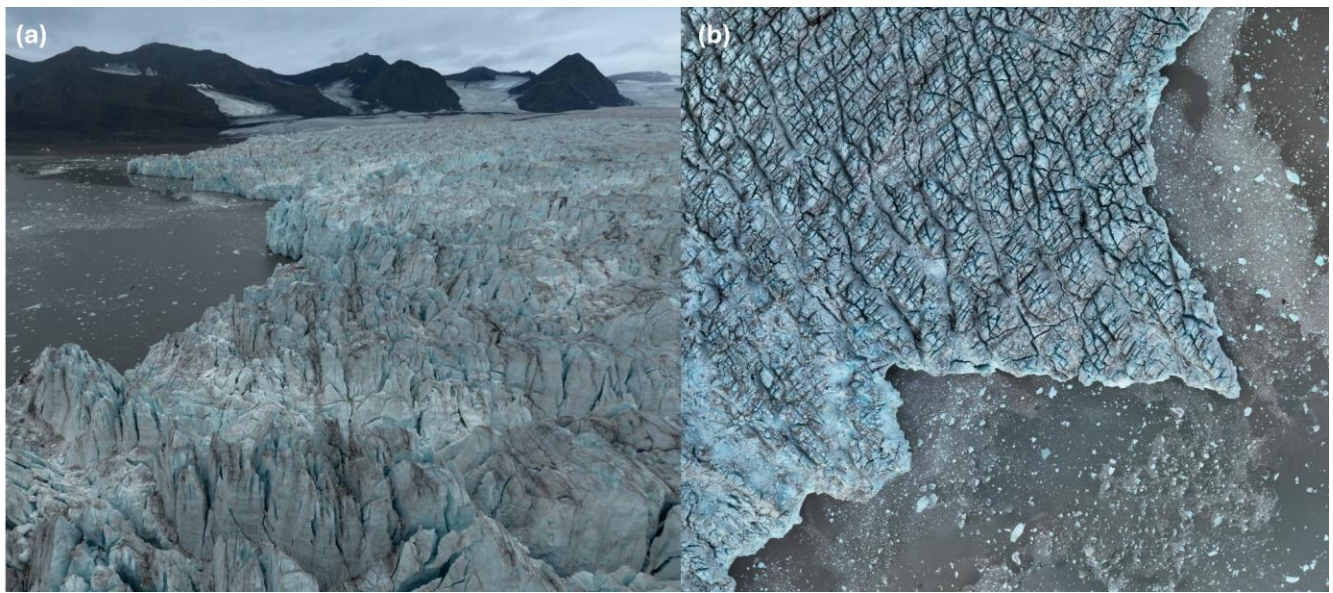
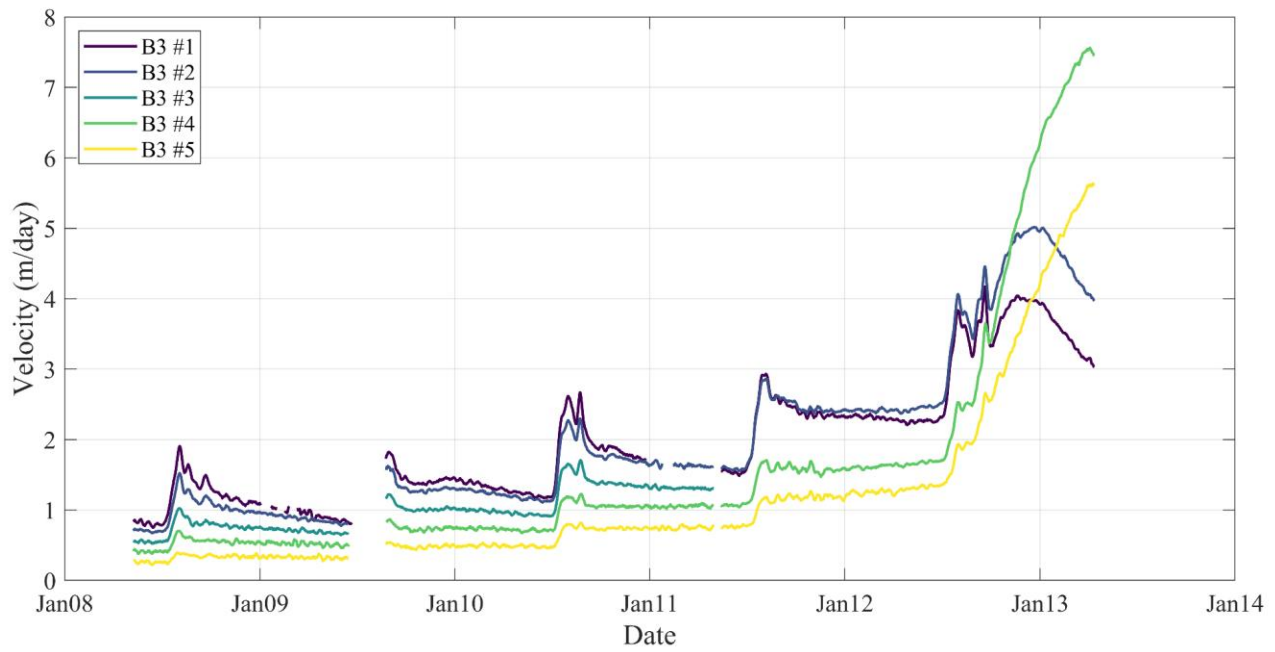


Figure 8 UAV imagery captured in (a) oblique and (b) nadir-looking geometry over Borebreen (78.42°N, 14.02°E).



1496

1497 **Figure 9:** Flow velocities along the centreline of the fast-flow region of Basin-3, Austfonna (79.42°N,
 1498 25.36°E), between May 2008 and May 2013. GPS stations are numbered from 1 at the lowest elevation
 1499 to 5 at the highest. Data replotted from Dunse et al. (2015). Data credit: Torben Dunse.

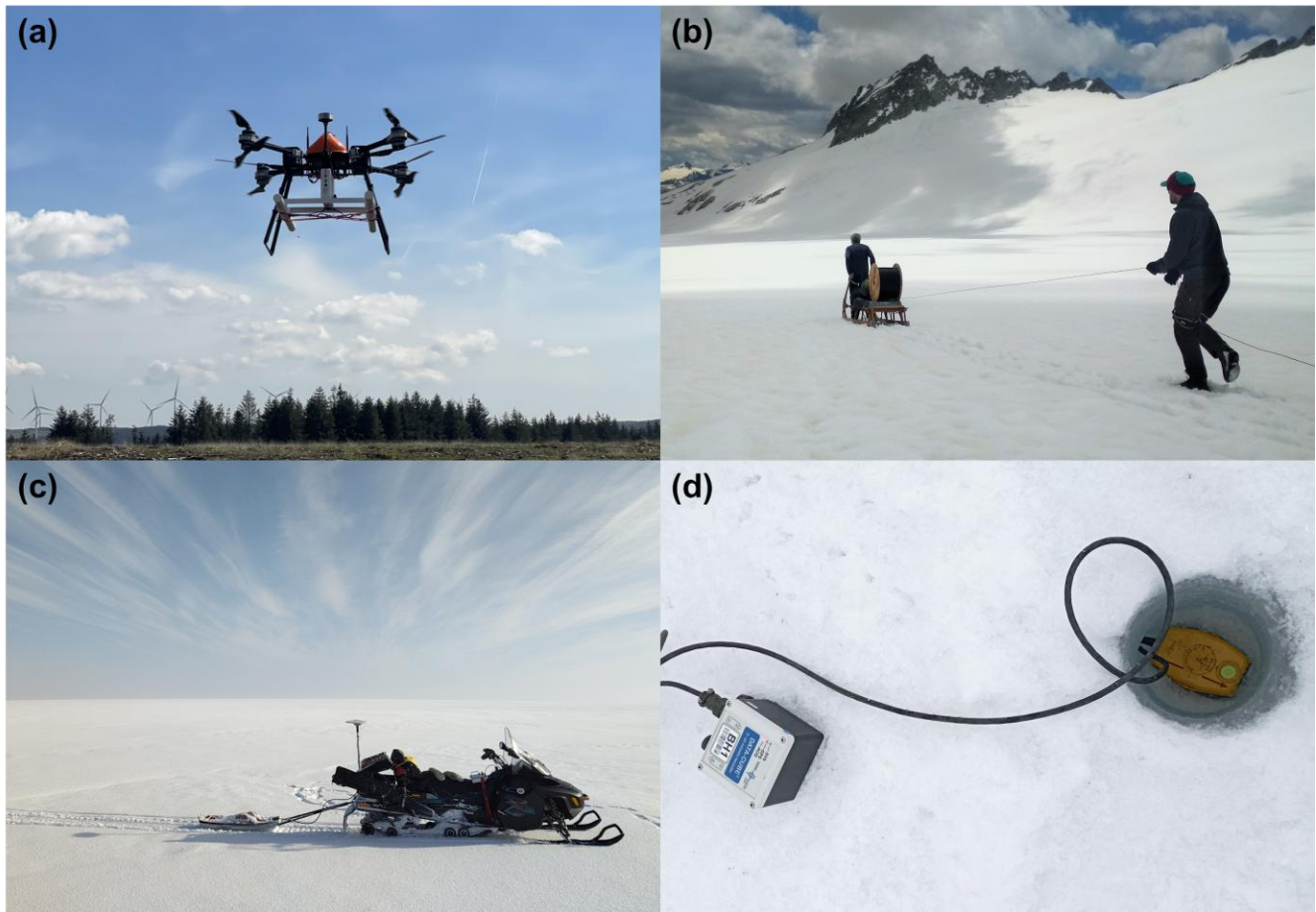
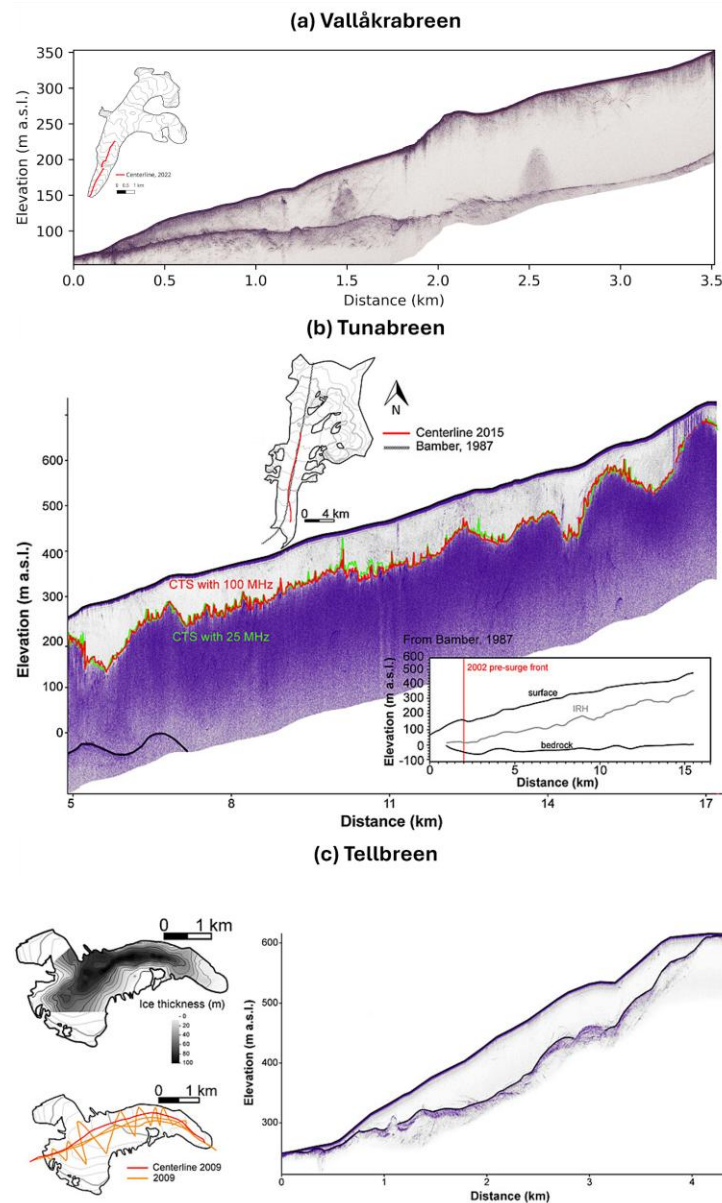


Figure 10 Examples of Ground Penetrating Radar (GPR) and seismic instruments in the field. (a) Airborne-GPR setup, GeoDrone 80MHz radar mounted on a Vulcan Harrier UAV flown in the Rhigos Mountains of South Wales, photo credit: Jon Walker (Swansea University); (b) A fibre-optic cable for Distributed Acoustic Sensing (DAS) being deployed on Rhônegletscher, Swiss Alps. The interrogator is located in the tent at the cable end. Photo by Wojciech Gajek; (c) Land-based GPR setup in Svalbard. The GPS and radar unit are installed on the snowmobile while the antenna is towed behind it. Photo by Erik Mannerfelt; (d) Traditional seismological instrument: DIGOS DataCUBE recorder next to a 30cm deep borehole equipped with a 4.5 Hz 3-component geophone (to be enclosed with ice and snow) on Hansbreen, Svalbard. The DataCUBE is equipped with internal GPS for time synchronisation and is powered with a pair of D20 batteries. Photo by Mateusz Olszewski.



1514

1515 **Figure 11** Examples of Ground Penetrating Radar (GPR) data collected for glaciers in Svalbard. (a)
 1516 Survey over the surge bulge (at 2 km) of Vallåkrabreen (77.84°N, 17.08°E) collected in 2022 with a
 1517 100 MHz antenna. (b) Centerline radargram of Tunabreen (78.46°N, 17.41°E) collected in 2015 with a
 1518 100 MHz antenna. The top pick marks the glacier surface, while the bottom pick follows the bed
 1519 reflector. The red line follows the CTS picked on the data collected with the 100 MHz antenna, while
 1520 the green line follows the CTS picked on the data collected with the 25 MHz antenna along the same
 1521 survey line. (c) Centreline radaragram collected in 2009 over Tellbreen (78.25°N, 16.20°E), corrected
 1522 for elevation. The top pick marks the glacier surface, whilst the bottom pick follows the bed reflector.
 1523 Panel (a) is an unpublished 2022 survey of Vallåkrabreen by Erik S. Mannerfelt. Panels (b) and (c) are
 1524 from Sevestre et al. (2015).

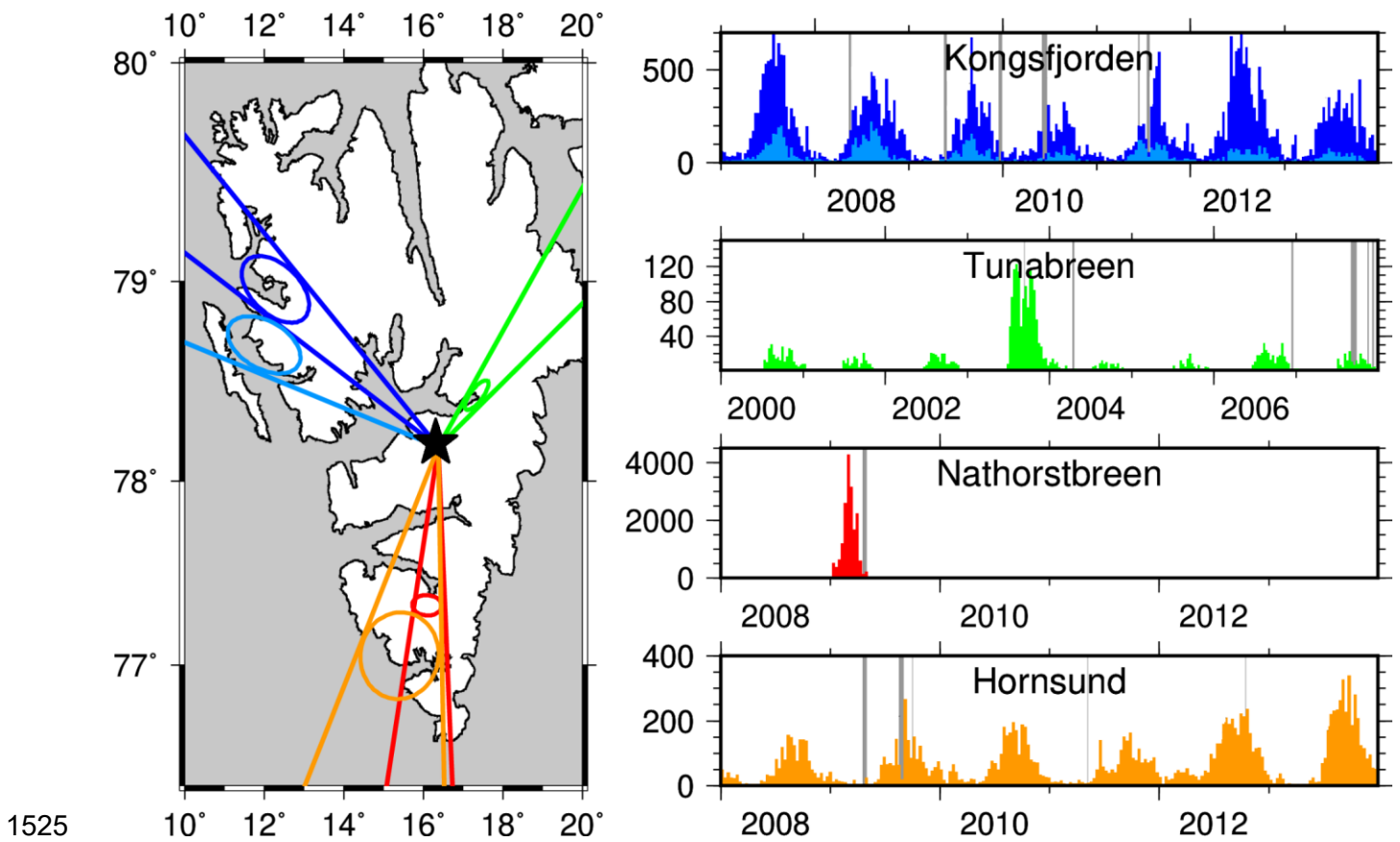
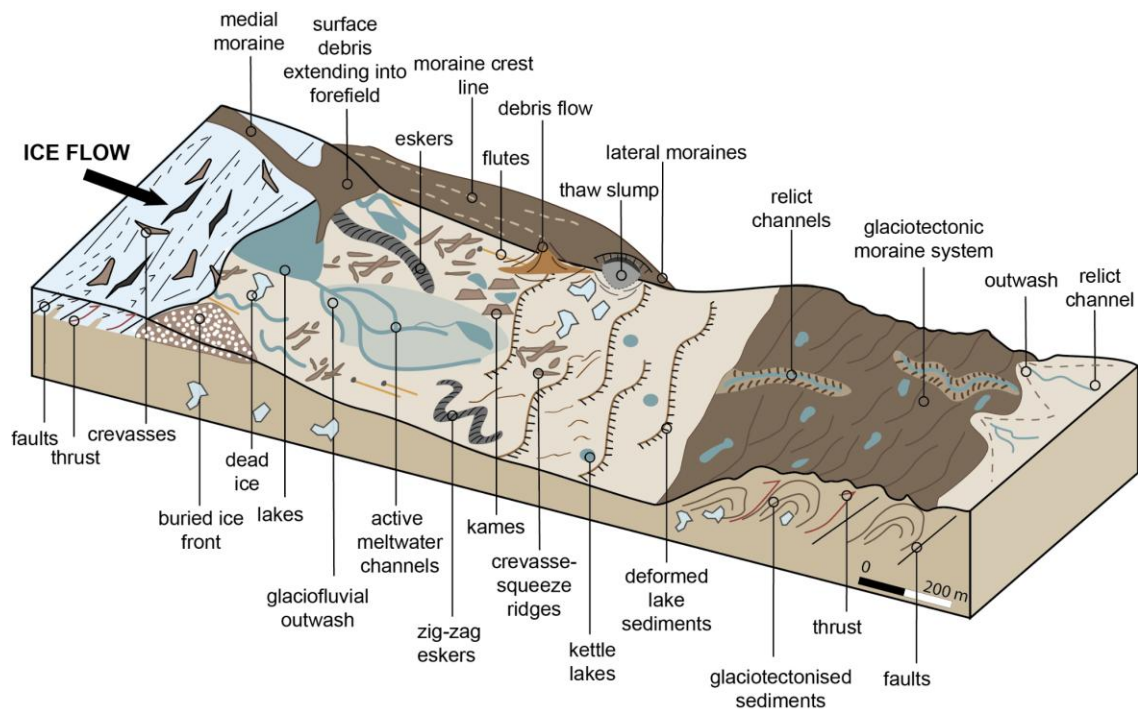
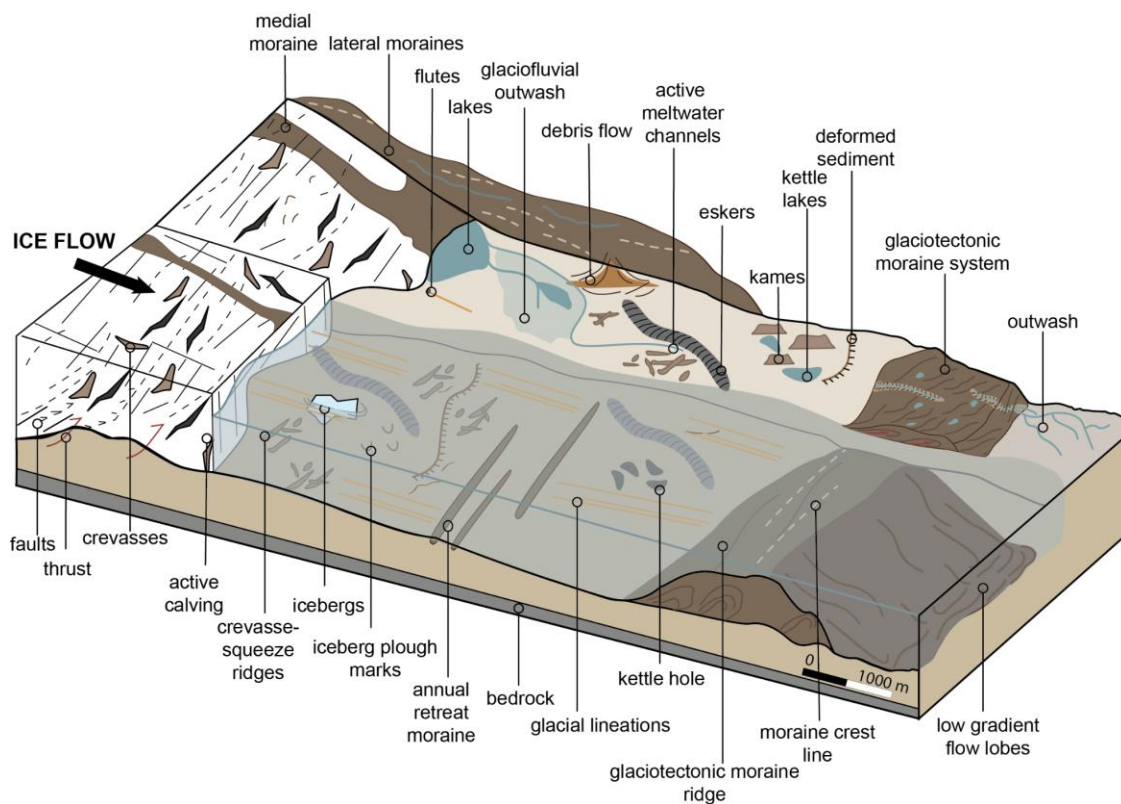


Figure 12 Temporal distribution of autonomous icequake detections obtained using regional seismic network stations. Lines and ellipses indicate individual source regions as seen in the data from the Spitsbergen seismic array (SPITS) marked as a black star. Temporal histograms present event counts per 10 days at each location. Light grey bars indicate days with data gaps. Seasonal temporal patterns at Kongsfjorden, Tunabreen and Hornsund are the result of glacier calving variability. High seismic activity at Nathorstbreen (2009; 77.27°N, 16.48°E) and Tunabreen (2003; 78.46°N, 17.41°E) was related to glacier surges. Modified from Köhler et al. (2015).



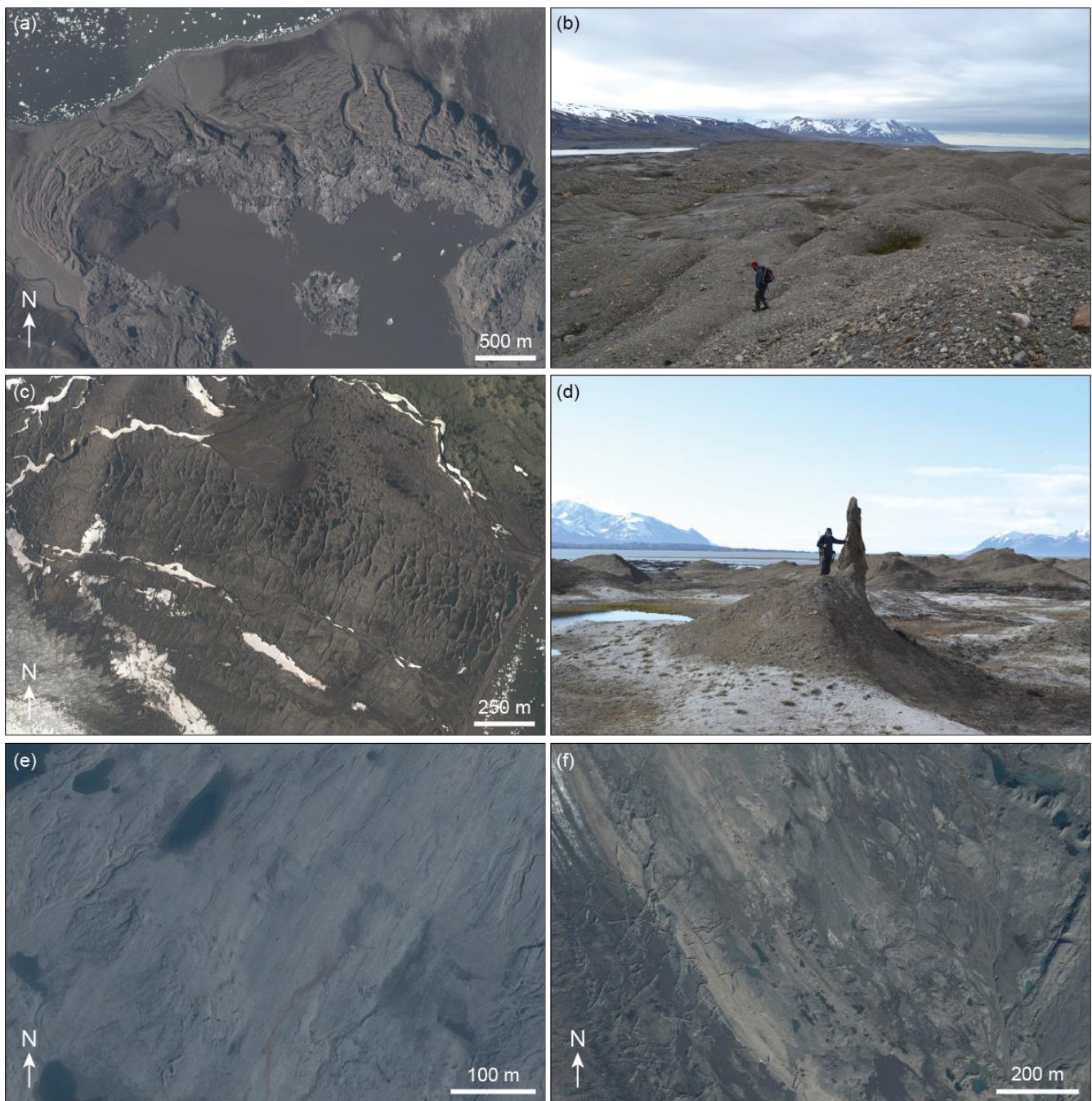
1533

1534 **Figure 13** Land-terminating surge-type glacier landsystem (from McCerery et al., 2025).



1535

1536 **Figure 14** Marine-terminating surge-type glacier landsystem (from McCerery et al., 2025). Note the
1537 fjord-adjacent terrestrial component where the surge extended on land (e.g. Aradóttir et al., 2019).



1538

1539

1540

1541

1542

1543

1544

1545

1546

Figure 15 Surge landforms present at terrestrial glacier margins. (a) Glaciotectionic moraine system at Penckbreen (77.49°N, 15.61°E). Note the smooth surface of the moraine system compared to the rest of the exposed foreland, the multiple ridge crests oriented perpendicular to glacier flow (broadly from S to N), the channels cut through the ridges, and the large proglacial lake. Aerial photograph captured by NPI in 2011 and accessed via TopoSvalbard (toposvalbard.npolar.no). (b) Photograph captured in 2012 looking west across the Penckbreen moraine system, with part of the proglacial lake visible in the left distance. Note the relatively homogenous gravel-sized surface sediment cover, which gives the smooth surface appearance seen in (a). Photo by Harold Lovell. (c) Crevasse-squeeze ridge (CSR)

1547 network exposed in front of Pettersenbreen (77.48°N, 23.43°E). Note the cross-cutting ridges oriented
1548 perpendicular and sub-perpendicular to ice flow (broadly from NW to SE), mimicking surface crevasse
1549 patterns. Aerial photograph captured by NPI in 2011 and accessed via TopoSvalbard
1550 (toposvalbard.npolar.no). (d) Photograph captured in 2012 of pinnacle-like CSR on Nathorstbreen's
1551 Nordre Nathorstmorenen (77.50°N, 16.13°E). Note other CSRs visible in the background. Photo by
1552 Harold Lovell. (e) Flutes in front of Elisebreen (78.62°N, 12.09°E). Ice flow was broadly from NE to
1553 SW, parallel to flute orientation. Note the cross-cutting meandering ridges and ridges oriented
1554 perpendicular to ice flow, interpreted by Christoffersen et al. (2005) as infilled basal meltwater conduits
1555 and CSR, respectively. A zig-zag esker can also be seen in the centre-left at the bottom of the image.
1556 Aerial photograph captured by NPI in 2011 and accessed via TopoSvalbard (toposvalbard.npolar.no).
1557 (f) Geometric ridge networks (bottom left of image) in front of Hørbye-breen (78.75°N, 16.35°E)
1558 interpreted as CSRs and zig-zag eskers by Evans et al. (2022). Ice flow was broadly from NW to SE.
1559 Note the sinuous esker in the top right of the image. Aerial photograph captured by NPI in 2011 and
1560 accessed via TopoSvalbard (toposvalbard.npolar.no).

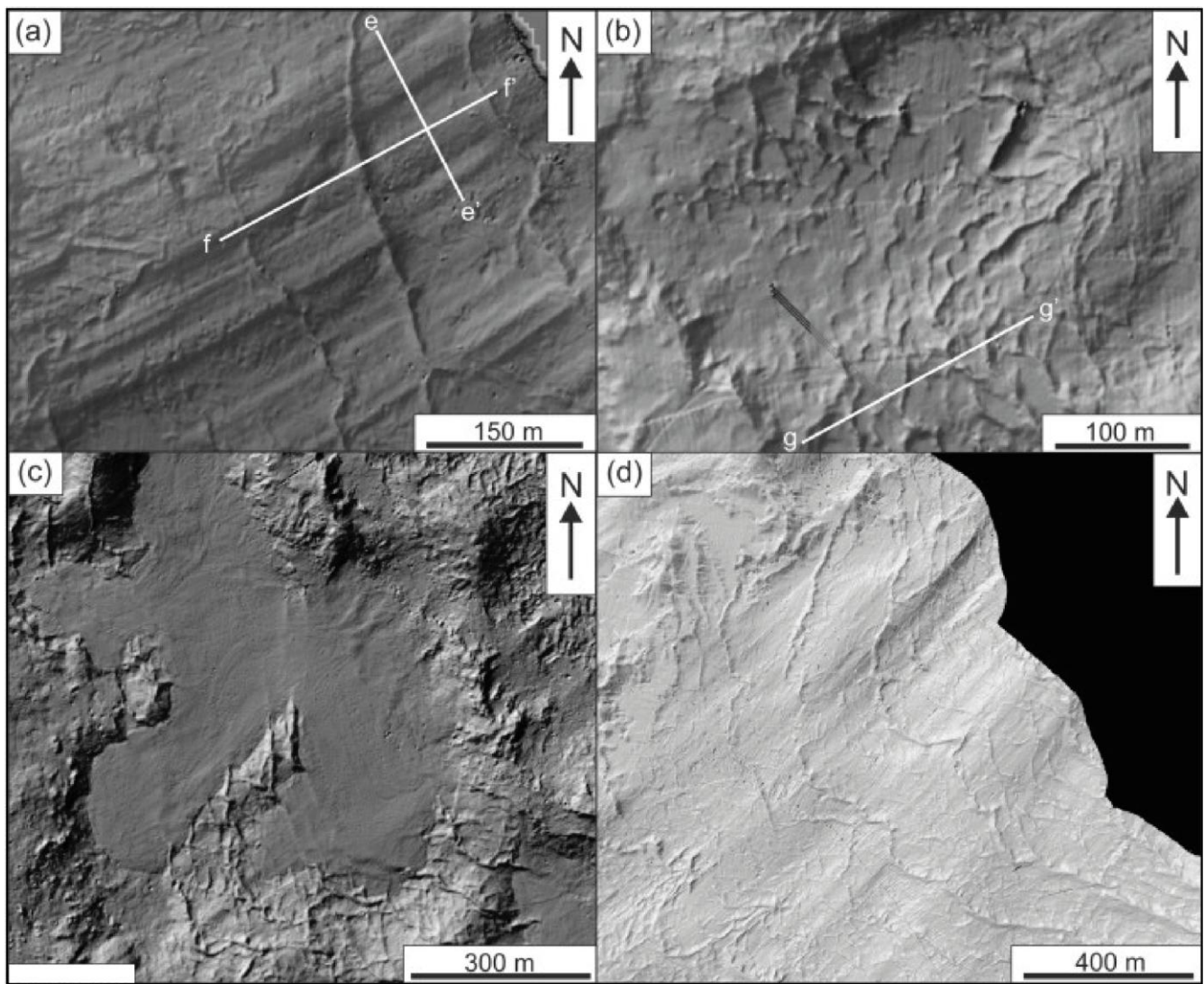
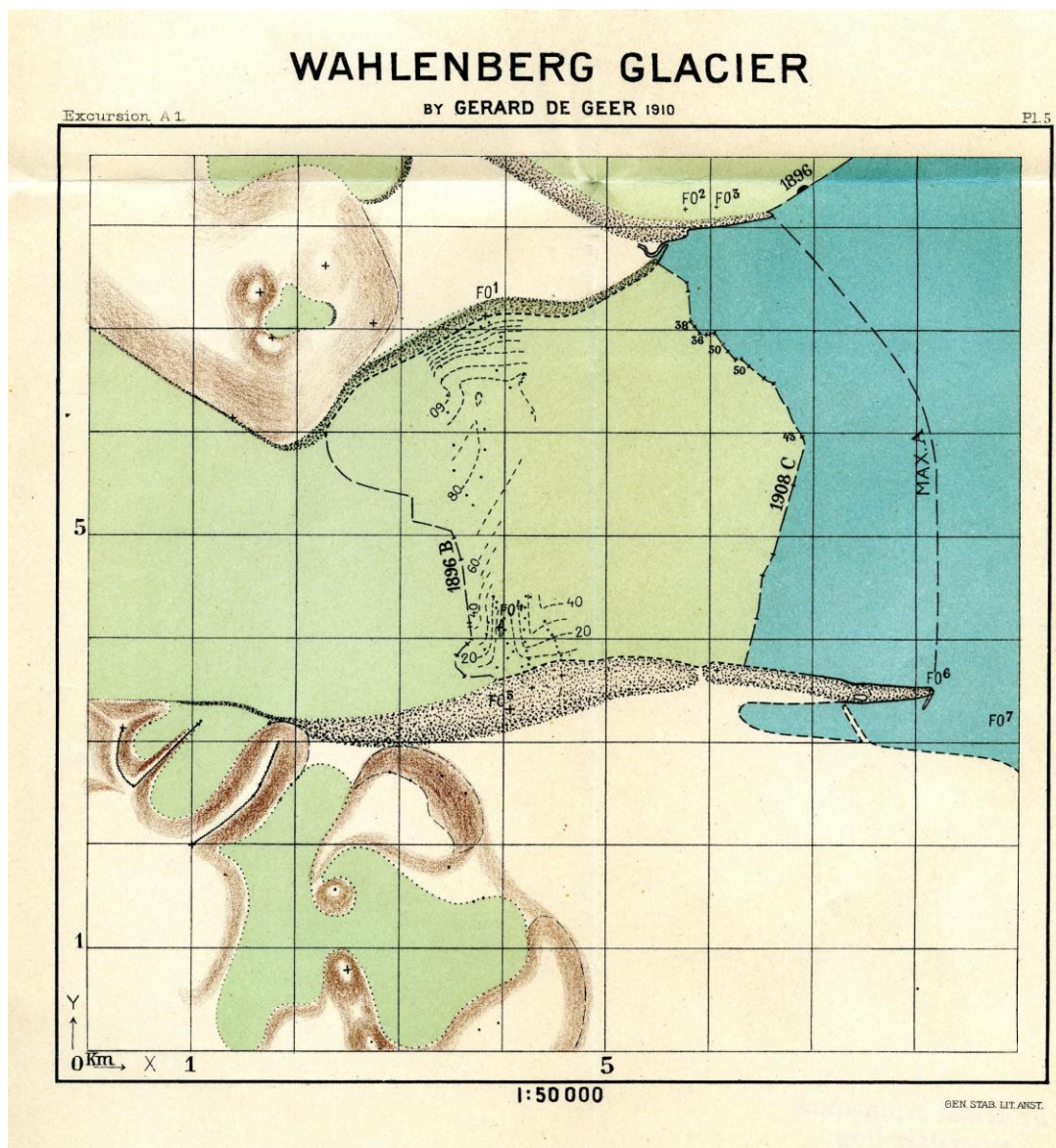
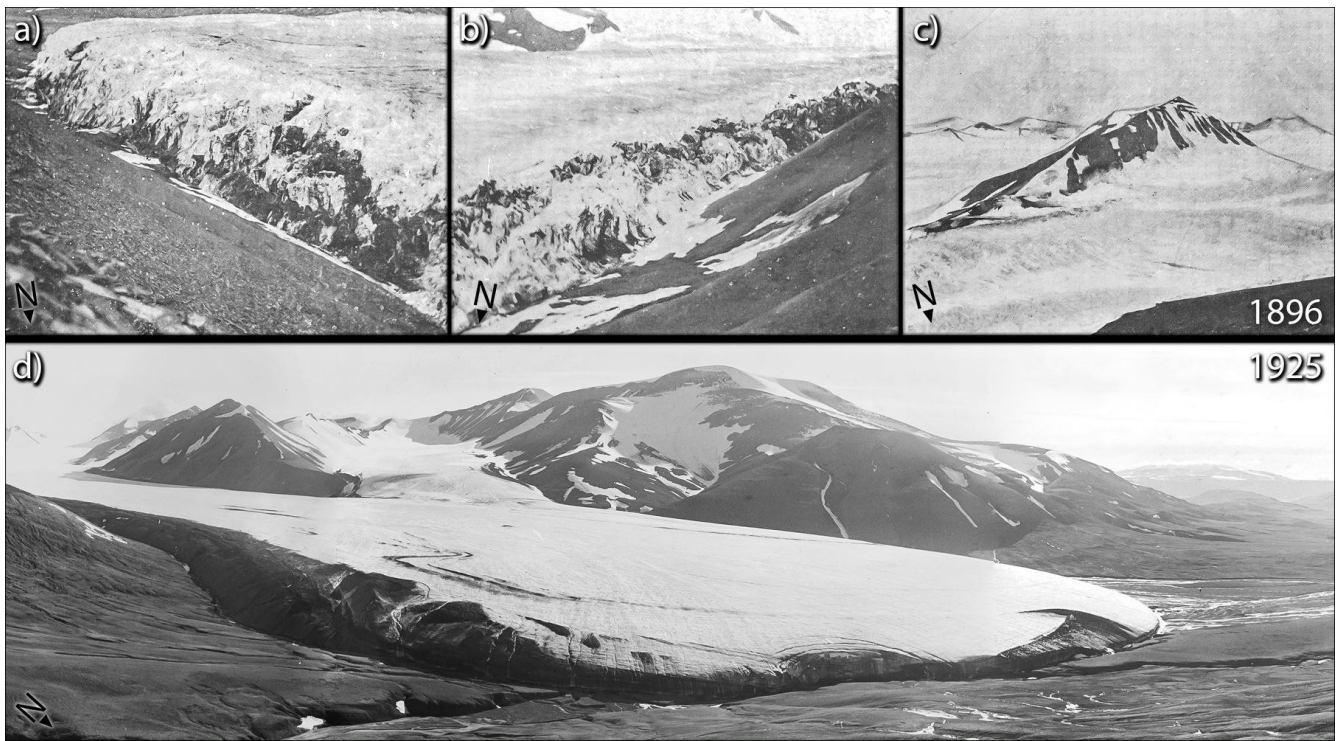


Figure 16 Examples of seafloor surge landforms in Tempelfjorden in front of Tunabreen (78.43°N, 17.31°E) from Flink et al. (2015). (a) Glacial lineations; (b) Crevasse-squeeze ridges (CSRs); (c) Debris-flow lobe covering older CSRs. (d) Annual retreat moraines.



1570

1571 **Figure 17** Historical map of the Wahlenbergreen terminus (78.47°N, 14.20°E) from repeat mapping
 1572 in the early 1900s (de Geer, 1910). An outline from their previous expedition in 1896 is drawn 3–4 km
 1573 behind the 1908 terminus position, indicating an ongoing surge that is also visible through extensive
 1574 crevassing in photographs from the latter year.



1575

1576

1577

1578

1579

Figure 18: Historical photographs from Drønbreen (78.13°N, 18.82°E), central Svalbard, indicating a surge around 1896 (a-c) and subsequent quiescence in 1925 (d). Photographs (a-c) are from Garwood and Gregory (1898), and (d) taken by Adolf Hoel, kept at the Norwegian Polar Institute library.

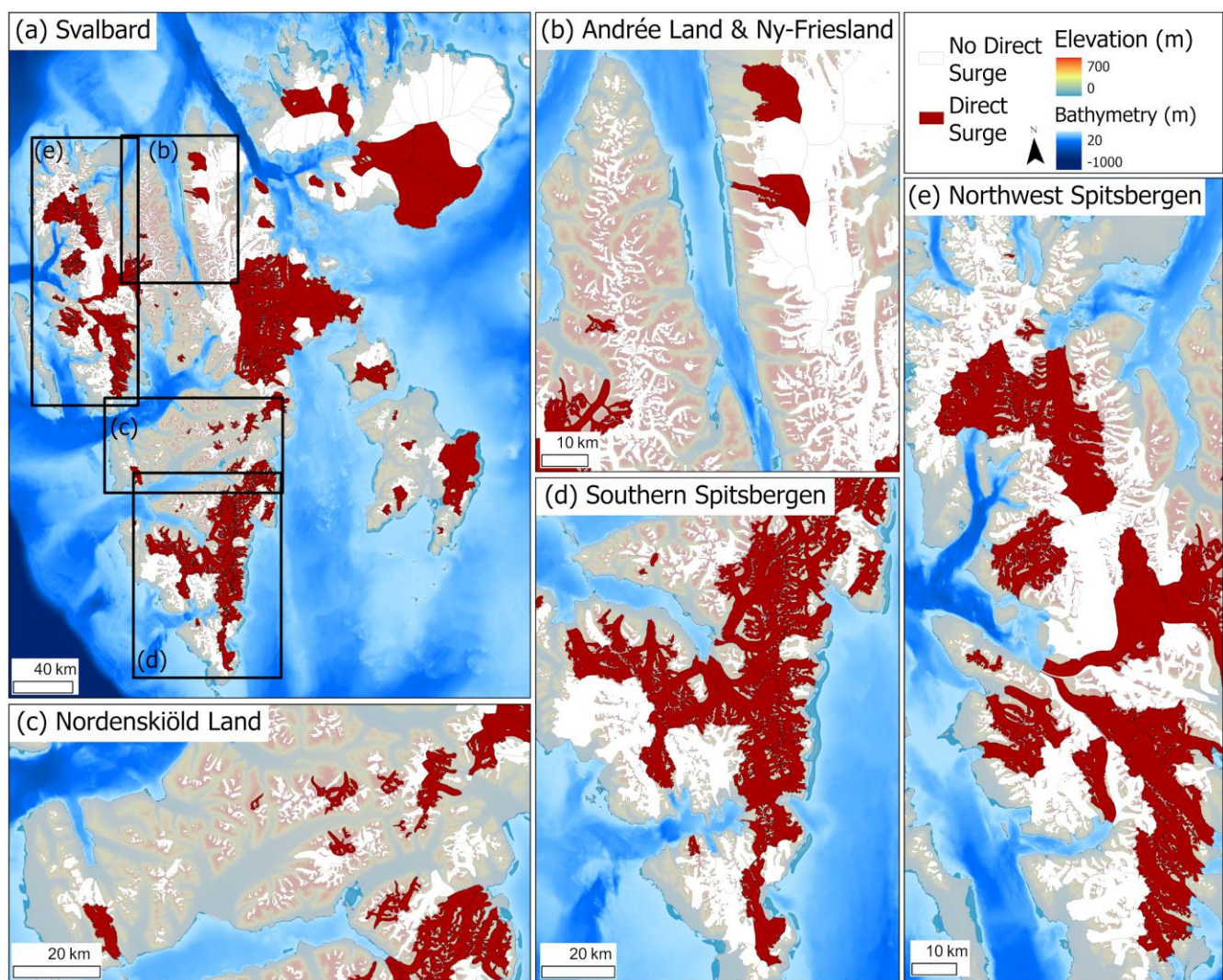


Figure 19 (a) Spatial distribution of glaciers directly observed to surge in Svalbard. Regions consisting of several small glaciers are expanded for (b) Andrée Land & Ny Friesland, (c) Nordenskiöld Land, (d) Southern Spitsbergen, and (e) Northwest Spitsbergen. Bathymetry data is taken from the International Bathymetric Chart of the Arctic Ocean (IBCAO) (Jakobsson et al., 2024).

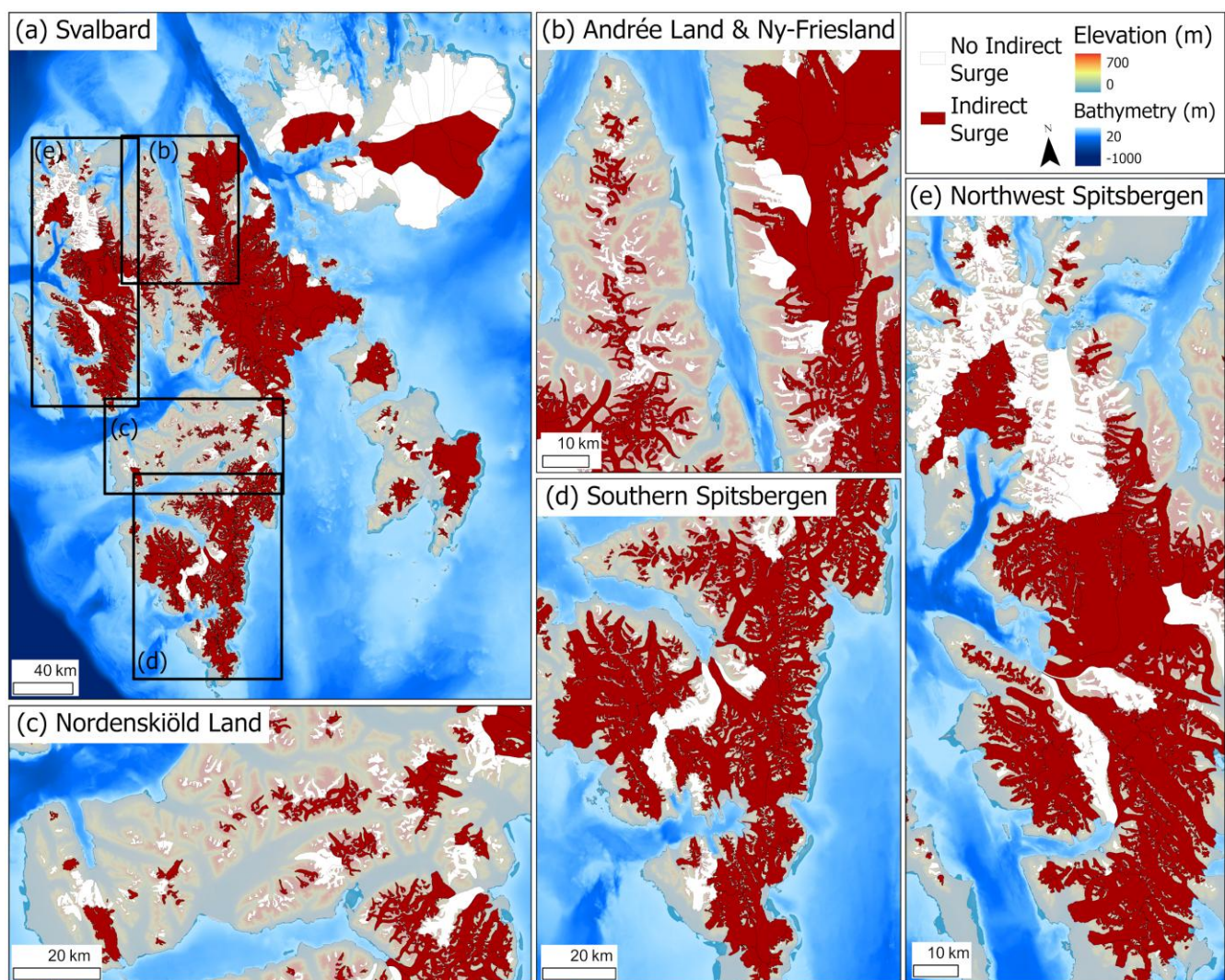


Figure 20 (a) Spatial distribution of glaciers indirectly (e.g. landforms, historical records) observed to surge in Svalbard. Regions consisting of several small glaciers are expanded for (b) Andrée Land & Ny Friesland, (c) Nordenskiöld Land, (d) Southern Spitsbergen, and (e) Northwest Spitsbergen. Bathymetry data is taken from the International Bathymetric Chart of the Arctic Ocean (IBCAO) (Jakobsson et al., 2024).

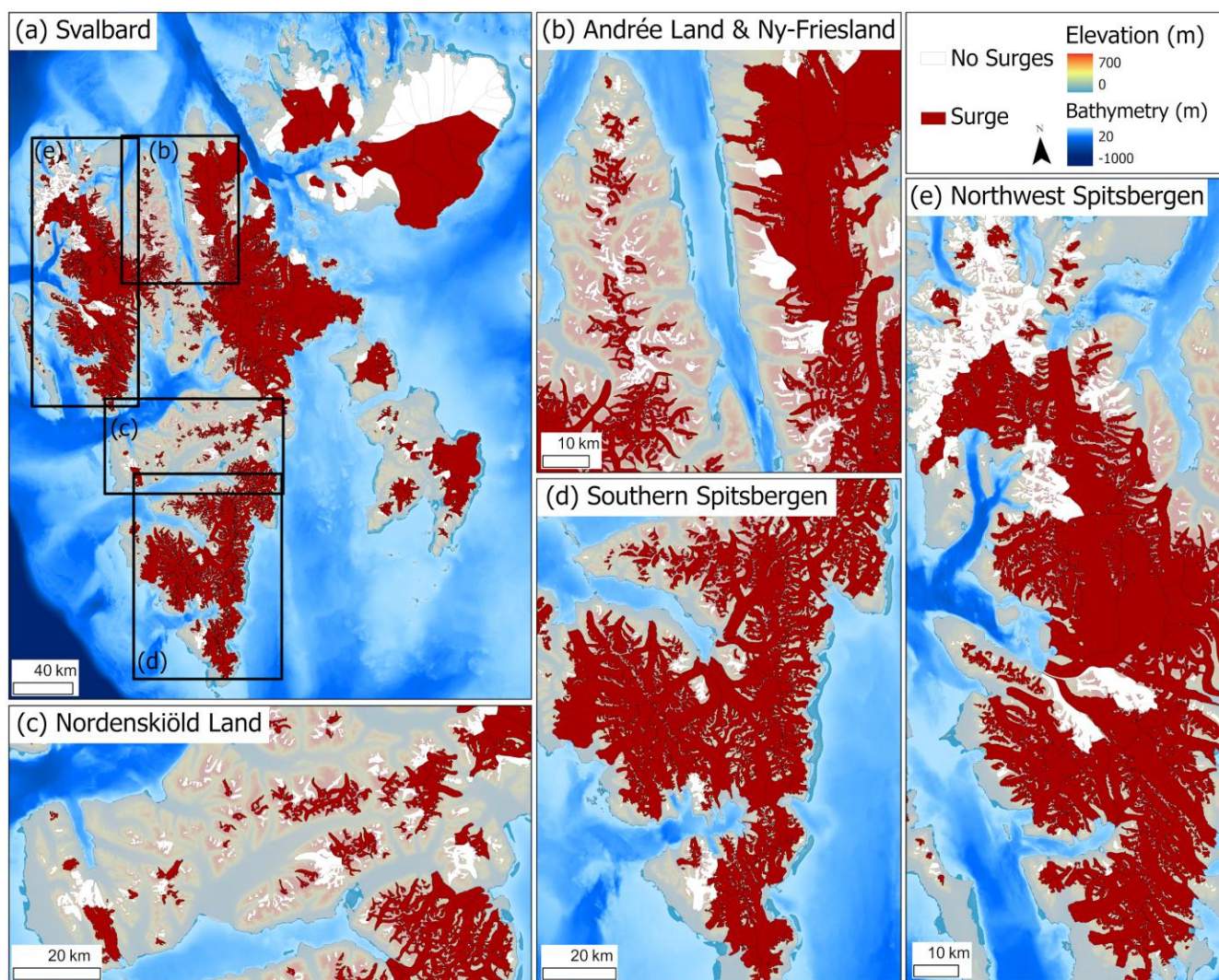


Figure 21 (a) Spatial distribution of all glaciers directly and indirectly (e.g. based on surge landforms, historical records) observed to surge in Svalbard. Regions consisting of several small glaciers are expanded for (b) Andrée Land & Ny Friesland, (c) Nordenskiöld Land, (d) Southern Spitsbergen, and (e) Northwest Spitsbergen. Bathymetry data is taken from the International Bathymetric Chart of the Arctic Ocean (IBCAO) (Jakobsson et al., 2024).

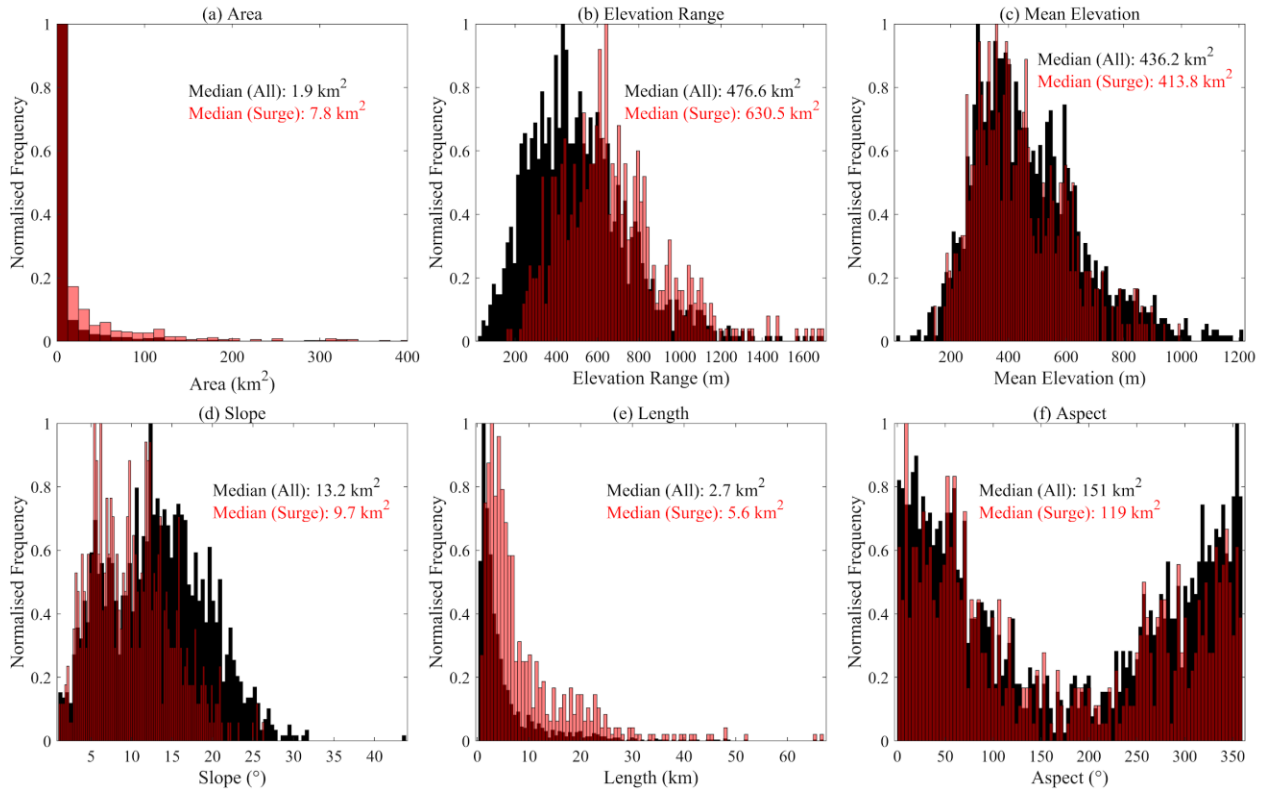


Figure 22 The characteristics of glaciers directly observed to surge (red) and all glaciers in Svalbard (black), including (a) area (km^2), (b) elevation range (m), (c) mean elevation (m), (d) Slope ($^\circ$), (e) length (m), and (f) aspect ($^\circ$). The glacier characteristics are taken from the RGI7.0 database.

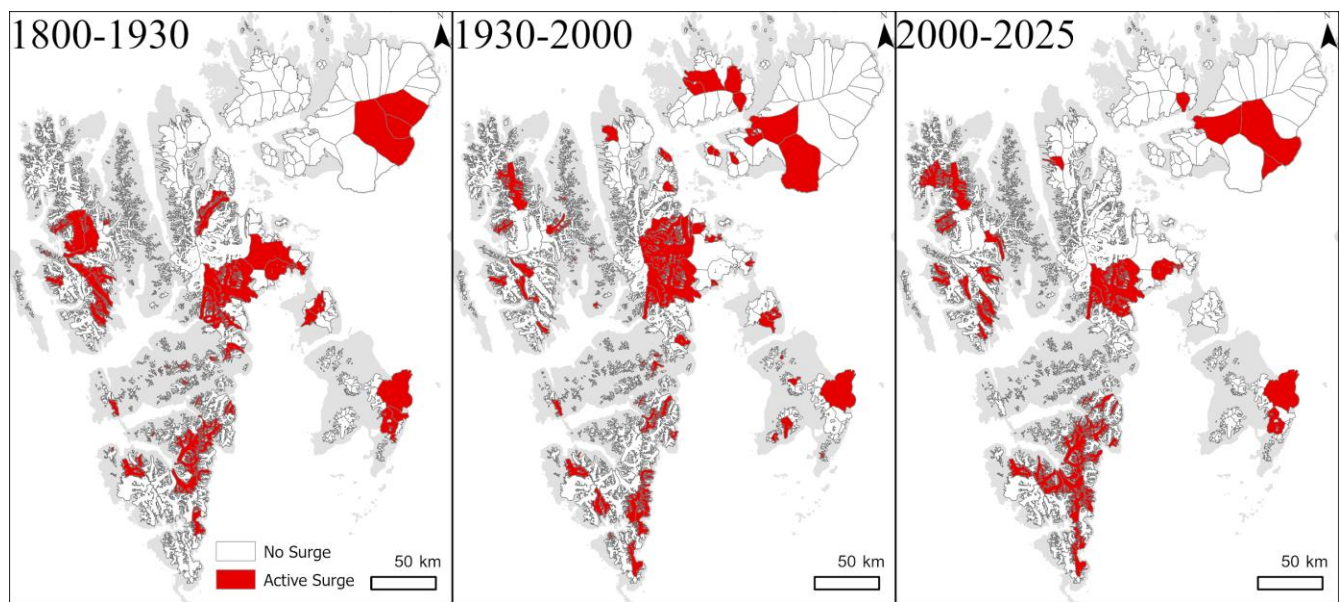
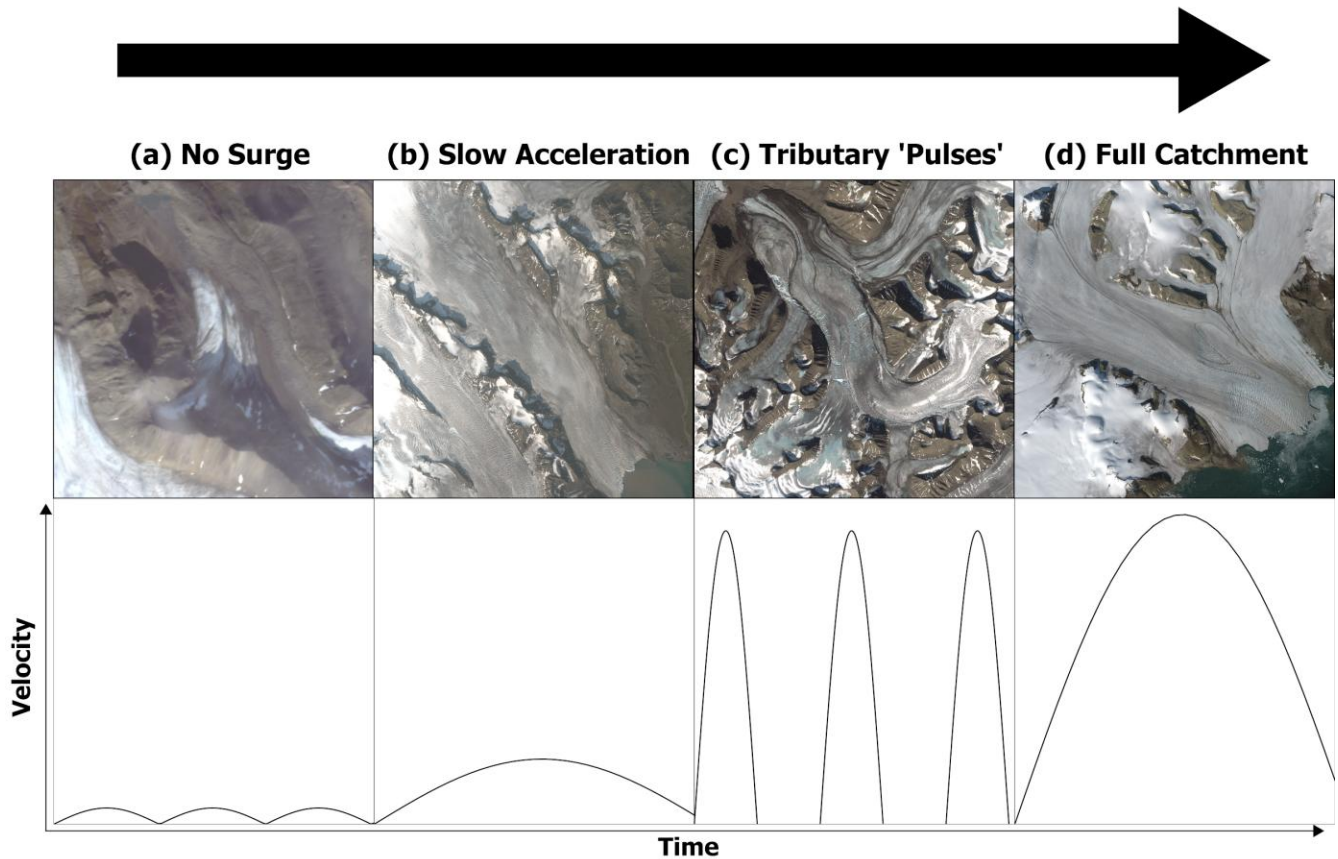


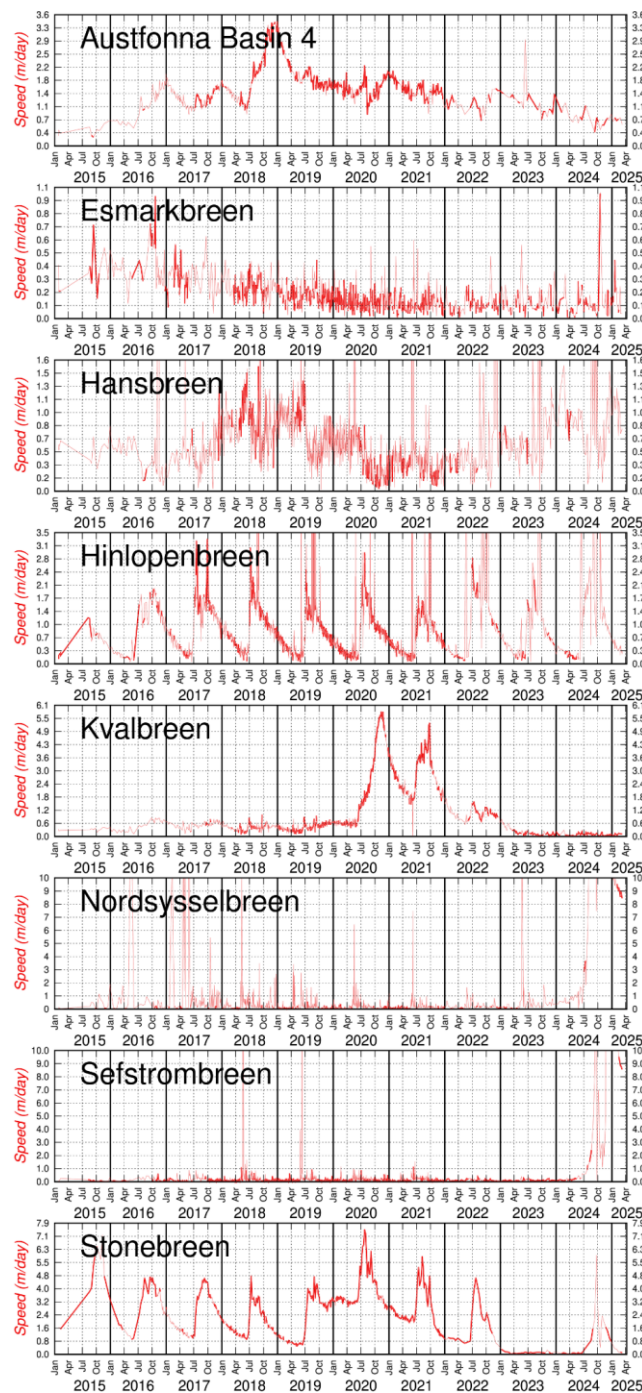
Figure 23 The temporal evolution of active surges across Svalbard in 1800-1930 (left), 1930-2000 (middle), and 2000-2025 (right) based on available, but likely incomplete, data. Active surges are shown in red.

Continuum of Glacier Surge Behaviour in Svalbard



1617

1618 **Figure 24** The continuum of surge-type behaviour in Svalbard. (a) Small glaciers are typically cold-
1619 based and do not surge, hence they represent an end-member of this continuum. (b) Some glaciers
1620 undergo a 'slow acceleration' but do not fully surge (e.g. pictured Sveabreen). (c) Moving along the
1621 continuum, glacier systems with several tributaries (e.g. pictured Paulabreen) are characterised by
1622 'Tributary Pulses'. (d) A 'Full Catchment' surge represents an end-member type and has been
1623 observed at glaciers such as Negribreen (pictured). The bottom panel indicates velocity profiles of
1624 each of the surge 'types' shown. The surge behaviours shown here are just a collection of a wider set
1625 of behaviours observed in Svalbard.



1626

1627 **Figure 25** Velocity time series of glaciers in Svalbard from 2015 to 2025 (10 years), generated using
 1628 Sentinel-1 feature-tracking. The time series demonstrate various surge-type behaviours ranging from:
 1629 well defined surges e.g. Nordsysselbreen (77.85°N, 17.93°E), Sefströmbreen (78.72°N, 14.21°E),
 1630 Kvalbreen (77.56°N, 17.92°E); seasonal cyclic behaviour e.g. Hinlopenbreen (79.08°N, 18.99°E),
 1631 Stonebreen (77.74°N, 23.97°E), low frequency multi-year cycles of fast and slow flow e.g. Hansbreen
 1632 (77.02°N, 15.63°E), and apparent speed-ups and multi-year slowdowns e.g. Austfonna Basin-4
 1633 (79.62°N, 25.58°E), Esmarkbreen (78.31°N, 13.85°E).

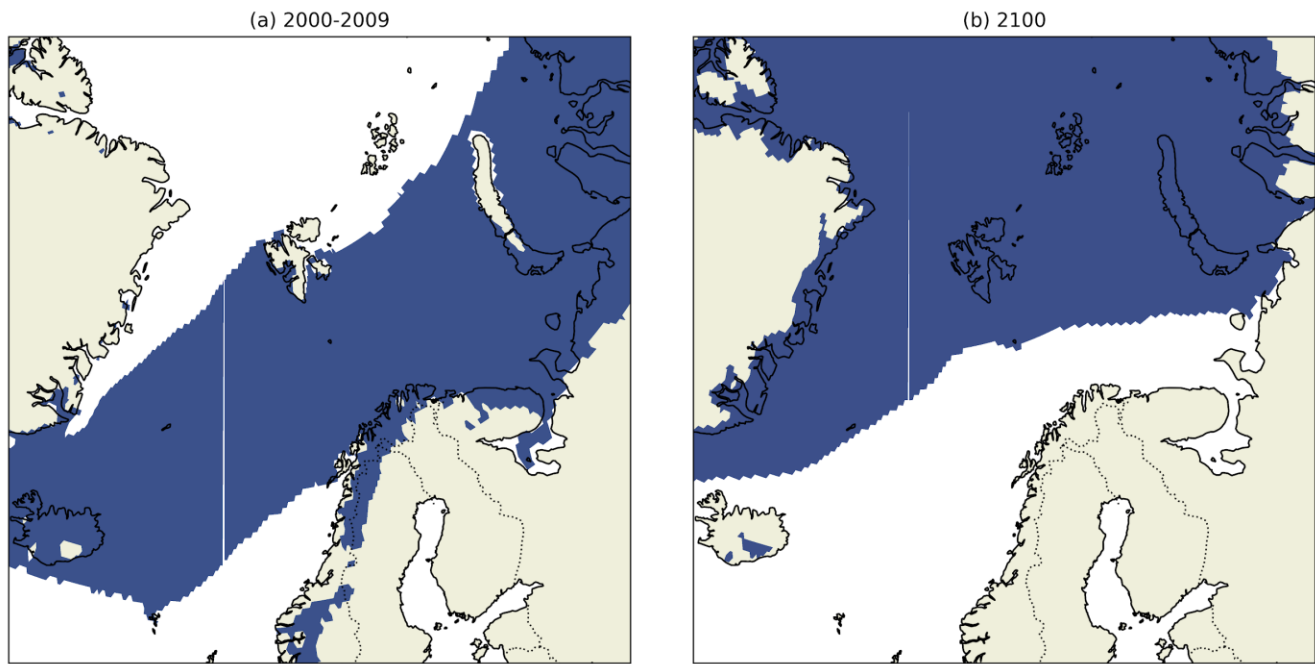


Figure 26: Climatic envelope (blue) encapsulating surge-type glaciers, derived from Sevestre and Benn (2015) and calculated from ERA5 reanalysis data. The panels show (a) the present-day climatic envelope, and b) the envelope simulated out to 2100 based on projections from Gutiérrez et al. (2021).

References

- Aradóttir, N., Ingólfsson, Ó., Noormets, R., Benediktsson, Í.Ö., Ben-Yehoshua, D., Håkansson, L., Schomacker, A. (2019). Glacial geomorphology of Trygghamna, western Svalbard - Integrating terrestrial and submarine archives for a better understanding of past glacial dynamics. *Geomorphology*, 344, 75-89. <https://doi.org/10.1016/j.geomorph.2019.07.007>
- Andreassen, K., Winsborrow, M.C.M., Bjarnadóttir, L.R., Ruther, D.C. (2014). Ice stream retreat dynamics inferred from an assemblage of landforms in the northern Barents Sea, *Quaternary Science Reviews*, 92, 246-257. <https://doi.org/10.1016/j.quascirev.2013.09.015>
- Aschwanden, A., Bueler, E., Khroulev, C., Blatter, H. (2012). An enthalpy formulation for glaciers and ice sheets, *Journal of Glaciology*, 58, 441-457. <https://doi.org/10.3189/2012JoG11J088>
- Aster, R. C., Winberry, J. P. (2017). Glacial seismology. *Reports on Progress in Physics*, 80, 126801. <https://doi.org/10.1088/1361-6633/aa8473>
- Bælum, K., Benn, D. I. (2011). Thermal structure and drainage system of a small valley glacier (Tellbreen, Svalbard), investigated by ground penetrating radar. *Cryosphere*, 5, 139-149. <https://doi.org/10.5194/tc-5-139-2011>
- Bahr, D.B., Pfeffer, W.T., Kaser, G. (2015). A review of volume-area scaling of glaciers, *Review of Geophysics*, 53, 95-140. <https://doi.org/10.1002/2014RG000470>
- Barrett, B. E., Murray, T., Clark, R., Matsuoka, K. (2008). Distribution and character of water in a surge-type glacier revealed by multifrequency and multipolarization ground-penetrating radar. *Journal of Geophysical Research: Earth Surface*, 113. <https://doi.org/10.1029/2007JF000972>
- Bartholomäus, T. C., Larsen, C. F., O'Neel, S., West, M. E. (2012). Calving seismicity from iceberg–sea surface interactions. *Journal of Geophysical Research: Earth Surface*, 117. <https://doi.org/10.1029/2012JF002513>
- Bartholomäus, T.C., Amundson, J.M., Walter, J.I., O'Neel, S., West, M.E., Larsen, C. F. (2015). Subglacial discharge at tidewater glaciers revealed by seismic tremor, *Geophysical Research Letters*, 42, 6391–6398. <https://doi.org/10.1002/2015GL064590>

1674 Barzycka, B., Błaszczyk, M., Grabiec, M., Jania, J. (2019). Glacier facies of Vestfonna (Svalbard)
 1675 based on SAR images and GPR measurements. *Remote Sensing of Environment*, 221, 373-385.
 1676 <https://doi.org/10.1016/j.rse.2018.11.020>.

1677 Barzycka, B., Grabiec, M., Błaszczyk, M., Ignatiuk, D., Laska, M., Hagen, J.O., Jania, J. (2020).
 1678 Changes of glacier facies on Hornsund glaciers (Svalbard) during the decade 2007-2017, *Remote*
 1679 *Sensing of Environment*, 251, 1-22. <https://doi.org/10.1016/j.rse.2020.112060>

1680 Ben-Yehoshua, D., Aradóttir, N., Farnsworth, W.R., Benediktsson, Í.Ö., Ingólfsson, Ó. (2023).
 1681 Formation of crevasse-squeeze ridges at Trygghamma, Svalbard, *Earth Surface Processes and*
 1682 *Landforms*, 48, 2334-2348. <https://doi.org/10.1002/esp.5631>.

1683 Benn, D.I., Kristensen, L., Gulley, J.D. (2009). Surge propagation constrained by a persistent
 1684 subglacial conduit, Bakaninbreen-Paulabreen, Svalbard, *Annals of Glaciology*, 50, 81-86.
 1685 <https://doi.org/10.3189/172756409789624337>

1686 Benn, D.I., Fowler, A.C., Hewitt, I., Sevestre, H. (2019a). A general theory of glacier surges, *Journal of*
 1687 *Glaciology*, 65, 701-716. <https://doi.org/10.1017/jog.2019.62>

1688 Benn, D.I., Jones, R.L., Luckman, A., Fürst, J.J., Hewitt, I., Sommer, C. (2019b). Mass and enthalpy
 1689 budget evolution during the surge of a polythermal glacier: A test of theory, *Journal of Glaciology*, 65,
 1690 717-731. <https://doi.org/10.1017/jog.2019.63>

1691 Benn, D.I., Hewitt, I.J., Luckman, A.J. (2022). Enthalpy balance theory unifies diverse glacier surge
 1692 behaviour, *Annals of Glaciology*, 63, 88-94. <https://doi.org/10.1017/aog.2023.23>

1693 Bennett, M. R., Hambrey, M. J., Huddart, D., Ghienne, J. F. (1996). The formation of a geometrical
 1694 ridge network by the surge-type glacier Kongsvegen, Svalbard. *Journal of Quaternary Science*:
 1695 *Published for the Quaternary Research Association*, 11(6), 437-449.
 1696 [https://doi.org/10.1002/\(SICI\)1099-1417\(199611/12\)11:6<437::AID-JQS269>3.0.CO;2-J](https://doi.org/10.1002/(SICI)1099-1417(199611/12)11:6<437::AID-JQS269>3.0.CO;2-J)

1697 Bintanja, R. (2018). The impact of Arctic warming on increased rainfall, *Scientific Reports*, 8, 16001.
 1698 <https://doi.org/10.1038/s41598-018-34450-3>

1699 Bjarnadóttir, L.R., Winsborrow, M.C.M, Andreassen, K. (2014). Deglaciation of the central Barents
 1700 Sea, *Quaternary Science Reviews*, 92, 208-226, <https://doi.org/10.1016/j.quascirev.2013.09.012>.

1701 Björnsson, H., Gjessing, Y., Hamran, S-E., Hagen, J.O., Liestøl, O., Pálsson, F., Erlingsson, B. (1996).
 1702 The thermal regime of sub-polar glaciers mapped by multi-frequency radio-echo sounding, *Journal of*
 1703 *Glaciology*, 42, 23-32. <https://doi.org/10.3189/S0022143000030495>

1704 Błaszczyk, M., Jania, J.A., Cieply, M., Grabiec, M., Ignatiuk, D., Kolondra, L., Kruss, A., Luks, B.,
 1705 Moskalik, M., Pastusiak, T., Strzelewicz, A., Walczowski, W., Wawrzyniak, T. (2021). Factors
 1706 controlling terminus position of Hansbreen, a tidewater glacier in Svalbard, *Journal of Geophysical*
 1707 *Research: Earth Surface*, 126, 1-20. <https://doi.org/10.1029/2020JF005763>

1708 Bouchayer, C., Aiken, J.M., Thøgersen, K., Renard, F., Schuler, T.V. (2022). A machine learning
 1709 framework to automate the classification of surge-type glaciers in Svalbard, *Journal of Geophysical*
 1710 *Research: Earth Surface*, 127, 1-26. <https://doi.org/10.1029/2022JF006597>.

1711 Bouchayer, C., Nanni, U., Lefeuvre, P-M., Hult, J., Schmidt, L.S., Kohler, J., Renard, F., Schuler, T.V.
 1712 (2024). Multi-scale variations of subglacial hydro-mechanical conditions at Kongsvegen glacier,
 1713 Svalbard, *Cryosphere*, 18, 2939-2968. <https://doi.org/10.5194/tc-18-2939-2024>.

1714 Boulton, G.S., Van Der Meer, J.J.M., Hart, J., Beets, D., Ruegg, G.H.J., Van Der Wateren, F.M.,
 1715 Jarvis, J. (1996). Till and moraine emplacement in a deforming bed surge – An example from a marine
 1716 environment, *Quaternary Science Reviews*, 15, 961-987. [https://doi.org/10.1016/0277-3791\(95\)00091-](https://doi.org/10.1016/0277-3791(95)00091-7)
 1717 [7](https://doi.org/10.1016/0277-3791(95)00091-7).

1718 Boulton, G.S., van der Meer, J.J.M., Beets, D.J., Hart, J.K., Ruegg, G.H.J. (1999). The sedimentary
 1719 and structural evolution of a recent push moraine complex: Holmströmbreen, Spitsbergen. *Quaternary*
 1720 *Science Reviews*, 18, 339-371. [https://doi.org/10.1016/S0277-3791\(98\)00068-7](https://doi.org/10.1016/S0277-3791(98)00068-7)

1721 Brandt, O., Kohler, J., Lüthje, M. (2008). Spatial mapping of multi-year superimposed ice on the
 1722 glacier Kongsvegen, Svalbard, *Journal of Glaciology*, 54, 73-80.
 1723 <https://doi.org/10.3189/002214308784409080>

1724 Clarke, G.K.C. (1976). Thermal regulation of glacier surging, *Journal of Glaciology*, 74, 231-250.
 1725 <https://doi.org/10.3189/S0022143000031567>

1726 Chandler, B.M.P., Lovell, H., Boston, C.M., Lukas, S., Barr, I.D., Benediktsson, Í.Ö., Benn, D.I., Clark,
 1727 C.D., Darvill, C.M., Evans, D.J.A., Ewertowski, M.W., Loibl, D., Margold, M., Otto, J-C., Roberts, D.H.,
 1728 Stokes, C.R., Storrar, R.D., Stroeve, A.P. (2018). Glacial geomorphological mapping: A review of
 1729 approaches and frameworks for best practice, *Earth Science Reviews*, 185, 806-846.
 1730 <https://doi.org/10.1016/j.earscirev.2018.07.015>

1731 Christoffersen, P., Piotrowski, J. A., & Larsen, N. K. (2005). Basal processes beneath an Arctic glacier
 1732 and their geomorphic imprint after a surge, Elisebreen, Svalbard. *Quaternary Research*, 64, 125-137.
 1733 <https://doi.org/10.1016/j.yqres.2005.05.009>

1734 Cichowicz, A. (1983). Icequakes and glacier motion: the Hans Glacier, Spitsbergen, *Pure and Applied*
 1735 *Geophysics*, 121, 27-38. <https://doi.org/10.1007/BF02590118>

1736 Commission scientifique du Nord (1852). *Voyages de la commission scientifique du Nord, en*
 1737 *Scandinavie, en Laponie, au Spitzberg et aux Féroë pendant les années 1838, 1839 et 1840*. Vol. 1.
 1738 Paris: Gide et J. Baudry, p. 300. Available at:
 1739 https://archive.org/details/FOLSC0948_1NOR/page/n273/mode/2up [Accessed 6 Apr. 2025].

1740 Conway, W.M. (1897). The First Crossing of Spitsbergen, *The Geographical Journal*, 9, 353-365.
 1741 <https://doi.org/10.2307/1774475>

1742 Crary, A.P. (1955). A brief study of ice tremors. *Bulletin of the Seismological Society of America*, 45, 1-
 1743 9. <https://doi.org/10.1785/BSSA0450010001>

1744 Croot DG (1988) Glaciotectonics and surging glaciers: a correlation based on Vestspitsbergen,
 1745 Svalbard, Norway. In: Croot DG (ed) *Glaciotectonics: forms and processes*. Balkema, Amsterdam, pp
 1746 49–62.

1747 Dachauer, A., Hann, R., Hodson, A.J. (2021). Aerodynamic roughness length of crevassed tidewater
 1748 glaciers from UAV mapping, *Cryosphere*, 15, 5513-5528. <https://doi.org/10.5194/tc-15-5513-2021>.

1749 de Geer, G. (1910). Guide de l'excursion au Spitsberg: Excursion A1 (Guide to excursions on
 1750 Spitsbergen: Excursion A1), paper presented at XI International Geological Congress. Exec. Comm.,
 1751 Stockholm.

1752 Delf, R., Bingham, R.G., Curtis, A., Singh, S., Giannopoulos, A., Schwarz, B., Borstad, C.P. (2022).
 1753 Reanalysis of polythermal glacier thermal structure using radar diffraction focusing, *Journal of*
 1754 *Geophysical Research: Earth Surface*, 127, e2021JF006382. <https://doi.org/10.1029/2021JF006382>

1755 Dowdeswell, J.A. Collin, R.L. (1990). Fast-flowing outlet glaciers on Svalbard ice caps, *Geology*, 18,
 1756 778-781. [https://doi.org/10.1130/0091-7613\(1990\)018%3C0778:FFOGOS%3E2.3.CO;2](https://doi.org/10.1130/0091-7613(1990)018%3C0778:FFOGOS%3E2.3.CO;2).

1757 Dowdeswell, J.A., Hamilton, G.S., Hagen, J.O. (1991). The duration of the active phase on surge-type
 1758 glaciers: Contrasts between Svalbard and other regions, *Journal of Glaciology*, 37, 388-400.
 1759 <https://doi.org/10.3189/S0022143000005827>

1760 Dowdeswell, J.A., Hodgkins, R., Nuttall, A-M., Hagen, J.O., Hamilton, G.S. (1995). Mass balance
 1761 change as a control on the frequency and occurrence of glacier surges in Svalbard, Norwegian High
 1762 Arctic, *Geophysical Research Letters*, 22, 2909-2912. <https://doi.org/10.1029/95GL02821>

1763 Dunse, T., Schuler, T.V., Hagen, J.O., Eiken, T., Brandt, O., Høgda, K.A. (2009). Recent fluctuations
 1764 in the extent of the firn area of Austfonna, Svalbard, inferred from GPR. *Annals of Glaciology*, 50, 155-
 1765 162. <https://doi.org/10.3189/172756409787769780>

1766 Dunse, T., Schuler, T.V., Hagen, J.O., Reijmer, C.H. (2012). Seasonal speed-up of two outlet glaciers
 1767 of Austfonna, Svalbard, inferred from continuous GPS measurements, *Cryosphere*, 6, 453-466.
 1768 <https://doi.org/10.5194/tc-6-453-2012>.

1769 Dunse, T., Schellenberger, T., Hagen, J. O., Kääb, A., Schuler, T. V., & Reijmer, C. H. (2015). Glacier-
 1770 surge mechanisms promoted by a hydro-thermodynamic feedback to summer melt. *Cryosphere*, 9,
 1771 197-215. <https://doi.org/10.5194/tc-9-197-2015>.

1772 Dyrda, M., Kułak, A., Trześniowski, Z., Trześniowski, M., Trześniowski, T., Worek, C., Ziętara, K.
 1773 (2023). Spectral ground penetrating radar - An innovative tool for multispectral subsurface probing and
 1774 modelling, NSG2023 29th European Meeting of Environmental and Engineering Geophysics, 1-5.
 1775 <https://doi.org/10.3997/2214-4609.202320038>

1776 Eiken, T., Hagen, J.O., Melvold, K. (1997). Kinematic GPS survey of geometry changes on Svalbard
 1777 glaciers, *Annals of Glaciology*, 24, 157-163. <https://doi.org/10.3189/S0260305500012106>.

1778 Evans, D.J.A., Rea, B.R. (1999). Geomorphology and sedimentology of surging glaciers: A land-
 1779 systems approach, *Annals of Glaciology*, 28, 75-82. <https://doi.org/10.3189/172756499781821823>.

1780 Evans, D.J.A. (2005). *Glacial landsystems*, London, Arnold.

1781 Evans, D.J.A., Ewertowski, M., Roberts, D.H., Tomczyk, A.M. (2022). The historical emergence of a
 1782 geometric and sinuous ridge network at the Hørbyebreen polythermal glacier snout, Svalbard and its
 1783 use in the interpretation of ancient glacial landforms, *Geomorphology*, 406, 1-22.
 1784 <https://doi.org/10.1016/j.geomorph.2022.108213>.

1785 Farnsworth, W.R., Ingólfsson, Ó., Retelle, M., Schomacker, A. (2016). Over 400 previously
1786 undocumented Svalbard surge-type glaciers identified, *Geomorphology*, 264, 52-60.
1787 <https://doi.org/10.1016/j.geomorph.2016.03.025>.

1788 Farnsworth, W.R., Allaart, L., Ingólfsson, Ó., Alexanderson, H., Forwick, M., Noormets, R., Retelle, M.,
1789 Schomacker, A. (200). Holocene glacial history of Svalbard: Status, perspectives and challenges,
1790 *Earth Science Reviews*, 208, 103249. <https://doi.org/10.1016/j.earscirev.2020.103249>

1791 Flink, A.E., Noormets, R. (2018). Submarine glacial landforms and sedimentary environments in
1792 Vaigattbogen, *Marine Geology*, 402, 244-263. <https://doi.org/10.1016/j.margeo.2017.07.019>

1793 Flink, A.E., Noormets, R., Kirchner, N., Benn, D.I., Luckman, A., Lovell, H. (2015). The evolution of a
1794 submarine landform record following recent and multiple surges of Tunabreen glacier, Svalbard,
1795 *Quaternary Science Reviews*, 108, 37-50. <https://doi.org/10.1016/j.quascirev.2014.11.006>

1796 Flink, A.E., Noormets, R., Fransner, O., Hogan, K.A., O'Regan, M., Jakobsson, M. (2017). Past ice
1797 flow in Wahlenbergfjorden and its implications for late Quaternary ice sheet dynamics in northeastern
1798 Svalbard. *Quaternary Science Reviews*, 163, 162-179. <https://doi.org/10.1016/j.quascirev.2017.03.021>

1799 Flink, A.E., Hill, P., Noormets, R., Kirchner, N. (2018). Holocene glacial evolution of Mohnbukta in
1800 eastern Spitsbergen. *Boreas*, 47, 390-409. <https://doi.org/10.1111/bor.12277>

1801 Fowler, A.C. (1987). A theory of glacier surges, *Journal of Geophysical Research: Solid Earth*, 92,
1802 9111-9120. <https://doi.org/10.1029/JB092iB09p09111>

1803 Fowler, A.C., Murray, T., Ng, F.S.L. (2001). Thermally controlled glacier surging, *Journal of*
1804 *Glaciology*, 47, 527-538. <https://doi.org/10.3189/172756501781831792>

1805 Friedl, P., Seehaus, T., Braun, M. (2021). Global time series and temporal mosaics of glacier surface
1806 velocities derived from Sentinel-1 data, *Earth System Science Data*, 13, 4653-4675.
1807 <https://doi.org/10.5194/essd-13-4653-2021>

1808 Fürst, J.J., Navarro, F., Gillet-Chaulet, F., Huss, M., Moholdt, G., Fettweis, X., Lang, C., Seehaus, T.,
1809 Ai, S., Benham, T.J., Benn, D.I., Björnsson, H., Dowdeswell, J.A., Grabiec, M., Kohler, J., Lavrentiev,
1810 I., Lindbäck, K., Melvold, K., Pettersson, R., Rippin, D., Saintenoy, A., Sánchez-Gómez, P., Schuler,
1811 T.V., Sevestre, H., Vasilenko, E., Braun, M.H. (2018). The ice-free topography of Svalbard,
1812 *Geophysical Research Letters*, 45, 11760-11769. <https://doi.org/10.1029/2018GL079734>

1813 Gajek, W., Trojanowski, J., Malinowski, M. (2017). Automating long-term glacier dynamics monitoring
 1814 using single-station seismological observations and fuzzy logic classification: a case study from
 1815 Spitsbergen, *Journal of Glaciology*, 63, 581-592. <https://doi.org/10.1017/jog.2017.25>

1816 Gajek, W., Gräff, D., Hellmann, S., Rempel, A. W., Walter, F. (2021). Diurnal expansion and
 1817 contraction of englacial fracture networks revealed by seismic shear wave splitting, *Communications*
 1818 *Earth & Environment*, 2, 209. <https://doi.org/10.1038/s43247-021-00279-4>

1819 Gajek, W., Köhler, A., Wuestefeld, A., & Hanssen, A. (2024). Hornsund 2023–2024 geophone seismic
 1820 data (FROST). *Dataset*.
 1821 https://doi.org/10.25171/InstGeoph_PAS_IGData_FROST_geophone_seismic_data_Hornsund_2023_2024
 1822 [2024](https://doi.org/10.25171/InstGeoph_PAS_IGData_FROST_geophone_seismic_data_Hornsund_2023_2024)

1823 Gajek W., Luckman A., Harcourt W. D, Pearce D. M., Hann R. (2025) Utilising seismic station internal
 1824 GPS for tracking surging glacier sliding velocity. *Journal of Glaciology*, 71, e40.
 1825 <https://doi.org/10.1017/jog.2025.30>

1826 Gardner, A.S., Greene, C.A., Kennedy, J.H., Fahnestock, M.A., Liukis, M., López, L.A., Lei, Y.,
 1827 Scambos, T.A., Dehecq, A. (2025). ITS_LIVE global glacier velocity data in near real time, *EGUsphere*
 1828 [preprint]. <https://doi.org/10.5194/egusphere-2025-392>

1829 Garwood, E. J., Gregory, J. W. (1898). Contributions to the glacial geology of Spitsbergen, *Quarterly*
 1830 *Journal of the Geological Society*, 54, 197–227. <https://doi.org/10.1144/GSL.JGS.1898.054.01-04.1>

1831 Geyman, E.C., van Pelt, W.J.J., Maloof, A.C., Aas, H.F., Kohler, J. (2022). Historical glacier change
 1832 on Svalbard predicts doubling of mass loss by 2100, *Nature*, 601, 374-379.
 1833 <https://doi.org/10.1038/s41586-021-04314-4>

1834 Gilbert, A., Gimbert, F., Thørgersen, K., Schuler, T.V., Käab, A. (2022). A consistent framework for
 1835 coupling basal friction with subglacial hydrology on hard-bedded glaciers, *Geophysical Research*
 1836 *Letters*, 49, e2021gl097507. <https://doi.org/10.1029/2021GL097507>

1837 Gillet-Chaulet, F., Hindmarsh, R. C., Corr, H. F., King, E. C., Jenkins, A. (2011). In-situ quantification
 1838 of ice rheology and direct measurement of the Raymond Effect at Summit, Greenland using a phase-
 1839 sensitive radar. *Geophysical Research Letters*, 38, L24503. <https://doi.org/10.1029/2011GL049843>

1840 Gimbert, F., Tsai, V. C., Amundson, J. M., Bartholomaeus, T. C., Walter, J. I. (2016). Subseasonal
 1841 changes observed in subglacial channel pressure, size, and sediment transport. *Geophysical*
 1842 *Research Letters*, 43(8), 3786-3794. <https://doi.org/10.1002/2016GL068337>

1843 Girod, L., Nuth, C., Kääh, A., Etzelmüller, B., Kohler, J. (2017). Terrain changes from images acquired
 1844 on opportunistic flights by SfM photogrammetry, *Cryosphere*, 11, 827-840. [https://doi.org/10.5194/tc-](https://doi.org/10.5194/tc-11-827-2017)
 1845 [11-827-2017](https://doi.org/10.5194/tc-11-827-2017)

1846 Glasser, N.F., Coulson, S.J., Hodkinson, I.D., Webb, N.R. (2004). Photographic evidence of the return
 1847 period of a Svalbard surge-type glacier: A tributary of Pedersenbreen, Kongsfjord, *Journal of*
 1848 *Glaciology*, 50, 307-308. <https://doi.org/10.3189/172756504781830060>.

1849 Górski, M., Teisseyre, R. (1991). Seismic events in Hornsund, Spitsbergen, *Polish Polar Research*,
 1850 12, 345-352.

1851 Gräff, D., & Walter, F. (2021). Changing friction at the base of an Alpine glacier, *Scientific reports*, 11,
 1852 10872. <https://doi.org/10.1038/s41598-021-90176-9>

1853 Gregory, J. W., Garwood, M., Trevor-Battye, M. (1897). The First Crossing of Spitsbergen: Discussion.
 1854 *The Geographical Journal*, 9, 365–368. <https://doi.org/10.2307/1774476>

1855 Gripp, K. (1929). Glaciologische und geologische Ergebnisse der Hamburgischen Spitzbergen-
 1856 Expedition 1927. *Abhandlungen aus dem Gebiete der Naturwissenschaften*, 22(3/4), 145-249.

1857 Gutiérrez, J.M., Jones, R.G., Narisma, G.T., Alves, L.M., Amjad, M., Gorodetskaya, I.V., Grose, M.,
 1858 Klutse, N.A.B., Krakovska, S., Li, J., Martinez-Castro, D., Mearns, L.O., Mernild, S.H., Ngo-Duc, T.,
 1859 van den Hurk, B., Yoon, J-H. (2021). Atlas. In *Climate Change 2021: The Physical Science Basis*.
 1860 Contribution of Working Group I to the Sixth Assessment Report of the Intergovernmental Panel on
 1861 Climate Change [Masson-Delmotte, V., Zhai, P., Pirano, A., Connors, S.L., Péan, C., Berger, S.,
 1862 Caud, N., Chen, Y., Goldfarb, L., Gomis, M.I., Huang, M., Leitzell, K., Lonnoy, E., Matthews, J.B.R.,
 1863 Maycock, T.K., Waterfield, T., Yelekçi, O., Yu, R., Zhou, B. (eds.)]. Cambridge University Press,
 1864 Cambridge, United Kingdom and New York, NY, USA, pp. 1927–2058, doi:
 1865 <https://doi.org/10.1017/9781009157896.021>

1866 Haas, C. , Happ, L. , Landy, J. and Krumpen, T. (2024): Campaign Report: IceBird Summer 2023 -
 1867 Polar 5 / C. Haas (editor) , [Other]

1868 Haga, O.N., McNabb, R., Nuth, C., Altena, B., Schellenberger, T., Kääb, A. (2020). From high friction
1869 zone to frontal collapse: Dynamics of an ongoing tidewater glacier surge, Negribreen, Svalbard,
1870 Journal of Glaciology, 66, 742-754, <https://doi.org/10.1017/jog.2020.43>

1871 Hagen, J.O., Liestøl, O., Roland, E., Jørgensen, T. (1993). Glacier Atlas of Svalbard and Jan Mayen,
1872 Norwegian Polar Institute, Oslo, Norway.

1873 Hagen J.O., Eiken, T., Kohler, J., Melvold, K. (2005). Geometry changes on Svalbard glaciers: Mass-
1874 balance or dynamic response, Annals of Glaciology, 42, 255-261.
1875 <https://doi.org/10.3189/172756405781812763>.

1876 Hald, M., Dahlgren, T., Olsen, T.E., Lebesbye, E., (2001). Late Holocene palaeoceanography in Van
1877 Mijenfjorden, Svalbard. Polar Research, 20, 23-35. <https://doi.org/10.3402/polar.v20i1.6497>

1878 Hamberg, A. (1894). En resa till norra Ishafvet sommaren 1892. Ymer, 14:25–61.

1879 Hamilton, G.S., Dowdeswell, J.A. (1996). Controls on glacier surging in Svalbard, Journal of
1880 Glaciology, 42, 157-168. <https://doi.org/10.3189/S0022143000030616>.

1881 Hann, R., Altstädter, B., Betlem, P., Deja, K., Dragańska-Deja K., Ewertowski, M., Hartvich, F.,
1882 Jonassen, M., Lampert, A., Laska, M., Sobota, I., Storvold, R., Tomczyk, A., Wojtysiak, K. Zagórski P.
1883 (2021). Scientific Applications of Unmanned Vehicles in Svalbard. SESS Report 2020, Svalbard
1884 Integrated Arctic Earth Observing System. doi.org/10.5281/zenodo.4293283

1885 Hann, R., Betlem, P., Deja, K., Hartvich, F., Jonassen, M., Lampert, A., Laska, M., Sobota, I.,
1886 Storvold, R., Zagórski P. (2022). Update to Scientific Applications of Unmanned Vehicles in Svalbard.
1887 SESS Report 2021, Svalbard Integrated Arctic Earth Observing System.
1888 doi.org/10.5281/zenodo.5751959

1889 Hann, R., Betlem, P., Deja, K., Ewertowski, M., Harm-Altstädter, B., Jonassen, M., Lampert, A., Laska,
1890 M., Sobota, I., Storvold, R., Tomczyk, A., & Zagorski, P. (2023). Practical Guidelines for Scientific
1891 Application of Uncrewed Aerial Vehicles in Svalbard (UAV Svalbard 3). In SESS report 2022 - The
1892 State of Environmental Science in Svalbard - an annual report (pp. 142–152). Svalbard Integrated
1893 Arctic Earth Observing System. <https://doi.org/10.5281/zenodo.7371141>.

1894 Hann, R., Rodes, N. Gajek, W. Pearce, D., Harcourt, W.D. (2024). Drone-based mapping of calving
1895 rates of Borebreen in Svalbard, <https://doi.org/10.18710/B553MB>, DataverseNO, V1

1896 Hansen, S. (2003). From surge-type to non-surge-type glacier behaviour: Midre Lovénbreen,
1897 Svalbard, *Annals of Glaciology*, 36, 97-102. <https://doi.org/10.3189/172756403781816383>

1898 Hanssen-Bauer, I., Førland, E.J., Hisdal, H., Mayer, S., Sandø, A.B., Sorteberg, A. (eds) (2019)
1899 Climate in Svalbard 2100 - a knowledge base for climate adaptation. Norway, Norwegian Centre of
1900 Climate Services (NCCS) for Norwegian Environment Agency (Miljødirektoratet), 208pp. (NCCS report
1901 1/2019). DOI: <http://dx.doi.org/10.25607/OBP-888>

1902 Harcourt, W.D., Robertson, D.A., Macfarlane, D.G., Rea, B.R., Spagnolo, M., Benn, D.I., James, M.R.,
1903 (2022). Glacier monitoring using real-aperture 94 GHz radar. *Annals of Glaciology*, 63, 116-120.
1904 <https://doi.org/10.1017/aog.2023.30>

1905 Harcourt, W.D., Gajek, W., Pearce, D., Hann, R., Luckman, A., Rea, B.R., Benn, D.I., James, M.R.,
1906 Spagnolo, M., Nanni, U. (2024). Surge initiation at the terminus of Borebreen (Svalbard): Drivers and
1907 impact on calving. EGU General Assembly 2024, Vienna, Austria. [https://doi.org/10.5194/egusphere-](https://doi.org/10.5194/egusphere-egu24-1505)
1908 [egu24-1505](https://doi.org/10.5194/egusphere-egu24-1505)

1909 Harcourt, W.D., Pearce, D.M., Gajek, W., Lovell, H., Luckman, A., Benn, D., Kohler, J., Kääh, A.,
1910 Hann, R. (2025a). Surging glaciers in Svalbard: Current knowledge and perspectives for monitoring
1911 (SvalSurge). In SESS report 2024 - The State of Environmental Science in Svalbard - an annual report
1912 (pp. 84–105). Svalbard Integrated Arctic Earth Observing System.
1913 <https://doi.org/10.5281/zenodo.14425522>

1914 Harcourt, W.D., Pearce, D., Gajek, W., Lovell, H., Mannerfelt, E.S., Kääh, A., Benn, D., Luckman, A.,
1915 Hann, R., Kohler, J. (2025b). Svalbard Surge Database 2024 (RGI2000-v7.0-G-07) [Data set].
1916 Zenodo. <https://doi.org/10.5281/zenodo.15240754>

1917 Hart, J.K., Watts, R.J. (1997). A comparison of the styles of deformation associated with two recent
1918 push moraines, south van Keulenfjorden, Svalbard, *Earth Surface Processes and Landforms*, 22,
1919 1089-1107. [https://doi.org/10.1002/\(SICI\)1096-9837\(199712\)22:12<1089::AID-ESP804>3.0.CO;2-8](https://doi.org/10.1002/(SICI)1096-9837(199712)22:12<1089::AID-ESP804>3.0.CO;2-8)

1920 Hatherton, T., Evison, F.F. (1962). A special mechanism for some Antarctic earthquakes, *New*
1921 *Zealand Journal of Geology and Geophysics*, 5, 864-873.
1922 <https://doi.org/10.1080/00288306.1962.10417642>

1923 Hodgkins, R., Hagen, J.O., Hamran, S-E. (1999). 20th century mass balance and thermal regime
1924 change at Scott Turnerbreen, Svalbard, *Annals of Glaciology*, 28, 216-220.
1925 <https://doi.org/10.3189/172756499781821986>

1926 Hodgkins, R., Fox, A., Nuttall, A-M. (2007). Geometry change between 1990 and 2003 at
 1927 Finsterwalderbreen, a Svalbard surge-type glacier, from GPS profiling, *Annals of Glaciology*, 46, 131-
 1928 135. <https://doi.org/10.3189/172756407782871189>.

1929 Hoel, A. 1914: Exploration du Nord-ouest Spitsbergen entreprise sous les auspices de S.A.S. le
 1930 Prince de Monaco par la Mission Isachsen. Troisieme partie. RPsultats des campagnes scienrifiques
 1931 accomplies sur son yachtpar ler Prince Souuerain de Monaco, farc. XLII, 1-160.

1932 Holmlund, P., Martinsson, T. (2016). Den norsk-brittisk-svenska Antarktisexpeditionen (NSBX). In: J.
 1933 Hedberg, ed., *Frusna ögonblick: Svensk polarfotografi 1861–1980*. Stockholm: Art and Theory
 1934 Publishing, pp.216–229.

1935 Hopwood, M.J., Carroll, D., Dunse, T., Hodson, A., Holding, J.M., Iriarte, J.L., Ribeiro, S., Achterberg,
 1936 E.P., Cantoni, C., Carlson, D.F., Chierici, M., Clarke, J.S., Cozzi, S., Fransson, A., Juul-Pedersen, T.,
 1937 Winding, M.H.S., Meire, L. (2020). Review article: How does glacier discharge affect marine
 1938 biogeochemistry and primary production in the Arctic, *Cryosphere*, 14, 1347-1383.
 1939 <https://doi.org/10.5194/tc-14-1347-2020>

1940 How, P., Benn, D.I., Hulton, N.R.J., Hubbard, B., Luckman, A., Sevestre, H., van Pelt, W.J.J.,
 1941 Lindbäck, K., Kohler, J., Boot, W. (2017). Rapidly changing subglacial hydrological pathways at a
 1942 tidewater glacier revealed through simultaneous observations of water pressure, supraglacial lakes,
 1943 meltwater plumes and surface velocities, *Cryosphere*, 11, 2691-2710. [https://doi.org/10.5194/tc-11-](https://doi.org/10.5194/tc-11-2691-2017)
 1944 [2691-2017](https://doi.org/10.5194/tc-11-2691-2017)

1945 Howe, J.A., Husum, K., Inall, M.E., Coogan, J., Luckman, A., Arosio, R., Abernethy, C., Verchili, D.
 1946 (2019). Autonomous underwater vehicle (AUV) observations of recent tidewater glacier retreat,
 1947 western Svalbard, *Marine Geology*, 417. <https://doi.org/10.1016/j.margeo.2019.106009>

1948 Hudson, T.S., Baird, A.F., Kendall, J.M., Kufner, S.K., Brisbourne, A.M., Smith, A.M., Butcher, A.,
 1949 Chalari, A., Clarke, A. (2021). Distributed Acoustic Sensing (DAS) for natural microseismicity studies:
 1950 A case study from Antarctica. *Journal of Geophysical Research: Solid Earth*, 126, e2020JB021493.
 1951 <https://doi.org/10.1029/2020JB021493>

1952 Inall, M.E., Sundfjord, A., Cottier, F., Korte, M-L., Slater, D.A., Venables, E.J., Coogan, J. (2024).
 1953 Mixing, water transformation, and melting close to a tidewater glacier, *Geophysical Research Letters*,
 1954 51, e2024GL108421, <https://doi.org/10.1029/2024GL108421>

1955 Ingólfsson, Ó., Landvik, J.Y. (2013). The Svalbard-Barents ice-sheet - Historical, current and future
1956 perspectives, Quaternary Science Reviews, 64, 33-60. <https://doi.org/10.1016/j.quascirev.2012.11.034>

1957 Jakobsson, M., Mohammad, R., Karlsson, M., Salas-Romero, S., Vacek, F., Heinze, F., Bringensparr,
1958 C., Castro, C.F., Johnson, P., Kinney, J., Cardigos, S., Bogonko, M., Accettella, D., Amblas, D., An, L.,
1959 Bohan, A., Brandt, A., Bünz, S., Canals, M., Casamor, J.L., Coakley, B., Cornish, N., Danielson, S.,
1960 Demarte, M., Di Franco, D., Dickson, M-L., Dorschel, B., Dowdeswell, J.A., Dreutter, S., Freman, A.C.,
1961 Hall, J.K., Hally, B., Holland, D., Hongm J.K., Ivaldi, R., Knutz, P.C., Krawczyk, D.W., Kristofferson, Y.,
1962 Lastras, G., Leck, C., Lucchi, R.G., Masetti, G., Morlighem, M., Muchowski, J., Nielsen, T., Noormets,
1963 R., Plaza-Faverola, A., Prescott, M.M., Purser, A., Rasmussen, T.L., Rebesco, M., Rignot, E.,
1964 Rysgaard, S., Silyakova, A., Snoeijs-Leijonmalm, P., Sørensen, A., Straneo, F., Sutherland, D.A.,
1965 Tate, A.J., Travaglini, P., Trenholm, N., van Wijk, E., Wallace, L., Willis, J.K., Wood, M., Zimmerman,
1966 M., Zinglensen, K.B., Mayer, L. (2024). The International Bathymetric Chart of the Arctic Ocean version
1967 5.0, Scientific Reports, 11, 1420. <https://doi.org/10.1038/s41597-024-04278-w>

1968 Jenssen, R-O.R., Vickers, H., Ricker, R., Malnes, E., Jacobsen, S. (2024). Drone-mounted snow radar
1969 system - Quantitative field validation of terrestrial snow measurements, Proceedings of the
1970 International Snow Science Workshop, Tromsø, Norway, 1073-1078.

1971 Jiskoot, H., Boyle, P., Murray, T. (1998). The incidence of glacier surging in Svalbard: Evidence from
1972 multivariate statistics, Computers and Geoscience, 24, 387-399. [https://doi.org/10.1016/S0098-](https://doi.org/10.1016/S0098-3004(98)00033-8)
1973 [3004\(98\)00033-8](https://doi.org/10.1016/S0098-3004(98)00033-8).

1974 Jiskoot, H., Murray, T., Boyle, P. (2000). Controls on the distribution of surge-type glaciers in
1975 Svalbard, Journal of Glaciology, 46, 412-422. <https://doi.org/10.3189/172756500781833115>.

1976 Kääb, A., Jacquemart, M., Gilbert, A., Leinss, S., Girod, L., Huggel, C., Falaschi, D., Ugalde, F.,
1977 Petrakov, Chernomorets, S., Dokukin, M., Paul, F., Gascoin, S., Berthier, E., Kargel, J.S. (2021).
1978 Sudden large-volume detachments of low-angle mountain glaciers - more frequent than thought?,
1979 Cryosphere, 15, 1751-1785. <https://doi.org/10.5194/tc-15-1751-2021>

1980 Kääb, A., Bazilova, V., Leclercq, P.W., Mannerfelt, E.S., Strozzi, T. (2023). Global clustering of recent
1981 glacier surges from radar backscatter data, 2017-2022, Journal of Glaciology, 69, 1515-1523.
1982 <https://doi.org/10.1017/jog.2023.35>.

1983 Kamb, B. (1987). Glacier surge mechanism based on linked cavity configuration of the basal water
1984 conduit system, *Journal of Geophysical Research: Solid Earth*, 92, 9083-9200.
1985 <https://doi.org/10.1029/JB092iB09p09083>

1986 Kamb, B., Raymond, C.F., Harrison, W.D., Engelhardt, H., Echelmeyer, K.A., Humphrey, N.,
1987 Brugman, M.M., Pfeffer, T. (1985). Glacier surge mechanism: 1982-1983 surge of Variegated Glacier,
1988 Alaska, *Science*, 227, 469-479. <https://doi.org/10.1126/science.227.4686.469>

1989 Karušs, J., Lamsters, K., Ješkins, J., Sobota, I., Džeriņš, P. (2022). UAV and GPR data integration in
1990 glacier geometry reconstruction: a case study from Irenebreen, Svalbard. *Remote Sensing*, 14, 456.
1991 <https://doi.org/10.3390/rs14030456>

1992 Kavan, J., Tallentire, G.D., Demidionov, M., Dudek, J., Strzelecki, M.C. (2022). Fifty years of tidewater
1993 glacier surface elevation and retreat dynamics along the south-east coast of Spitsbergen (Svalbard
1994 Archipelago), *Remote Sensing*, 13, 354. <https://doi.org/10.3390/rs14020354>.

1995 Kavan, J., Luláková, P., Malecki, J., Strzelecki, C. (2024). Capturing the transition from marine to land-
1996 terminating glacier from the 126-year retreat history of Nordenskiöldbreen, Svalbard, *Journal of*
1997 *Glaciology*, 70, e70. <https://doi.org/10.1017/jog.2023.92>

1998 Kempf, P., Forwick, M., Laberg, J.S., Vorren, T.O. (2013). Late Weichselian and Holocene sedimentary
1999 palaeoenvironment and glacial activity in the high-arctic van Keulenfjorden, Spitsbergen, *Holocene*, 23,
2000 1607-1618. <https://doi.org/10.1177/0959683613499055>

2001 King, O., Hambrey, M.J., Irvine-Flynn, T.D.L., Holt, T.O. (2016). The structural, geometric and
2002 volumetric changes of a polythermal Arctic glacier during a surge cycle: Comfortlessbreen, Svalbard,
2003 *Earth Surface Processes and Landforms*, 41, 162-177. <https://doi.org/10.1002/esp.3796>

2004 Kingslake, J., Hindmarsh, R.C.A., Aðalgeirsdóttir, G., Conway, H., Corr, H.F.J., Gillet-Chaulet, F.,
2005 Martín, C., King, E.C., Mulvaney, R., Pritchard, H.D. (2014). Full-depth englacial vertical ice sheet
2006 velocities measured using phase-sensitive radar. *Journal of Geophysical Research: Earth Surface*,
2007 119, 2604-2618.

2008 Kleber, G., Hodson, A.J., Magerl, L., Mannerfelt, E.S., Bradbury, H.J., Zhu, Y., Trimmer, M., Turchyn,
2009 A.V. (2023). Groundwater springs formed during glacial retreat are a large source of methane in the
2010 high Arctic, *Nature Geoscience*, 16, 597-604. <https://doi.org/10.1038/s41561-023-01210-6>

2011 Kleber, G.E., Magerl, L., Turchyn, A.V., Schloemer, S., Trimmer, M., Zhu, Y., Hodson, A. (2025).
 2012 Proglacial methane emissions driven by meltwater and groundwater flushing in a high-Arctic glacial
 2013 catchment, Biogeosciences, 22, 659-674. <https://doi.org/10.5194/bg-22-659-2025>

2014 Koch, M., Seehaus, T., Friedl, P., Braun, M. (2023). Automated detection of glacier surges from
 2015 Sentinel-1 surface velocity time series – An example from Svalbard, Remote Sensing, 15, 1545.
 2016 <https://doi.org/10.3390/rs15061545>

2017 Köhler, A., Nuth, C., Schweitzer, J., Weidle, C., Gibbons, S.J. (2015). Regional passive seismic
 2018 monitoring reveals dynamic glacier activity on Spitsbergen, Svalbard, Polar Research, 34, 26178.
 2019 <https://doi.org/10.3402/polar.v34.26178>

2020 Köhler, A., Nuth, C., Kohler, J., Berthier, E., Weidle, C., Schweitzer, J. (2016). A 15 year record of
 2021 frontal glacier ablation rates estimated from seismic data, Geophysical Research Letters, 43, 12155-
 2022 12164. <https://doi.org/10.1002/2016GL070589>

2023 Köhler, A., Pętllicki, M., Lefeuivre, P-M., Buscaino, G., Nuth, C., Weidle, C. (2019). Contribution of
 2024 calving to frontal ablation quantified from seismic and hydroacoustic observations calibrated with lidar
 2025 volume measurements, Cryosphere, 13, 3117-3137. <https://doi.org/10.5194/tc-13-3117-2019>.

2026 Köhler, A., Gajek, W., Malinowski, M., Schweitzer, J., Majdanski, M., Geissler, W. H., Chamarczuk,
 2027 M., & Wuestefeld, A. (2020). Seismological monitoring of Svalbard's cryosphere: current status and
 2028 knowledge gaps. In SESS report 2019 - The State of Environmental Science in Svalbard - an annual
 2029 report (pp. 136–159). Svalbard Integrated Arctic Earth Observing System.
 2030 <https://doi.org/10.5281/zenodo.4704584>

2031 Kolar, J., Haas, C., Helm, V. (2025): 2023 Glacier surface elevation data from airborne laser scanner
 2032 survey in Svalbard [dataset]. PANGAEA, <https://doi.org/10.1594/PANGAEA.974592>

2033 Kristensen, L., Benn, D.I. (2012). A surge of the glaciers Skobreen-Paulabreen, Svalbard, observed by
 2034 time-lapse photographs and remote sensing data, Polar Research, 31, 1-9.
 2035 <https://doi.org/10.3402/polar.v31i0.11106>

2036 Kristensen, L., Benn, D.I., Hormones, A., Ottesen, D. (2009). Mud aprons in front of Svalbard surge
 2037 moraines: Evidence of subglacial deforming layers or proglacial glaciotectionics?, Geomorphology,
 2038 111, 206-221. <https://doi.org/10.1016/j.geomorph.2009.04.022>

- 2039 Kurjanski, B., Rea, B.R., Spagnolo, M., Winsborrow, M., Cornwell, D., Andreassen, K., Howell, J.
2040 (2019). Morphological evidence for marine ice stream shutdown, central Barents Sea. *Marine*
2041 *Geology*, 414, 64-76. <https://doi.org/10.1016/j.margeo.2019.05.001>
- 2042 Langley, K., Hamran, S-E., Høgda, K.A., Storvold, R., Brandt, O., Hagen, J.O., Kohler, J. (2007). Use
2043 of C-band ground penetrating radar to determine backscatter sources within glaciers, *IEEE*
2044 *Transactions on Geoscience and Remote Sensing*, 45, 1236-1246.
2045 <https://doi.org/10.1109/TGRS.2007.892600>
- 2046 Langley, K., Lacroix, P., Hamran, S-E., Brandt, O. (2009). Sources of backscatter at 5.3 GHz from a
2047 superimposed ice and firn area revealed by multi-frequency GPR and cores, *Journal of Glaciology*, 55,
2048 373-383. <https://doi.org/10.3189/002214309788608660>
- 2049 Larsen, D.J., Geirsdóttir, Á., Miller, G.H. (2015). Precise chronology of Little Ice Age expansion and
2050 repetitive surges of Langjökull, central Iceland, *Geology*, 43, 167-170.
2051 <https://doi.org/10.1130/G36185.1>
- 2052 Larsen, E., Lyså, A., Rubensdotter, L., Farnsworth, W.R., Jensen, M., Nadeau, M.J., Ottesen, D.
2053 (2018). Lateglacial and Holocene glacier activity in the van Mijenfjorden area, western Svalbard,
2054 *Arktos*, 4. <https://doi.org/10.1007/s41063-018-0042-2>
- 2055 Leclercq, P.W., Käab, A., Altena, B. (2021). Brief communication: Detection of glacier surge activity
2056 using cloud computing of Sentinel-1 radar data, *Cryosphere*, 15, 4901-4907. [https://doi.org/10.5194/tc-](https://doi.org/10.5194/tc-15-4901-2021)
2057 [15-4901-2021](https://doi.org/10.5194/tc-15-4901-2021).
- 2058 Lefauconnier, B., Hagen, J.O. (1991). Surging and calving glaciers in eastern Svalbard, Norsk
2059 Polarinstitut, Meddelelser NR. 116.
- 2060 Lei, Y., Gardner, A.S., Agram, P. (2022). Processing methodology for the ITS_LIVE Sentinel-1 ice
2061 velocity products, *Earth System Science Data*, 14, 5111-5137. [https://doi.org/10.5194/essd-14-5111-](https://doi.org/10.5194/essd-14-5111-2022)
2062 [2022](https://doi.org/10.5194/essd-14-5111-2022).
- 2063 Lewandowska, H., & Teisseyre, R. (1964). Investigations of the ice microtremors on Spitsbergen in
2064 1962. *Biul Inf Komisji Wypraw Geof PAN*, 37, 1-5.
- 2065 Li, T., Heidler, K., Mou, L., Ignéczi, Á., Zhu, X.X., Bamber, J.L. (2024). A high-resolution calving front
2066 data product for marine-terminating glaciers in Svalbard, *Earth System Science Data*, 16, 919-939.
2067 <https://doi.org/10.5194/essd-16-919-2024>.

2068 Li, T., Hofer, S., Moholdt, G., Igneczi, A., Heidler, K., Zhu, X.X., Bamber, J. (2025). Pervasive glacier
 2069 retreats across Svalbard from 1985 to 2023, *Nature Communications*, 16, 1-11.
 2070 <https://doi.org/10.1038/s41467-025-55948-1>

2071 Lliboutry, L. (1968). General theory of subglacial cavitation and sliding of temperate glaciers, *Journal*
 2072 *of Glaciology*, 7, 21-58. <https://doi.org/10.3189/S0022143000020396>

2073 Lok, L. B., Brennan, P. V., Nicholls, K. W., & Corr, H. F. (2014). ApRES: Autonomous phase-sensitive
 2074 FMCW radar, for basal monitoring and imaging of Antarctic ice shelves, *IET Colloquium on Antennas,*
 2075 *Wireless and Electromagnetics*, 7. <https://doi.org/10.1049/ic.2014.0019>

2076 López, Y.Á., Garcia-Fernandez, M., Alvarez-Narciandi, G., Andrés, F.L.H. (2022). Unmanned aerial
 2077 vehicle-based ground-penetrating radar systems: A review. *IEEE Geoscience and Remote Sensing*
 2078 *Magazine*, 10, 66-86. <https://doi.org/10.1109/MGRS.2022.3160664>

2079 Lovell, H., Boston, C.M. (2017). Glacitectonic composite ridge systems and surge-type glaciers: An
 2080 updated correlation based on Svalbard, Norway, *Arktos*, 3. [https://doi.org/10.1007/s41063-017-0028-](https://doi.org/10.1007/s41063-017-0028-5)
 2081 [5](https://doi.org/10.1007/s41063-017-0028-5).

2082 Lovell, H., Fleming, E.J. (2023). Structural evolution during a surge in the Paulabreen glacier system,
 2083 Svalbard, *Journal of Glaciology*, 69, 141-152. <https://doi.org/10.1017/jog.2022.53>

2084 Lovell, H., Fleming, E.J., Benn, D.I., Hubbard, B., Lukas, S., Naegeli, K. (2015a). Former dynamic
 2085 behaviour of a cold-based valley glacier on Svalbard revealed by basal ice and structural glaciology
 2086 investigations. *Journal of Glaciology*, 61, 309-328. <https://doi.org/10.3189/2015JoG14J120>

2087 Lovell, H., Fleming, E.J., Benn, D.I., Hubbard, B., Lukas, S., Rea, B.R., Noormets, R., Flink, A.E.
 2088 (2015b). Debris entrainment and landform genesis during tidewater glacier surges, *Journal of*
 2089 *Geophysical Research: Earth Surface*, 120, 1574-1595. <https://doi.org/10.1002/2015JF003509>

2090 Lovell, H., Benn, D.I., Lukas, S., Spagnolo, M., Cook, S.J., Swift, D.A., Clark, C.D., Yde, J.C., Watts,
 2091 T. (2018a). Geomorphological investigation of multiphase glacitectonic composite ridge systems in
 2092 Svalbard, *Geomorphology*, 300, 176-188. <https://doi.org/10.1016/j.geomorph.2017.10.024>

2093 Lovell, H., Benn, D.I., Lukas, S., Ottesen, D., Luckman, A., Hardiman, M., Barr, I.D., Boston, C.M.,
 2094 Sevestre, H. (2018b). Multiple late Holocene surges of a high-Arctic tidewater glacier system in
 2095 Svalbard, *Quaternary Science Reviews*, 201, 162-185. <https://doi.org/10.1016/j.quascirev.2018.10.024>

2096 Luckman, A., Murray, T., Strozzi, T. (2002). Surface flow evolution throughout a glacier surge
 2097 measured by satellite radar interferometry, *Geophysical research Letters*, 29, 2095.
 2098 <https://doi.org/10.1029/2001GL014570>

2099 Luckman, A., Benn, D.I., Cottier, F., Bevan, S., Nilsen, F., Inall, M. (2015). Calving rates at tidewater
 2100 glaciers vary strongly with ocean temperature, *Nature Communications*, 8566, 8566.
 2101 <https://doi.org/10.1038/ncomms9566>

2102 Lyså, A., Larsen, E.A., Høgaas, F., Jensen, M.A., Klug, M., Rubensdotter, L., Szczuciński, W. (2018).
 2103 A temporary glacier-surge ice-dammed lake, Braganzavågen, Svalbard, *Boreas*, 47, 837-854.
 2104 <https://doi.org/10.1111/bor.12302>

2105 Małecki, J., Faucherre, S., Strzelecki, M.C. (2013). Post-surge geometry and thermal structure of
 2106 Hørbyebreen, central Spitsbergen, *Polish Polar Research*, 34, 305-321.
 2107 <https://doi.org/10.2478/popore-2013-0019>

2108 Mannerfelt, E.S., Hodson, A.J., Håkansson, L., Lovell, H. (2024). Dynamic LIA advances hastened the
 2109 demise of small valley glaciers in central Svalbard, *Arctic Science*, 10, 815-833.
 2110 <https://doi.org/10.1139/as-2024-0024>

2111 Mannerfelt, E.S., Schellenberger, T, Kääb, A.M. (2025). Tracking glacier surge evolution using
 2112 interferometric SAR coherence – examples from Svalbard. *Journal of Glaciology*, 71, e43.
 2113 <https://doi.org/10.1017/jog.2025.27>

2114 Mansell, D., Luckman, A., Murray, T. (2012). Dynamics of tidewater surge-type glaciers in northwest
 2115 Svalbard, *Journal of Glaciology*, 58, 110-118. <https://doi.org/10.3189/2012JoG11J058>.

2116 McCerery, R., Davies, B.J., Lovell, H., Pearce, D.A., Calvo-Ryan, R., Małecki, J., Woodward, J.
 2117 (2024). Terrestrial glacial geomorphology of surge-type and non-surge-type glaciers on Svalbard,
 2118 *Journal of Maps*, 20, 2362277. <https://doi.org/10.1080/17445647.2024.2362277>

2119 McCerery, R., Davies, B.J., Lovell, H., Calvo-Ryan, R., Pearce, D.A., Małecki, J., Woodward, J.
 2120 (2025). Landsystem models from remote and field based geomorphological mapping reveal diverse
 2121 glacier dynamics on Svalbard, *Geomorphology*, 484, 109854.
 2122 <https://doi.org/10.1016/j.geomorph.2025.109854>

2123 McCrystall, M.R., Stroeve, J., Serreze, M., Forbes, B.C., Screen, J.A. (2021). New climate models
 2124 reveal faster and larger increases in Arctic precipitation than previously projected, Nature
 2125 Communications, 12, 6765. <https://doi.org/10.1038/s41467-021-27031-y>

2126 McMillan, M., Shepherd, A., Gourmelen, N., Dehecq, A., Leeson, A., Ridout, A., Flament, T., Hogg, A.,
 2127 Gilbert, L., Benham, T., van den Broeke, M., Dowdeswell, J.A., Fettweis, X., Noël, B., Strozzi, T.
 2128 (2014). Rapid dynamic activation of a marine-based Arctic ice cap, Geophys Research Letters, 41,
 2129 8902-8909. <https://doi.org/10.1002/2014GL062255>.

2130 Meier, M.F., Post, A. (1969). What are glacier surges?, Canadian Journal of Earth Sciences, 6, 807-
 2131 817. <https://doi.org/10.1139/e69-081>

2132 Melvold, K., Hagen, J.O. (1998). Evolution of a surge-type glacier in its quiescent phase: Kongsvegen,
 2133 Spitsbergen, 1964-95, Journal of Glaciology, 44, 394-404.
 2134 <https://doi.org/10.3189/S0022143000002720>.

2135 Mikesell, T. D., van Wijk, K., Haney, M. M., Bradford, J. H., Marshall, H. P., & Harper, J. T. (2012).
 2136 Monitoring glacier surface seismicity in time and space using Rayleigh waves. Journal of Geophysical
 2137 Research: Earth Surface, 117, F02020. <https://doi.org/10.1029/2011JF002259>

2138 Minchew, B.M., Meyer, C.R. (2020). Dilation of subglacial sediment governs incipient surge motion in
 2139 glaciers with deformable beds, Proceedings of the Royal Society A, 476, 20200033.
 2140 <https://doi.org/10.1098/rspa.2020.0033>

2141 Morris, A., Moholdt, G., Gray, L. (2020). Spread of Svalbard glacier mass loss to Barents Sea margins
 2142 revealed by CryoSat-2, Journal of Geophysical Research: Earth Surface, 125, 1-20.
 2143 <https://doi.org/10.1029/2019JF005357>

2144 Murray, T., Porter, P.R. (2001). Basal conditions beneath a soft-bedded polythermal surge-type
 2145 glacier: Bakaninbreen, Svalbard, Quaternary International, 86, 103-116.
 2146 [https://doi.org/10.1016/S1040-6182\(01\)00053-2](https://doi.org/10.1016/S1040-6182(01)00053-2)

2147 Murray, T., Booth, A.D. (2010). Imaging glacial sediment inclusions in 3-D using ground-penetrating
 2148 radar at Kongsvegen, Svalbard, Journal of Quaternary Science, 25, 754-761.
 2149 <https://doi.org/10.1002/jqs.1351>

2150 Murray, T., Dowdeswell, J.A., Drewry, D.J., Frearson, I. (1998). Geometric evolution and ice dynamics
 2151 during a surge of Bakaninbreen, Svalbard, *Journal of Glaciology*, 44, 263-272.
 2152 <https://doi.org/10.3189/S0022143000002604>

2153 Murray, T., Stuart, G.W., Miller, P.J., Woodward, J., Smith, A.M., Porter, P. R., Jiskoot, H. (2000).
 2154 Glacier surge propagation by thermal evolution at the bed. *Journal of Geophysical Research: Solid*
 2155 *Earth*, 105, 13491-13507. <https://doi.org/10.1029/2000JB900066>

2156 Murray, T., Strozzi, T., Luckman, A., Jiskoot, H., Christakos, P. (2003a). Is there a single surge
 2157 mechanism? Contrasts in dynamics between glacier surges in Svalbard and other regions, *Journal of*
 2158 *Geophysical Research: Solid Earth*, 108, 2237. <https://doi.org/10.1029/2002JB001906>

2159 Murray, T., Luckman, A., Strozzi, T., Nuttall, A-M., (2003b). The initiation of glacier surging at
 2160 Fridtjovbreen, Svalbard, *Annals of Glaciology*, 36, 110-116.
 2161 <https://doi.org/10.3189/172756403781816275>.

2162 Murray, T., James, T.D., Macheret, Y., Lavrentiev, I., Glazovsky, A., Sykes, H. (2012). Geometric
 2163 changes in a tidewater glacier in Svalbard during its surge cycle, *Arctic Antarctic, and Alpine*
 2164 *Research*, 44, 359-367. <https://doi.org/10.1657/1938-4246-44.3.359>.

2165 Nanni, U., Gimbert, F., Vincent, C., Gräff, D., Walter, F., Piard, L., & Moreau, L. (2020). Quantification
 2166 of seasonal and diurnal dynamics of subglacial channels using seismic observations on an Alpine
 2167 glacier, *Cryosphere*, 14, 1475-1496. <https://doi.org/10.5194/tc-14-1475-2020>

2168 Navarro, F. J., Martín-Español, A., Lapazaran, J. J., Grabiec, M., Otero, J., Vasilenko, E. V., &
 2169 Puczkó, D. (2014). Ice volume estimates from ground-penetrating radar surveys, Wedel Jarlsberg
 2170 Land glaciers, Svalbard, *Arctic, Antarctic, and Alpine Research*, 46, 394-406.
 2171 <https://doi.org/10.1657/1938-4246-46.2.394>

2172 Nuth, C., Moholdt, G., Kohler, J., Hagen, J.O., Kääb, A. (2010). Svalbard glacier elevation changes
 2173 and contribution to sea level rise, *Journal of Geophysical Research*, 115, F01008.
 2174 <https://doi.org/10.1029/2008JF001223>

2175 Nuth, C., Gilbert, A., Köhler, A., McNabb, R., Schellenberger, T., Sevestre, H., Weidle, C., Girod, L.,
 2176 Luckman, A., Kääb, A. (2019). Dynamic vulnerability revealed in the collapse of an Arctic tidewater
 2177 glacier, *Scientific Reports*, 9, 5541. <https://doi.org/10.1038/s41598-019-41117-0>.

2178 Nuttall, A-M., Hagen, J.O., Dowdeswell, J. (1997). Quiescent-phase changes in velocity and geometry
2179 of Finsterwalderbreen, a surge-type glacier in Svalbard, *Annals of Glaciology*, 24, 249-254.
2180 <https://doi.org/10.3189/S0260305500012258>.

2181 Ødegård, R.S., Hamran, S-E., Bø, P.H., Etzelmüller, B., Vatne, G., Sollid, J.L. (1992). Thermal regime
2182 of a valley glacier, Erikbreen, northern Spitsbergen, *Polar Research*, 11, 69-79.
2183 <https://doi.org/10.3402/polar.v11i2.6718>

2184 Oerlemans, J. (2018). Modelling the late Holocene and future evolution of Monacobreen, northern
2185 Spitsbergen, *Cryosphere*, 12, 3001-3015. <https://doi.org/10.5194/tc-12-3001-2018>.

2186 Onarheim, I.H., Eldevik, T., Smedsrud, L.H., Stroeve, J.C. (2018). Seasonal and regional
2187 manifestation of Arctic sea ice loss, *Journal of Climate*, 31, 4917-4932. [https://doi.org/10.1175/JCLI-D-](https://doi.org/10.1175/JCLI-D-17-0427.1)
2188 [17-0427.1](https://doi.org/10.1175/JCLI-D-17-0427.1)

2189 Osika, A., Jania, J. (2024). Geomorphological and historical records of the surge-type behaviour of
2190 Hansbreen (Svalbard). *Journal of Glaciology*, 65, e31. <https://doi.org/10.1017/aog.2024.32>

2191 Ottesen, D., Dowdeswell, J.A. (2006). Assemblages of submarine landforms produced by tidewater
2192 glaciers in Svalbard, *Journal of Geophysical Research: Earth Surface*, 11, F01016.
2193 <https://doi.org/10.1029/2005JF000330>

2194 Ottesen, D., Dowdeswell, J.A., Benn, D.I., Kristensen, L., Christiansen, H.H., Christensen, O.,
2195 Hansen, L., Lebesbye, E., Forwick, M., Vorren, T.O. (2008). Submarine landforms characteristic of
2196 glacier surges in two Spitsbergen fjords, *Quaternary Science Reviews*, 27, 1583-1599.
2197 <https://doi.org/10.1016/j.quascirev.2008.05.007>.

2198 Ottesen, D., Dowdeswell, J.A., Bellec, V.K., Bjarnadóttir, L.R. (2017). The geomorphic imprint of
2199 glacier surges into open-marine waters: Examples from eastern Svalbard. *Marine Geology*, Volume
2200 392, 1-29, <https://doi.org/10.1016/j.margeo.2017.08.007>

2201 Pełlicki, M., Cieplý, M., Jania, J. A., Promińska, A., Kinnard, C. (2015). Calving of a tidewater glacier
2202 driven by melting at the waterline, *Journal of Glaciology*, 61, 851-863.
2203 <https://doi.org/10.3189/2015JoG15J062>

2204 Podolskiy, E.A., Walter, F. (2016). Cryoseismology, *Reviews of Geophysics*, 54, 708-758.
2205 <https://doi.org/10.1002/2016RG000526>

2206 Podolskiy, E.A., Murai, Y., Kanna, N., Sugiyama, S. (2021). Ocean-bottom and surface seismometers
 2207 reveal continuous glacial tremor and slip, *Nature Communications*, 12, 3929.
 2208 <https://doi.org/10.1038/s41467-021-24142-4>

2209 Pohjola, V.A., Christoffersen, P., Kolondra, L., Moore, J.C., Pettersson, R., Schäfer, M., Strozzi, T.,
 2210 Reijmer, C.H. (2011). Spatial distribution and change in the surface ice-velocity field of Vestfonna ice
 2211 cap, Nordaustlandet, Svalbard, 1995-2010 using geodetic and satellite interferometry data,
 2212 *Geografiska Annaler: Series A, Physical geography*, 93, 323-335. [https://doi.org/10.1111/j.1468-](https://doi.org/10.1111/j.1468-0459.2011.00441.x)
 2213 [0459.2011.00441.x](https://doi.org/10.1111/j.1468-0459.2011.00441.x)

2214 Rantanen, M., Karpechko, A.Y., Lipponen, A., Nordling, K., Hyvärinen, O., Ruosteenoja, K., Vihma, T.,
 2215 Laaksonen, A. (2022). The Arctic has warmed nearly four times faster than the globe since 1979,
 2216 *Communications Earth & Environment*, 3, 168. <https://doi.org/10.1038/s43247-022-00498-3>

2217 Raymond, C.F. (1987). How do glaciers surge? A review, *Journal of Geophysical Research: Solid*
 2218 *Earth*, 92, 9121-9134. <https://doi.org/10.1029/JB092iB09p09121>

2219 Raymond, C.F., Malone, S. (1986). Propagating strain anomalies during mini-surges of Variegated
 2220 Glacier, Alaska, USA, *Journal of Glaciology*, 32, 178-191.
 2221 <https://doi.org/10.3189/S00222143000015495>

2222 Rea, B.R., Evans, D.J.A. (2011). An assessment of surge-induced crevassing and the formation of
 2223 crevasse squeeze ridges, *Journal of Geophysical Research: Earth Surface*, 16, F04005.
 2224 <https://doi.org/10.1029/2011JF001970>

2225 RGI 7.0 Consortium (2023). Randolph Glacier Inventory - A Dataset of Global Glacier Outlines,
 2226 Version 7.0. Boulder, Colorado USA. NSIDC: National Snow and Ice Data Center.
 2227 doi:10.5067/f6jmovy5navz. Online access: <https://doi.org/10.5067/f6jmovy5navz>.

2228 Rieke, O., Årthun, M., Dörr, J.S. (2023). Rapid sea ice changes in the future Barents Sea, *Cryosphere*,
 2229 17, 1445-1456. <https://doi.org/10.5194/tc-17-1445-2023>

2230 Robinson, P., Dowdeswell, J.A. (2011). Submarine landforms and the behavior of a surging ice cap
 2231 since the last glacial maximum: The open-marine setting of eastern Austfonna, Svalbard, *Marine*
 2232 *Geology*, 286, 82-94. <https://doi.org/10.1016/j.margeo.2011.06.004>

2233 Rolstad, C., Amlien, J., Hagen, J.O., Lundén, B. (1997). Visible and near-infrared digital images for
 2234 determination of ice velocities and surface elevation during a surge on Osbornebreen, a tidewater
 2235 glacier in Svalbard, *Annals of Glaciology*, 24, 255-261. <https://doi.org/10.3189/S026030550001226X>

2236 Rösli, C., Walter, F., Husen, S., Andrews, L.C., Lüthi, M.P., Catania, G.A., Kissling, E. (2014).
 2237 Sustained seismic tremors and icequakes detected in the ablation zone of the Greenland ice sheet,
 2238 *Journal of Glaciology*, 60, 563-575. <https://doi.org/10.3189/2014JoG13J210>

2239 Røthe, T.O., Bakke, J., Vasskog, K., Gjerde, M., D'Andrea, W.J., Bradley, R.S. (2015). Arctic
 2240 Holocene glacier fluctuations reconstructed from lake sediments at Mitrahavøya, Spitsbergen,
 2241 *Quaternary Science Reviews*, 109, 111-125. <https://doi.org/10.1016/j.quascirev.2014.11.017>

2242 Röthlisberg, H. (1955). Studies in glacier physics on the Penny Ice Cap, Baffin Island, 1953: Part III:
 2243 seismic sounding, *Journal of Glaciology*, 2, 539-552. <https://doi.org/10.3189/002214355793702064>

2244 Saintenoy, A., Friedt, J. M., Booth, A. D., Tolle, F., Bernard, E., Laffly, D., Marlin, C., Griselin, M.
 2245 (2013). Deriving Ice Thickness, Glacier Volume and Bedrock Morphology of Austre Lovénbreen
 2246 (Svalbard) Using GPR, *Near Surface Geophysics*, 11, 253–262. <https://doi.org/10.3997/1873-0604.2012040>
 2247

2248 Schomacker, A., Kjær, K.H. (2008). Quantification of dead-ice melting in ice-cored moraines at the
 2249 high-Arctic glacier Holmströmbreen, Svalbard, *Boreas*, 37, 211-225. <https://doi.org/10.1111/j.1502-3885.2007.00014.x>
 2250

2251 Schoof, C. (2005). The effect of cavitation on glacier sliding, *Proceedings of the Royal Society A*, 461,
 2252 609-627. <https://doi.org/10.1098/rspa.2004.1350>

2253 Sevestre, H., Benn, D.I. (2015). Climatic and geometric controls on the global distribution of surge-
 2254 type glaciers: Implications for a unifying model of surging, *Journal of Glaciology*, 61, 646-662.
 2255 <https://doi.org/10.3189/2015JoG14J136>.

2256 Sevestre, H., Benn, D.I., Hulton, N.R.J., Bælum, K. (2015). Thermal structure of Svalbard glaciers and
 2257 implications for thermal switch models of glacier surging, *Journal of Geophysical Research: Earth*
 2258 *Surface*, 120, 2220-2236. <https://doi.org/10.1002/2015JF003517>.

2259 Sevestre, H., Benn, D.I., Luckman, A., Nuth, C., Kohler, J., Lindbäck, K., Pettersson, R. (2018).
 2260 Tidewater glacier surges initiated at the terminus, *Journal of Geophysical Research: Earth Surface*,
 2261 123, 1035-1051. <https://doi.org/10.1029/2017JF004358>.

2262 Sharp, M. (1985). "Crevasse-fill" ridges - A landform type characteristics of surging glaciers?,
 2263 Geografiska Annaler: Series A, Physical Geography, 67, 213-220.
 2264 <https://doi.org/10.1080/04353676.1985.11880147>

2265 Smith, A.M., Murray, T., Davison, B.M., Clough, A.F., Woodward, J., Jiskoot, H. (2002). Late surge
 2266 glacial conditions on Bakaninbreen, Svalbard, and implications for surge termination, Journal of
 2267 Geophysical Research: Solid Earth, 107, 2152. <https://doi.org/10.1029/2001JB000475>

2268 Smith, M.W., Carrivick, J.L., Quincey, D.J. (2016). Structure from motion photogrammetry in physical
 2269 geography, Progress in physical geography, 40, 247-275. <https://doi.org/10.1177/03091333156158>

2270 Sochor, L., Seehaus, T., Braun, M.H. (2021). Increased ice thinning over Svalbard measured by
 2271 ICESat/ICESat-2 laser altimetry, Remote Sensing, 13, 2089. <https://doi.org/10.3390/rs13112089>

2272 Solbø, S., & Storvold, R. (2013). Mapping svalbard glaciers with the cryowing UAS. The International
 2273 Archives of the Photogrammetry, Remote Sensing and Spatial Information Sciences, 40, 373-377.

2274 Streuff, K., Forwick, M., Szczuciński, W., Andreassen, K., Ó Cofaigh, C. (2015). Submarine landform
 2275 assemblages and sedimentary processes related to glacier surging in Kongsfjorden, Svalbard, Arktos,
 2276 1. <https://doi.org/10.1007/s41063-015-0003-y>

2277 Streuff, K., Ó Cofaigh, C., Noormets, R., Lloyd, J. (2018). Submarine landform assemblages and
 2278 sedimentary processes in front of Spitsbergen tidewater glaciers, Marine Geology, 402, 209-227.
 2279 <https://doi.org/10.1016/j.margeo.2017.09.006>

2280 Striberger, J., Björk, S., Benediktsson, Í.Ö., Snowball, I., Uvo, C.B., Ingólfsson, Ó., Kjær, K.H. (2011).
 2281 Climatic control of the surge periodicity of an Icelandic outlet glacier, Journal of Quaternary Science,
 2282 26, 561-565. <https://doi.org/10.1002/jqs.1527>

2283 Strozzi, T., Paul, F., Wiesmann, A., Schellenberger, T., Kääb, A. (2017). Circum-Arctic changes in the
 2284 flow of glaciers and ice caps from satellite SAR data between the 1990s and 2017, Remote Sensing,
 2285 9, 947. <https://doi.org/10.3390/rs9090947>.

2286 Stuart, G., Murray, T., Brisbourne, A., Styles, P., Toon, S. (2005). Seismic emissions from a surging
 2287 glacier: Bakaninbreen, Svalbard. Annals of Glaciology, 42, 151-157.
 2288 <https://doi.org/10.3189/172756405781812538>

2289 Sund, M., Eiken, T. (2010). Recent surges on Blomstrandbreen, Comfortlessbreen and Nathorstbreen,
2290 Svalbard, Journal of Glaciology, 56, 182-184. <https://doi.org/10.3189/002214310791190910>

2291 Sund, M., Eiken, T., Hagen, J.O., Kääb, A. (2009). Svalbard surge dynamics derived from geometric
2292 changes, Annals of Glaciology, 50, 50-60. <https://doi.org/10.3189/172756409789624265>.

2293 Sund, M., Lauknes, T.R., Eiken, T. (2014). Surge dynamics in the Nathorstbreen glacier system,
2294 Svalbard, Cryosphere, 8, 623-638. <https://doi.org/10.5194/tc-8-623-2014>.

2295 Swirad, Z.M., Johansson, A.M., Malnes, E. (2024). Extent, duration and timing of the sea ice cover in
2296 Hornsund, Svalbard, from 2014-2023, Cryosphere, 18, 895-910. [https://doi.org/10.5194/tc-18-895-](https://doi.org/10.5194/tc-18-895-2024)
2297 [2024](https://doi.org/10.5194/tc-18-895-2024)

2298 Tedstone, A.J., Nienow, P.W., Gourmelen, N., Dehecq, A., Goldberg, D., Hanna, E. (2015). Decadal
2299 slowdown of a land-terminating sector of the Greenland Ice Sheet despite warming, Nature, 526, 692-
2300 695. <https://doi.org/10.1038/nature15722>

2301 Temminghoff, M., Benn, D.I., Gulley, J.D., Sevestre, H. (2019). Characterization of the englacial and
2302 subglacial drainage system in a high Arctic cold glacier by speleological mapping and ground-
2303 penetrating radar, Geografiska Annaler: Series A, Physical Geography, 101, 98-117.
2304 <https://doi.org/10.1080/04353676.2018.1545120>

2305 Terleth, Y., van Pelt, W.J.J., Pohjola, V.A., Pettersson, R. (2021). Complementary approaches
2306 towards a universal model of glacier surges, Frontiers in Earth Science, 9.
2307 <https://doi.org/10.3389/feart.2021.732962>.

2308 Thøgersen, K., Gilbert, A., Schuler, T.V., Malthe-Sørenssen, A. (2019). Rate-and-state friction
2309 explains glacier surge propagation, Nature Communications, 10, 2823.
2310 <https://doi.org/10.1038/s41467-019-10506-4>

2311 Thøgersen, K., Gilbert, A., Bouchayer, C., Schuler, T.V. (2024). Glacier surges controlled by the close
2312 interplay between subglacial friction and drainage, Journal of Geophysical Research: Earth Surface,
2313 129, E2023JF007441. <https://doi.org/10.1029/2023JF007441>

2314 Trantow, T., Herzfeld, U.C. (2018). Crevasses as indicators of surge dynamics in the Bering Bagley
2315 glacier system, Alaska: Numerical experiments and comparison to image data analysis, Journal of
2316 Geophysical Research: Earth Surface, 123, 1615-1637. <https://doi.org/10.1029/2017JF004341>

2317 Trantow, T., Herzfeld, U.C. (2025). Progression of the surge in the Negribreen glacier system from two
 2318 years of ICESat-2 measurements, *Journal of Glaciology*, 71, e2. <https://doi.org/10.1017/jog.2024.58>

2319 Truffer, M., Kääb, A., Harrison, W.D., Osipova, G.B., Nosenko, G.A., Espizua, L., Gilbert, A., Fischer,
 2320 L., Huggel, C., Craw Burns, P.A., Lai, A.W. (2021): Chapter 13 - Glacier surges. In: W. Haeberli and
 2321 C. Whiteman (Eds.), *Snow and Ice-Related Hazards, Risks, and Disasters* (Second Edition). Elsevier.
 2322 417-466. <https://doi.org/10.1016/B978-0-12-817129-5.00003-2>

2323 Vallot, D., Adinugroho, S., Strand, R., How, P., Pettersson, R., Benn, D.I., Hulton, N.R. (2019).
 2324 Automatic detection of calving events from time-lapse imagery at Tunabreen, Svalbard, *Geoscientific*
 2325 *Instrumentation, Methods and Data Systems*, 8, 113-127. <https://doi.org/10.5194/gi-8-113-2019>.

2326 Van Pelt, W., Frank, T. (2025). New glacier thickness and bed topography maps for Svalbard,
 2327 *Cryosphere*, 19, 1-17. <https://doi.org/10.5194/tc-19-1-2025>

2328 Van Pelt, W., Pohjola, V., Pettersson, R., Marchenko, S., Kohler, J., Luks, B., Hagen, J.O., Schuler,
 2329 T.V., Dunge, T., Noël, B., Reijmer, C. (2019). A long-term dataset of climatic mass balance, snow
 2330 conditions, and runoff in Svalbard (1957-2018), *Cryosphere*, 13, 2259-2280. [https://doi.org/10.5194/tc-](https://doi.org/10.5194/tc-13-2259-2019)
 2331 [13-2259-2019](https://doi.org/10.5194/tc-13-2259-2019)

2332 Van Pelt, W.J.J., Schuler, T.V., Pohjola, V.A., Pettersson, R. (2021). Accelerating future mass loss of
 2333 Svalbard glaciers from a multi-model ensemble, *Journal of Glaciology*, 67, 485-499.
 2334 <https://doi.org/10.1017/jog.2021.2>

2335 Walter, F., Roux, P., Roeoesli, C., Lecointre, A., Kilb, D., Roux, P.F. (2015). Using glacier seismicity
 2336 for phase velocity measurements and Green's function retrieval, *Geophysical Journal International*,
 2337 201, 1722-1737. <https://doi.org/10.1093/gji/ggv069>

2338 Walter, F., Gräff, D., Lindner, F., Paitz, P., Köpfli, M., Chmiel, M., Fichtner, A. (2020). Distributed
 2339 acoustic sensing of microseismic sources and wave propagation in glaciated terrain. *Nature*
 2340 *Communications*, 11, 2436. <https://doi.org/10.1038/s41467-020-15824-6>

2341 Weaver, C.S., Malone, S.D. (1979). Seismic evidence for discrete glacier motion at the rock-ice
 2342 interface, *Journal of Glaciology*, 23, 171-184. <https://doi.org/10.3189/S0022143000029816>

2343 Weertman, J. (1957). On the sliding of glaciers, *Journal of Glaciology*, 3, 33-38.
 2344 <https://doi.org/10.3189/S0022143000024709>

2345 Werner, C., Strozzi, T., Wiesmann, A., Wegmüller, U. (2008). GAMMA's portable radar interferometer.
2346 In: Proceedings of the 13th FIG International Symposium on Deformation Measurements and Analysis
2347 & 4th IAG Symposium on Geodesy for Geotechnical and Structural Engineering, Lisbon, Portugal,
2348 May 12–15, 2008.

2349 Woodward, J., Murray, McCaig, A. (2002). Formation and reorientation of structure in the surge-type
2350 glacier Kongsvegen, Svalbard, Journal of Quaternary Science, 17, 201-209.
2351 <https://doi.org/10.1002/jqs.673>

2352 Woodward, J., Murray, T., Clark, R.A., Stuart, G.W. (2003). Glacier surge mechanisms inferred from
2353 ground-penetrating radar: Kongsvegen, Svalbard, Journal of Glaciology, 49, 473-480.
2354 <https://doi.org/10.3189/172756503781830458>

2355 Woodward, J., Burke, M.J. (2007). Applications of ground-penetrating radar to glacial and frozen
2356 materials. Journal of Environmental & Engineering Geophysics, 12, 69-85.
2357 <https://doi.org/10.2113/JEEG12.1.69>

2358 Zagórski, P., Frydrych, K., Jania, J., Błaszczuk, M., Sund, M., Moskalik, M. (2023). Surges in three
2359 Svalbard glaciers derived from historic sources and geomorphic features, Annals of the American
2360 Association of Geographers, 113, 1835-1855. <https://doi.org/10.1080/24694452.2023.2200487>

2361 Zhan, Z. (2019). Seismic noise interferometry reveals transverse drainage configuration beneath the
2362 surging Bering Glacier. Geophysical Research Letters, 46(9), 4747-4756.
2363 <https://doi.org/10.1029/2019GL082411>